

Lectures on insulating and conducting quantum spin liquids

Subir Sachdev

Department of Physics, Harvard University, Cambridge, Massachusetts, 02138, USA.

Center for Computational Quantum Physics, Flatiron Institute,
162 5th Avenue, New York, NY 10010, USA.

The Abdus Salam International Centre for Theoretical Physics,
Strada Costiera 11, I-34151, Trieste, Italy.

sachdev@g.harvard.edu

Abstract

Two of the iconic phases of the hole-doped cuprate materials are the intermediate temperature pseudogap metal and the lower temperature d -wave superconductor. Following the prescient suggestion of P. W. Anderson, there were numerous early theories of these phases as doped quantum spin liquids. However, these theories have had difficulties with two prominent observations:

- (i) angle-dependent magnetoresistance measurements (ADMR) in the pseudogap metal, including observation of the Yamaji effect, present convincing evidence of small hole pockets which can tunnel coherently between square lattice layers (Fang *et al.*, *Nature Physics* 18, 558 (2022); Chan *et al.*, *Nature Physics* 21, 1753 (2025)) and
- (ii) the velocities of the nodal Bogoliubov quasiparticles in the d -wave superconductor are highly anisotropic, with $v_F \gg v_\Delta$ (Chiao *et al.*, *Phys. Rev. B* 62, 3554 (2000)).

These lecture notes review how the fractionalized Fermi Liquid (FL*) state, which dopes quantum spin liquids with gauge-neutral electron-like quasiparticles, resolves both difficulties. Theories of insulating quantum spin liquids employing fractionalization of the electron spin into bosonic or fermionic partons are discussed. Doping the bosonic parton theory leads to a holon metal theory: while not appropriate for the cuprate pseudogap, this theory is argued to apply to the Lieb lattice. Doping the fermionic parton theory leads to a d -wave superconductor with nearly isotropic quasiparticle velocities. The construction of the FL* state in a single band Hubbard-type model is described using a quantum dimer model, followed by a more realistic description using the Ancilla Layer Model (ALM), which is then used to obtain the theory of the pseudogap and the d -wave superconductor.

Advanced School and Conference on Quantum Matter, Dec 1-12, 2025
International Centre for Theoretical Physics, Trieste
Lecture Videos: [Lecture I](#), [Lecture II](#).

- Sections 1, 2 are mostly adapted from *Quantum Phases of Matter*, by Subir Sachdev, Cambridge University Press (2023).
- Sections 3, 5, 6 are mostly adapted from *Fractionalized Fermi liquids and the cuprate phase diagram*, Pietro M. Bonetti, Maine Christos, Alexander Nikolaenko, Aavishkar A. Patel, and Subir Sachdev, [arXiv:2508.20164](#).

Contents

1	Introduction	2
2	Spin density wave order in the Hubbard model	4
2.1	Fermi surface reconstruction	5
3	Bosonic spinon theory of quantum spin liquids	9
3.1	Mean-field theory	11
3.2	Gauge excitations	14
3.2.1	Square lattice	14
3.2.2	Triangular lattice	15
3.3	Topological excitations on the triangular lattice	17
3.4	Dynamics of excitations on the triangular lattice	19
3.4.1	Motion of spinons	19
3.4.2	Motion of visons	21
3.4.3	Semions and fermions	22
3.4.4	Complete \mathbb{Z}_2 gauge theory of spinons and visons	24
3.5	Dynamics of excitations on the square lattice	25
3.5.1	Quantum criticality	27
4	Fermionic spinon theory of quantum spin liquids	28
4.1	Low energy SU(2) gauge theory.	30
4.2	SO(5) non-linear σ -model	32
5	Holon metal from a quantum spin liquid with bosonic spinons	33
6	<i>d</i>-wave superconductor and charge orders from a quantum spin liquid with fermionic spinons	35
7	Fractionalized Fermi liquids (FL*)	40
7.1	FL* in single band models	41
7.1.1	ADMR	43
7.2	Layer construction with ancilla qubits	43
7.3	Mean field theory of the cuprate pseudogap.	45
7.4	Wavefunction for FL* and cold atom observations.	48
7.5	SU(2) gauge theory of the onset of nodal <i>d</i> -wave superconductivity from FL*	48
7.6	Anisotropic velocities in the <i>d</i> -wave superconductor	50
References		52

1 Introduction

These lectures begin by presenting the conventional Hartree-Fock theory of antiferromagnetic order in the square lattice Hubbard model in Section 2. The state with antiferromagnetic

order is generically a metal, with electron and/or hole pocket Fermi surfaces. However, precisely at half-filling, and *only if* the antiferromagnetic order is large enough, the Fermi surfaces disappear, and we obtain an insulating antiferromagnet.

Sections 3 and 4 present the theory of insulating quantum spin liquids in two spatial dimensions. These are states at half-filling which are insulating *without* any antiferromagnetic order or other broken symmetry. No such states appear in the theory of Section 2, or in other conventional approaches found in condensed matter texts published before the 1980s. We describe these states by the powerful parton method, which requires the presence of emergent gauge fields. Section 3 expresses the electron spin operator in terms of bosonic partons, while Section 4 employs fermionic partons.

The bosonic parton theory on triangular lattice leads to the theory of the \mathbb{Z}_2 spin liquid [1–3]. This is the simplest quantum spin liquid which can have time-reversal symmetry, and its spectrum of fractionalized ‘anyon’ excitations is the same as that of the toric code [4].

The bosonic parton theory on the square lattice leads to a U(1) gauge theory which maps at low energy to the \mathbb{CP}^1 field theory, along with additional Berry phases for Dirac monopole configurations in the U(1) gauge field [5,6] (Section 3.5). This theory describes the transition from the antiferromagnetically ordered Néel state to a valence bond solid (VBS), with a gapless spin liquid regime between them.

The fermionic parton theory on the square lattice is discussed in Section 4. Its low energy theory is a SU(2) gauge theory with 2 flavors ($N_f = 2$) of massless Dirac spinons [7–10]. Remarkably this SU(2) gauge theory has a duality mapping [11] to the U(1) gauge theory of Section 3.5.

Section 5 moves the bosonic parton theory of Section 3 away from half-filling. This leads a ‘holon metal’ state, which is relevant for the Hubbard model on the Lieb lattice. But holons cannot tunnel coherently between square lattice layers, and so we argue that ADMR experiments [12,13] imply that the holon metal cannot describe the cuprate pseudogap metal.

Section 6 moves the fermionic parton theory of Section 3 away from half-filling. This leads to a *d*-wave superconductor and also a variety of competing charge-order states. But the *d*-wave superconductor has nearly isotropic velocities for the Bogoliubov quasiparticles, in contrast to observations [14].

The Fractionalized Fermi liquid (FL*) state [15,16] is introduced in Section 7. The theory of FL* in a single-band Hubbard-type model is developed, and argued to resolve the problems with applications to the cuprates noted above.

The existence of the FL* state sets up the possibility of a quantum phase transition from FL* to the conventional Fermi liquid (FL): a transition between two metals without any broken symmetry order parameter. Such an underlying FL*-FL transition has been argued [17] to be the key to understanding the cuprate phase diagram across optimal doping, as is reviewed elsewhere [18], but will not be described in the present article beyond the discussion below.

A key constraint satisfied by the theory is that the FL and FL* states have a transition at low temperatures to the *same* *d*-wave superconductor, *i.e.* there is no transition within the superconducting state between over- and under-doping. In the over-doped regime, the transition from FL to the superconductor is described by the conventional BCS framework. In the under-doped regime, the transition from FL* to the *same* *d*-wave superconductor is described by a confinement transition of a SU(2) gauge theory [19–23], employing the SU(2) gauge field of Section 4. But an important point is that the underlying FL*-FL transition is visible within the superconducting state in the differences in the vortex core structure [23,24]: in the over-doped superconductor, the vortices exhibit [25] the Wang-MacDonald peak [26] obtained from a conventional BCS theory of a *d*-wave superconductor; in the under-doped superconductor the underlying FL* normal state leads to [23,24] modulations in the local density of states [27].

The underlying FL^* -FL transition is also useful in developing a theory of the strange metal phase at higher temperatures. In the presence of impurities, the strange metal has been argued [28–31] to be described by a two-dimensional extension of the Sachdev-Ye-Kitaev model [32, 33].

2 Spin density wave order in the Hubbard model

We consider the onset of magnetism at a non-zero wavevector in a metal, often called a spin density wave (SDW). We will focus on the case where the wavevector of the SDW is $\mathbf{K} = (\pi, \pi)$ on the square lattice, and so the ordering has the same symmetry as the Néel state in an insulating antiferromagnet. The main ingredient here will be a bosonic collective mode representing antiferromagnetic spin fluctuations in the metal: this boson is the ‘paramagnon’.

Near the transition from the Fermi liquid to the antiferromagnetic metal, it is possible to derive a systematic approach to the paramagnon modes of a metal. We begin with an electronic Hubbard model

$$H = \sum_{\mathbf{k}, \alpha} \varepsilon_{\mathbf{k}} c_{\mathbf{k}\alpha}^\dagger c_{\mathbf{k}\alpha} + U \sum_i n_{i\uparrow} n_{i\downarrow} \quad (1)$$

where $n_{i\uparrow} \equiv c_{i\uparrow}^\dagger c_{i\uparrow}$, and similarly for $n_{i\downarrow}$. Upon using the single-site identity

$$U \left(n_{i\uparrow} - \frac{1}{2} \right) \left(n_{i\downarrow} - \frac{1}{2} \right) = -\frac{2U}{3} S_i^2 + \frac{U}{4}, \quad (2)$$

(which is easily established from the electron commutation relations) it becomes possible to decouple the 4-fermion term in a particle-hole channel. We decouple the interaction term in the Hubbard model in (1), by the Hubbard-Stratonovich transformation

$$\exp \left(\frac{2U}{3} \sum_i \int d\tau S_i^2 \right) = \int \mathcal{D}\mathbf{P}_i(\tau) \exp \left(- \sum_i \int d\tau \left[\frac{3U}{8} \mathbf{P}_i^2 - U \mathbf{P}_i \cdot c_{i\alpha}^\dagger \frac{\boldsymbol{\sigma}_{\alpha\beta}}{2} c_{i\beta} \right] \right) \quad (3)$$

We now have a new field $\mathbf{P}_i(\tau)$ which will play the role of the paramagnon field.

The path integral of the Hubbard model can now be written exactly as:

$$\begin{aligned} \mathcal{Z} = & \int \mathcal{D}c_{i\alpha}(\tau) \mathcal{D}\mathbf{P}_i(\tau) \exp \left(- \int d\tau \left\{ \sum_{\mathbf{k}, \alpha} c_{\mathbf{k}\alpha}^\dagger \left[\frac{\partial}{\partial \tau} + \varepsilon_{\mathbf{k}} \right] c_{\mathbf{k}\alpha} \right. \right. \\ & \left. \left. + \sum_i \left[\frac{3U}{8} \mathbf{P}_i^2 - U \mathbf{P}_i \cdot c_{i\alpha}^\dagger \frac{\boldsymbol{\sigma}_{\alpha\beta}}{2} c_{i\beta} \right] \right\} \right). \end{aligned} \quad (4)$$

We can now formally integrate out the electrons, and obtain

$$\frac{\mathcal{Z}}{\mathcal{Z}_0} = \int \prod_i \mathcal{D}\mathbf{P}_i(\tau) \exp \left(- \mathcal{S}_{\text{paramagnon}} [\mathbf{P}_i(\tau)] \right), \quad (5)$$

where \mathcal{Z}_0 is the free electron partition function. Close to the onset of SDW order (but still on the non-magnetic side), we can expand the action in powers of \mathbf{P}

$$\mathcal{S}_{\text{paramagnon}} [\mathbf{P}_i(\tau)] = \frac{T}{2} \sum_{\mathbf{q}, \omega_n} |\mathbf{P}(\mathbf{q}, \omega_n)|^2 U \left[\frac{3}{4} - \frac{U \chi_0(\mathbf{q}, i\omega_n)}{2} \right] + \dots \quad (6)$$

where $\chi_0(\mathbf{q}, \omega_n)$ is the frequency-dependent Lindhard susceptibility, given by the particle-hole bubble graph shown in Fig. 1

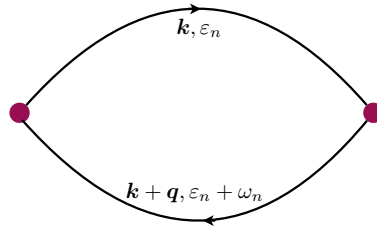


Figure 1: Feynman diagram leading to (7).

$$\chi_0(\mathbf{q}, i\omega_n) = -\frac{T}{V} \sum_{\mathbf{p}, \epsilon_n} \frac{1}{(i\epsilon_n - \epsilon_{\mathbf{k}})(i\epsilon_n + i\omega_n - \epsilon_{\mathbf{k}+\mathbf{q}})} \quad (7)$$

Performing the sum over frequencies by partial fractions, we obtain

$$\chi_0(\mathbf{q}, i\omega_n) = \frac{1}{V} \sum_{\mathbf{k}} \frac{f(\epsilon_{\mathbf{k}+\mathbf{q}}) - f(\epsilon_{\mathbf{k}})}{i\omega_n + \epsilon_{\mathbf{k}} - \epsilon_{\mathbf{k}+\mathbf{q}}}, \quad (8)$$

From the structure of the \mathbf{P} propagator, it is clear that \mathbf{P} will first condense at the wavevector \mathbf{q}_{\max} at which $\chi_0(\mathbf{q}, i\omega = 0)$ is a maximum, and \mathbf{q}_{\max} is then the wavevector of the SDW. In the mean field treatment of (6), the appearance of the this condensate requires that U is large enough to obey the ‘Stoner criterion’:

$$\frac{3}{4} - \frac{U\chi_0(\mathbf{q}_{\max}, i\omega = 0)}{2} < 0. \quad (9)$$

This wavevector is in turn determined by the dispersion $\epsilon_{\mathbf{k}}$ of the underlying fermions. For simplicity, we will only consider the case of a SDW with wavevector $\mathbf{K} = (\pi, \pi)$. The frequency dependence of $\chi_0(\mathbf{q}, i\omega)$ also has an important influence on the dynamics of the paramagnon fluctuations.

2.1 Fermi surface reconstruction

Let us now move into the antiferromagnetic metal phase, where we assume there is a \mathbf{P} condensate at wavevector $\mathbf{K} = (\pi, \pi)$

$$\langle \mathbf{P}_i \rangle = \eta_i \mathcal{N} \hat{\mathbf{z}}, \quad (10)$$

where the factor

$$\eta_i = \pm 1 \quad (11)$$

on the two checkerboard sublattices of the square lattice, and \mathcal{N} measuring the strength of the Néel ordered moment shown in Fig. 2.

We wish to describe the excitations of this state. One class of excitations are spin waves: these can be obtained by considering transverse fluctuations of \mathbf{P} about the condensate in (10) using the full action in (5). However, there are also low energy fermionic excitations in the antiferromagnetic metal, which are gapped in the insulator. We can determine the spectrum of the fermions by inserting (10) into the Yukawa coupling; using $\eta_i = e^{i\mathbf{K} \cdot \mathbf{r}_i}$, with $\mathbf{K} = (\pi, \pi)$, we can write the fermion Hamiltonian in momentum space

$$H_{\text{AFM}} = \sum_{\mathbf{k}} [\epsilon_{\mathbf{k}} c_{\mathbf{k}\alpha}^\dagger c_{\mathbf{k}\alpha} - \Delta c_{\mathbf{k}\alpha}^\dagger \sigma_{\alpha\alpha}^z c_{\mathbf{k}+\mathbf{K},\alpha}] + \text{constant}. \quad (12)$$

This is the analog of the BCS Hamiltonian for superconductivity, and the analog of the pairing gap is the energy

$$\Delta = \mathcal{N}. \quad (13)$$

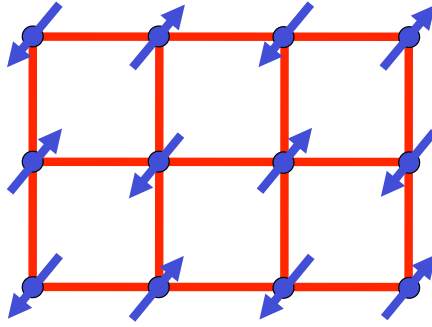


Figure 2: Antiferromagnetic (Néel) order \mathcal{N} of the spin density wave state. This can be an insulator at $p = 0$, provided $\Delta = \mathcal{N}$ is large enough, as shown in Fig. 4. Otherwise, it is a metal with electron and/or hole pocket Fermi surfaces, as shown in Fig. 4-6.

But, in general, the spectrum of H_{AFM} does not have a gap, as we will see below. As in BCS theory, the value of \mathcal{N} has to be determined self-consistently from the mean-field equations.

To obtain the fermionic excitation spectrum, we have to perform the analog of the Bogoliubov rotation in BCS theory. This is achieved by writing H_{AFM} in a 2×2 matrix form by using the fact that $2K$ is a reciprocal lattice vector, and so $\varepsilon_{k+2K} = \varepsilon_k$; correspondingly, the prime over the summation indicates that it only extends over half the Brillouin zone of the underlying lattice, shown in the left panel of Fig. 4, which is the Brillouin zone of the lattice with Néel order.

$$H_{\text{AFM}} = \sum'_{\mathbf{k}} (c_{\mathbf{k}\alpha}^\dagger, c_{\mathbf{k}+K,\alpha}^\dagger) \begin{pmatrix} \varepsilon_{\mathbf{k}} & -\Delta\sigma_{\alpha\alpha}^z \\ -\Delta\sigma_{\alpha\alpha}^z & \varepsilon_{\mathbf{k}+K} \end{pmatrix} \begin{pmatrix} c_{\mathbf{k}\alpha} \\ c_{\mathbf{k}+K,\alpha} \end{pmatrix}. \quad (14)$$

It is now easy to diagonalize the 2×2 matrix in (14), and we obtain

$$E_{\mathbf{k}\pm} = \frac{\varepsilon_{\mathbf{k}} + \varepsilon_{\mathbf{k}+K}}{2} \pm \left[\left(\frac{\varepsilon_{\mathbf{k}} - \varepsilon_{\mathbf{k}+K}}{2} \right)^2 + \Delta^2 \right]^{1/2} \quad (15)$$

The spectrum in (15) is not gapped, or even positive definite. Rather, it is the spectrum of a metal, in which the negative energy states are filled, and bounded by a Fermi surface. For small Δ , the structure of the Fermi surface can be deduced from the pictorial argument in Fig. 3: gaps open at the ‘hotspots’ where both $\varepsilon_{\mathbf{k}}$ and $\varepsilon_{\mathbf{k}+K}$ vanish, reconstructing the large Fermi surface into small pockets. The Fermi surfaces so obtained is shown in Figs. 4, 5, 6 for different values of the electron density $1 - p$. Here p is conventionally the hole doping, and electron doping corresponds to $p < 0$. The dispersion $\varepsilon_{\mathbf{k}}$ has hoppings $t_{1,2,3}$ to first, second, and third neighbors with $t_{1,3} > 0$ and $t_2 < 0$ as appropriate for the cuprates.

We observe that the ‘large’ Fermi surface of the paramagnetic metal has ‘reconstructed’ into small pocket Fermi surfaces in the SDW state. The excitations of the SDW metal are hole-like quasiparticles on the Fermi surfaces surrounding the hole pockets, and electron-like quasiparticles on the Fermi surfaces surrounding the electron pockets. The spin wave excitations interact rather weakly with the fermionic quasiparticle excitations: this can be seen from a somewhat involved computation from the effective action.

Finally, we discuss the fate of the Luttinger relation in this metal. The Luttinger relation connects the volume enclosed by the Fermi surface to the density of electrons, modulo 2 electrons per unit cell. It should be applied in the Brillouin zone of the Néel state, which is half the size of the Brillouin zone of the underlying square lattice, as shown in Fig. 4. In real space, this corresponds to the fact that the unit cell has doubled, and so the density of electrons per unit cell is $2(1-p)$. For spinful electrons, the Luttinger relations measures electron density modulo

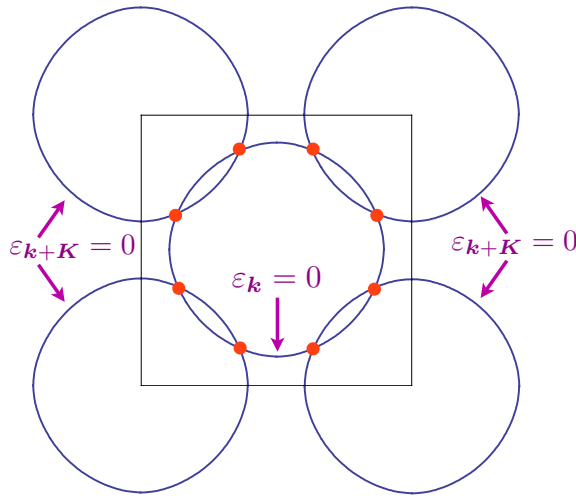


Figure 3: Fermi surface of the original dispersion ε_k , and those obtained by scattering off the antiferromagnetic order by a momentum K . The intersections of the Fermi surfaces are the hotspots, where the antiferromagnetism opens a gap. In this figure only, the center is the momentum K , around which the large hole-like Fermi surface is centered in the cuprates.

Square-lattice Hubbard model with no doping

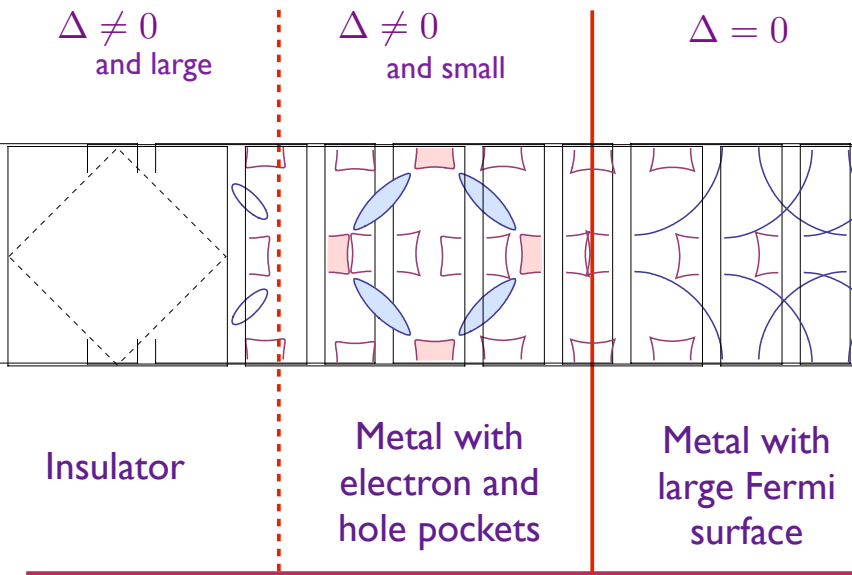


Figure 4: Fermi surfaces of the Néel state at half-filling, *i.e.* doping $p = 0$. The pockets intersecting the diagonals of the Brillouin zone have both bands in (15) empty and so form hole pockets, while the remaining pockets have both bands occupied and form electron pockets. The dashed line in the insulator shows the boundary of the Brillouin zone of the Néel state.

Square-lattice Hubbard model with hole doping

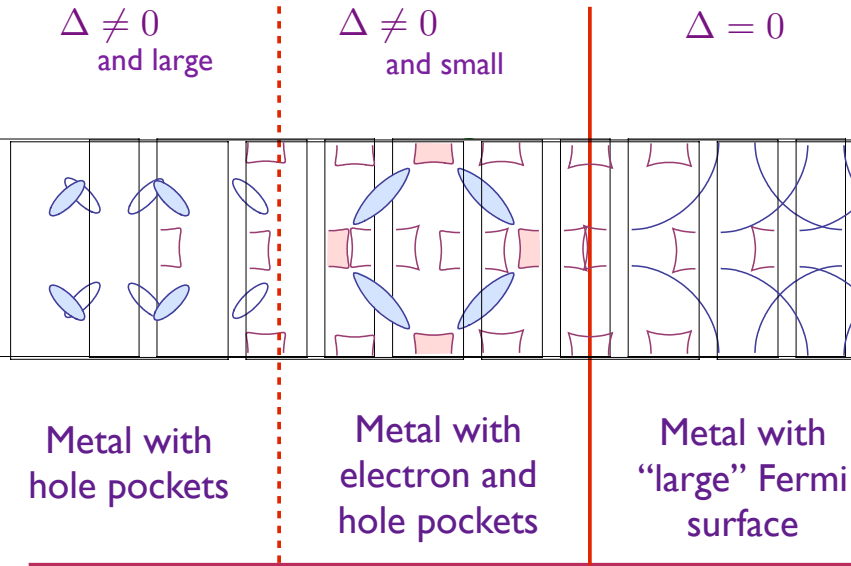


Figure 5: Fermi surfaces of the Néel state at $p > 0$. The pockets are as in Fig. 4. From (16), the area of each hole pocket on the left (when Δ is large and there are no electron pockets) is $p/4$, in units with the square lattice Brillouin zone having unit area. This follows from the existence of 2 independent hole pockets in the magnetic Brillouin zone, each with a spin degeneracy of 2.

Square-lattice Hubbard model with electron doping

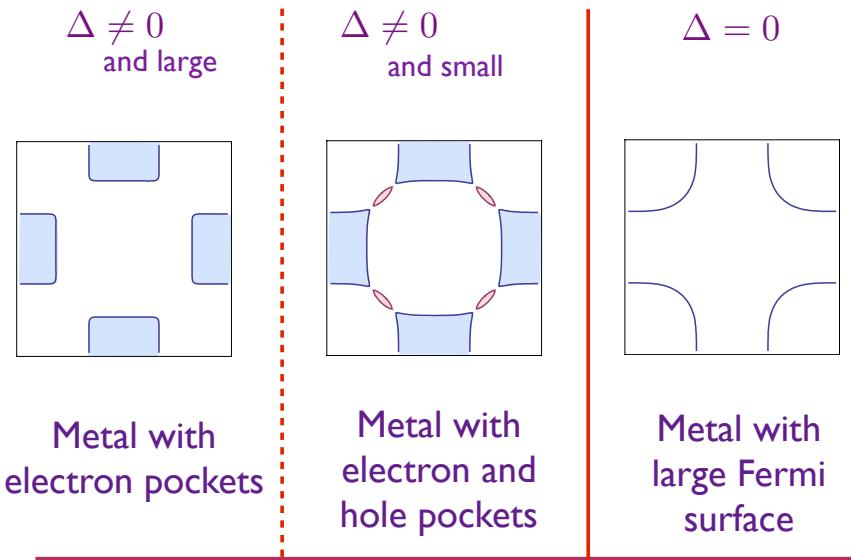


Figure 6: Fermi surfaces of the Néel state at $p < 0$, with pockets as in Figs. 4. From (16), the area of each electron pocket on the left (when Δ is large and there are no hole pockets) is $|p|/2$, in units with the square lattice Brillouin zone having unit area. This follows from the existence of 1 independent electron pocket in the magnetic Brillouin zone with a spin degeneracy of 2.

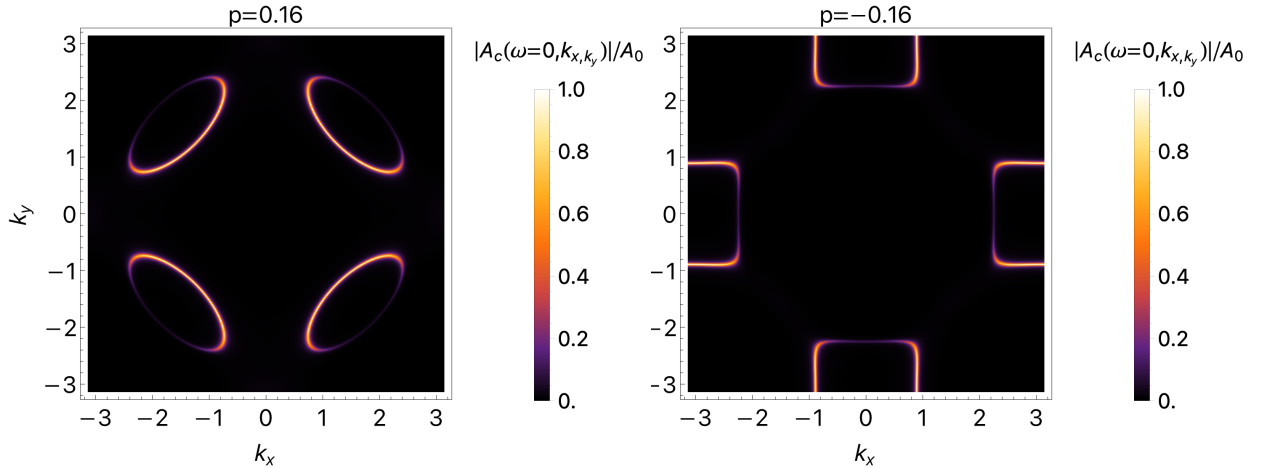


Figure 7: Spectral density of hole (left) and electron (right) pockets at $p = 0.16$ and $p = -0.16$ respectively for the SDW state. The fractional area of each hole pocket is $p/4$, and the fractional area of the electron pocket is $|p|/2$. Figure by A. Nikolaenko.

2, and so the density appearing in the Luttinger relation is $-2p$. This has to be equated to twice the volumes enclosed by the electron and hole pockets within the diamond shaped Brillouin zone in Fig. 4. Let \mathcal{A}_h be the area of a single elliptical hole pocket: there are 4 such pockets in the complete Brillouin zone of the square lattice or 2 pockets in the Brillouin zone of the Néel state, as is apparent from Figs. 4, 5, 6. Similarly, let \mathcal{A}_e be the area of a single elliptical electron pocket: there are 2 such pockets in the complete Brillouin zone of the square lattice or 1 pocket in the Brillouin zone of the Néel state. These arguments show that the Luttinger relation becomes

$$2 \times \frac{1}{(2\pi)^2/2} \times (-2\mathcal{A}_h + \mathcal{A}_e) = -2p. \quad (16)$$

On the left hand side, the first factor is the spin degeneracy, and the second factor is the inverse of the volume of the Brillouin zone of the Néel state. To reiterate, this is the conventional Luttinger relation applied after accounting for the doubling of the unit cell, and it determines a linear constraint on the areas of the electron and hole pockets.

Fig 7 shows the electron spectral density (as measured by photoemission) at zero frequency for both the electron and hole pockets. This is computed by taking the imaginary part of the Green's function $(\omega - H_{\text{AFM}} + i\eta)^{-1}$ of the matrix Hamiltonian in Eq. (14), where η is a positive infinitesimal.

3 Bosonic spinon theory of quantum spin liquids

Section 2 has obtained an insulator at $p = 0$ with Néel order \mathcal{N} . Decreasing \mathcal{N} eventually leads to a metallic state with $\mathcal{N} = 0$, even at $p = 0$. But there was no insulator at $p = 0$ with no broken symmetry, and no such insulator is possible within the conventional Hartree-Fock framework. In this section we show that an insulator can indeed be obtained at $p = 0$ without any broken symmetry, but only after introducing fractionalized spin excitations.

As long as the charge gap is finite, we can perform a canonical transformation of the Hubbard model in Eq. (1) to spin-only Heisenberg antiferromagnet

$$\mathcal{H}_J = \sum_{i < j} J_{ij} \mathbf{S}_i \cdot \mathbf{S}_j. \quad (17)$$

The J_{ij} are short-ranged antiferromagnetic exchange interactions between $S = 1/2$ spins S_i on sites i . We will consider here the square and triangular lattices with nearest neighbor interactions, but the methods generalize to a wide class of lattices and interaction ranges. Our analysis will be carried out for the nearest-neighbor Hamiltonian, and we will search for mean-field theories without any broken symmetries. In practice, we know that the nearest neighbor models on both the square and triangular lattices have antiferromagnetic order. But the strategy here is to understand the general structure of the spin liquid states, which can then be realized in more general Hamiltonians.

In this section, we employ a method which fractionalizes the spin operator into bosonic partons. On the square lattice, this leads to the low energy U(1) gauge theory with complex scalars in Eq. (75), and to the phase diagram in Fig. 17. This phase diagram is in good agreement with numerical studies [34–36] of the square lattice antiferromagnet with first and second neighbor exchange (the J_1 - J_2 model), and also of Sandvik’s J - Q model [37].

Section 4 fractionalizes the spin operator into fermionic partons. This leads ultimately to a seemingly different low energy theory on the square lattice: a SU(2) gauge theory with massless Dirac fermions in Eq. (90), which initially did not agree with numerical studies of square lattice antiferromagnets. Wang *et al.* [11] argued that the bosonic and fermionic theories are equivalent, and that the confining phases of the SU(2) gauge theory lead to the same phase diagram as the bosonic partons. This equivalence is powerful, as it yields a toolbox of different approaches to study the square lattice spin liquid. In particular, upon including charge fluctuations, it is the fermionic parton theory that allows study of the confining instability of the square lattice spin liquid to d -wave superconductivity that we study in Sections 6 and 7.6.

In the bosonic parton approach, we introduce the Schwinger boson description [38], in terms of elementary $S = 1/2$ bosons. For the group SU(2) the complete set of $(2S + 1)$ states on site i are represented as follows

$$|S, m\rangle \equiv \frac{1}{\sqrt{(S+m)!(S-m)!}} (b_{i\uparrow}^\dagger)^{S+m} (b_{i\downarrow}^\dagger)^{S-m} |0\rangle, \quad (18)$$

where $m = -S, \dots, S$ is the z component of the spin ($2m$ is an integer). We have introduced two flavors of Schwinger bosons on each site, created by the canonical operator $b_{i\alpha}^\dagger$, with $\alpha = \uparrow, \downarrow$, and $|0\rangle$ is the vacuum with no Schwinger bosons. The total number of Schwinger bosons, n_b , is the same for all the states; therefore

$$b_{i\alpha}^\dagger b_{i\alpha} = n_b \quad (19)$$

with

$$n_b = 2S. \quad (20)$$

The above representation of the states is completely equivalent to the operator identity between the spin and Schwinger boson operators

$$S_i = \frac{1}{2} b_{i\alpha}^\dagger \boldsymbol{\sigma}_{\alpha\beta} b_{i\beta} \quad (21)$$

where $\ell = x, y, z$ and the $\boldsymbol{\sigma}$ are the usual 2×2 Pauli matrices.

The spin-states on two sites i, j can combine to form a singlet in a unique manner - the wavefunction of the (unnormalized) singlet state is particularly simple in the boson formulation:

$$(\varepsilon_{\alpha\beta} b_{i\alpha}^\dagger b_{j\beta}^\dagger)^{2S} |0\rangle \quad (22)$$

Also, using the constraint in Eq. (19), the following Fierz-type identity can be established

$$(\varepsilon_{\alpha\beta} b_{i\alpha}^\dagger b_{j\beta}^\dagger)(\varepsilon_{\gamma\delta} b_{i\gamma} b_{j\delta}) = -2S_i \cdot S_j + n_b^2/2 + \delta_{ij} n_b \quad (23)$$

where ε is the totally antisymmetric 2×2 tensor

$$\varepsilon = \begin{pmatrix} 0 & 1 \\ -1 & 0 \end{pmatrix}. \quad (24)$$

This implies that \mathcal{H}_J can be rewritten in the form (apart from an additive constant)

$$\mathcal{H}_J = -\frac{1}{2} \sum_{i < j} J_{ij} (\varepsilon_{\alpha\beta} b_{i\alpha}^\dagger b_{j\beta}^\dagger) (\varepsilon_{\gamma\delta} b_{i\gamma} b_{j\delta}) \quad (25)$$

This form makes it clear that \mathcal{H}_J counts the number of singlet bonds.

3.1 Mean-field theory

We begin by the coherent state path integral of \mathcal{H}_J in imaginary time τ at a temperature $\beta = 1/T$

$$\mathcal{Z}_J = \int \mathcal{D}\mathcal{Q} \mathcal{D}b \mathcal{D}\lambda \exp \left(- \int_0^\beta \mathcal{L}_J d\tau \right), \quad (26)$$

where

$$\begin{aligned} \mathcal{L}_J = & \sum_i \left[b_{i\alpha}^\dagger \left(\frac{d}{d\tau} + i\lambda_i \right) b_{i\alpha} - i\lambda_i n_b \right] \\ & + \sum_{\langle i,j \rangle} \left[\frac{J_{ij} |\mathcal{Q}_{i,j}|^2}{2} - \frac{J_{ij} \mathcal{Q}_{i,j}^*}{2} \varepsilon_{\alpha\beta} b_{i\alpha} b_{j\beta} + H.c. \right]. \end{aligned} \quad (27)$$

Here the λ_i fix the boson number of n_b at each site; τ -dependence of all fields is implicit; \mathcal{Q} was introduced by a Hubbard-Stratonovich decoupling of \mathcal{H}_J . In contrast to the decoupling in Eq. (3), we have now decoupled in the spin-singlet channel as we are interested in states that preserve spin rotation invariance.

This procedure is similar to that employed in deriving the Landau-Ginzburg theory of superconductivity from electron pairing, with the crucial difference that now the Lagrangian \mathcal{L}_J has a $U(1)$ gauge invariance associated with the local constraint in Eq. (19):

$$\begin{aligned} b_{i\alpha}^\dagger & \rightarrow b_{i\alpha}^\dagger \exp(i\rho_i(\tau)) \\ \mathcal{Q}_{i,j} & \rightarrow \mathcal{Q}_{i,j} \exp(-i\rho_i(\tau) - i\rho_j(\tau)) \\ \lambda_i & \rightarrow \lambda_i + \frac{\partial \rho_i}{\partial \tau}(\tau). \end{aligned} \quad (28)$$

The functional integral over \mathcal{L}_J faithfully represents the partition function, but does require gauge fixing. This gauge invariance leads to emergent gauge field degrees of freedom, as we will see below.

We begin with mean-field saddle point of \mathcal{Z}_J over the path integrals of \mathcal{Q} and λ . The saddle-point approximation is valid in the limit of a large number of spin flavors, but we do not explore this here. With the saddle point values $\mathcal{Q}_{ij} = \bar{\mathcal{Q}}_{ij}$, $i\lambda_i = \bar{\lambda}_i$ we obtain a mean-field Hamiltonian for the $b_{i\alpha}$

$$\begin{aligned} \mathcal{H}_{J,MF} = & \sum_{\langle i,j \rangle} \left(\frac{J_{ij} |\bar{\mathcal{Q}}_{ij}|^2}{2} - \frac{J_{ij} \bar{\mathcal{Q}}_{ij}^*}{2} \varepsilon_{\alpha\beta} b_i^\alpha b_j^\beta + H.c. \right) \\ & + \sum_i \bar{\lambda}_i (b_{i\alpha}^\dagger b_{i\alpha} - n_b). \end{aligned} \quad (29)$$

This Hamiltonian is quadratic in the boson operators and all its eigenvalues can be determined by a Bogoliubov transformation. This leads in general to an expression of the form

$$\mathcal{H}_{J,MF} = E_{J,MF}[\bar{\mathcal{Q}}, \bar{\lambda}] + \sum_{\mu} \omega_{\mu}[\bar{\mathcal{Q}}, \bar{\lambda}] \gamma_{\mu\alpha}^{\dagger} \gamma_{\mu\alpha} \quad (30)$$

The index μ extends over 1...number of sites in the system, $E_{J,MF}$ is the ground state energy and is a functional of $\bar{\mathcal{Q}}$, $\bar{\lambda}$, ω_{μ} is the eigenspectrum of excitation energies which is also a function of $\bar{\mathcal{Q}}$, $\bar{\lambda}$, and the γ_{μ}^{α} represent the bosonic eigenoperators. The excitation spectrum thus consists of non-interacting spinor bosons. The ground state is determined by minimizing $E_{J,MF}$ with respect to the $\bar{\mathcal{Q}}_{ij}$ subject to the constraints

$$\frac{\partial E_{MF}}{\partial \bar{\lambda}_i} = 0 \quad (31)$$

The saddle-point value of the $\bar{\mathcal{Q}}$ satisfies

$$\bar{\mathcal{Q}}_{ij} = \langle \epsilon_{\alpha\beta} b_{i\alpha} b_{j\beta} \rangle \quad (32)$$

Note that $\bar{\mathcal{Q}}_{ij} = -\bar{\mathcal{Q}}_{ji}$ indicating that $\bar{\mathcal{Q}}_{ij}$ is a directed field - an orientation has to be chosen on every link.

These saddle-point equations have been solved for the square and triangular lattices with nearest neighbor exchange J , and they lead to stable and translationally invariant solutions for $\bar{\lambda}_i$ and $\bar{\mathcal{Q}}_{ij}$. The only saddle-point quantity which does not have the full symmetry of the lattice is the orientation of the $\bar{\mathcal{Q}}_{ij}$. Note that although it appears that such a choice of orientation appears to break inversion or reflection symmetries, such symmetries are actually preserved: the $\bar{\mathcal{Q}}_{ij}$ are not gauge-invariant, and all gauge-invariant observables do preserve all symmetries of the underlying Hamiltonian. For the square lattice, we have $\bar{\lambda}_i = \bar{\lambda}$, $\bar{\mathcal{Q}}_{i,i+\hat{x}} = \bar{\mathcal{Q}}_{i,i+\hat{y}} = \bar{\mathcal{Q}}$. Similarly, on the triangular lattice we have $\bar{\mathcal{Q}}_{i,i+\hat{e}_p} = \bar{\mathcal{Q}}$ for $p = 1, 2, 3$, where the unit vectors

$$\begin{aligned} \hat{e}_1 &= (1/2, \sqrt{3}/2) \\ \hat{e}_2 &= (1/2, -\sqrt{3}/2) \\ \hat{e}_3 &= (-1, 0) \end{aligned} \quad (33)$$

point between nearest neighbor sites of the triangular lattice. We sketch the orientation of the $\bar{\mathcal{Q}}_{ij}$ on the triangular lattice in Fig. 8.

We can also compute the dispersion $\omega_{\mathbf{k}}$ of the $\gamma_{\mathbf{k}}$ excitations. These are fractionalized bosonic particles which carry spin $S = 1/2$ and charge 0, named ‘spinons’. They should be contrasted from the spin-wave excitations of ordered magnets, which carry integer spin and charge 0. Their dispersion on the square lattice is

$$\omega_{\mathbf{k}} = (\bar{\lambda}^2 - J^2 \bar{\mathcal{Q}}^2 (\sin k_x + \sin k_y)^2)^{1/2} \quad (34)$$

while that on the triangular lattice is [3]

$$\omega_{\mathbf{k}} = (\bar{\lambda}^2 - J^2 \bar{\mathcal{Q}}^2 (\sin k_1 + \sin k_2 + \sin k_3)^2)^{1/2} \quad (35)$$

with $k_p = \mathbf{k} \cdot \hat{e}_p$. These are the spinons and the spinon dispersion on the triangular lattice is plotted in Fig. 9, and that on the square lattice in Fig. 10.

Notice that the spinons are gapped, and their minimum gaps are at two degenerate points in the Brillouin zone for both lattices. For the square lattice, the minima are at $\mathbf{k} = \pm(\pi/2, \pi/2)$ with an energy gap of $(\bar{\lambda}^2 - 4J^2 \bar{\mathcal{Q}}^2)^{1/2}$. For the triangular lattice they are at $\mathbf{k} = \pm(4\pi/3, 0)$

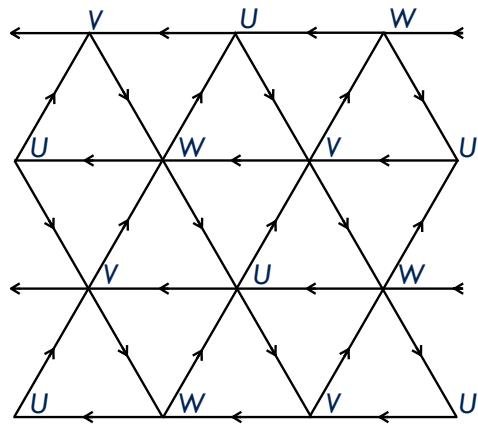


Figure 8: Orientation of the nearest neighbor \bar{Q}_{ij} on the triangular lattice. Also shown are the labels of the 3 sublattices.

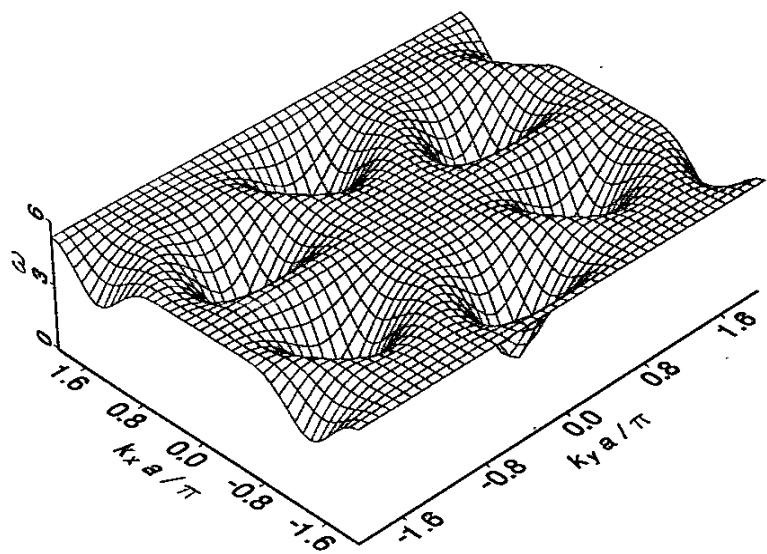


Figure 9: Spinon dispersion on the triangular lattice [3]. Reprinted with permission from APS.

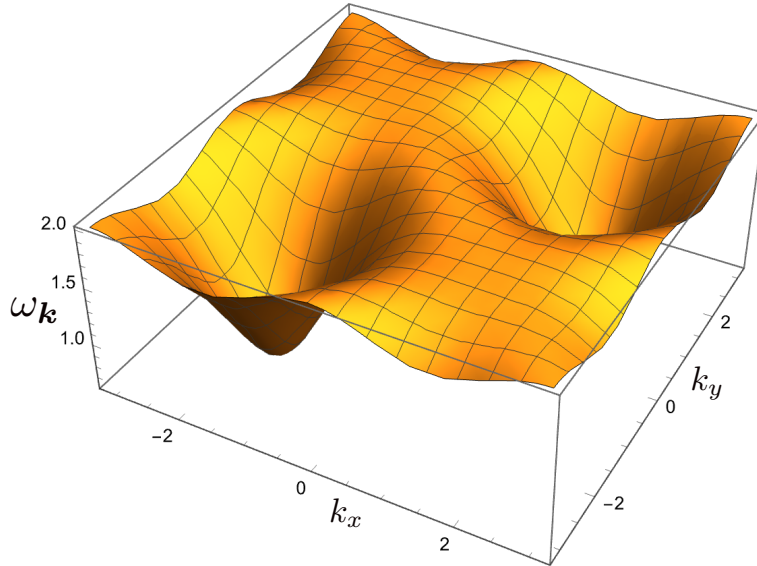


Figure 10: Dispersion of bosonic spinons in a square lattice spin liquid, from Eq. (34).

(and at wavevectors separated from these by reciprocal lattice vectors). So there are a total of 4 spinon excitations in both cases: 2 associated with the spin degeneracy of $S_z = \pm 1/2$, and 2 associated with the degeneracy in the Brillouin zone spectrum.

Next, we turn to spin-singlet excitations, *i.e.* understanding the nature of the spectrum of the \mathcal{Q}_{ij} and λ_i fluctuations about the saddle point described above. At the outset, it appears that we can view such fluctuations as composites of 2-spinon excitations, as both \mathcal{Q}_{ij} and λ_i couple to spinon pair operators, and so conclude that such excitations should not be viewed as the ‘elementary’ excitations of the quantum state found so far. Furthermore, the saddle-point has not broken any global symmetries of the Hamiltonian, and so it would appear that no such composite excitations has any reason to be low energy without fine-tuning.

However, it does turn out that there are separate elementary excitations in the singlet sector, and these arise from two distinct causes: (i) the gauge invariance in (28) leads to a gapless “photon” excitation; (ii) there are topologically non-trivial configurations of \mathcal{Q}_{ij} which lead to excitations which appear as new saddle points. Excitations in the class (i) arise in the square lattice case, while those in class (ii) appear on the triangular lattice, and these will be considered separately in the following subsections.

3.2 Gauge excitations

The gauge transformations in (28) act on the phases of the \mathcal{Q}_{ij} , and so it is appropriate to just focus on the fluctuations of the phases of the \mathcal{Q}_{ij} whose amplitudes are non-zero at the saddle-point.

3.2.1 Square lattice

We define

$$\begin{aligned} \mathcal{Q}_{i,i+\hat{x}} &= \bar{\mathcal{Q}} \exp(i\Theta_{ix}) \\ \mathcal{Q}_{i,i+\hat{y}} &= \bar{\mathcal{Q}} \exp(i\Theta_{iy}) \end{aligned} \quad (36)$$

Then, the gauge transformations in (28) can be written as

$$\begin{aligned}\Theta_{ix}(\tau) &\rightarrow \Theta_{ix}(\tau) - \rho_i(\tau) - \rho_{i+x}(\tau) \\ \Theta_{iy}(\tau) &\rightarrow \Theta_{iy}(\tau) - \rho_i(\tau) - \rho_{i+y}(\tau) \\ \lambda_i &\rightarrow \lambda_i + \frac{\partial \rho_i}{\partial \tau}(\tau).\end{aligned}\quad (37)$$

The question before us is whether (28) imposes on us the presence of a gapless photon in the low energy and long-wavelength limit. The answer is affirmative, and the needed result is obtained by parameterizing such fluctuations as follows

$$\begin{aligned}\Theta_{ix}(\tau) &= \eta_i a_x(\mathbf{r}, \tau) \\ \Theta_{iy}(\tau) &= \eta_i a_y(\mathbf{r}, \tau) \\ \lambda_i &= -i\bar{\lambda} - \eta_i a_\tau(\mathbf{r}, \tau)\end{aligned}\quad (38)$$

where the a_μ are assumed to be smooth functions of spacetime parameterized by the continuum spatial co-ordinate \mathbf{r} , and imaginary time τ ; the factor η_i , defined in Eq. (11), has opposite signs on any pair of nearest-neighbor sites. Then, taking the continuum limit of (37) with $\rho_i(\tau) = \eta_i \rho(r, \tau)$, we deduce from (38) that

$$\begin{aligned}a_x &\rightarrow a_x - \partial_x \rho \\ a_y &\rightarrow a_y - \partial_y \rho \\ a_\tau &\rightarrow a_\tau - \partial_\tau \rho\end{aligned}\quad (39)$$

So we reach the very important conclusion that a_μ transforms just like a continuum U(1) gauge field! Note that the factor η_i in this U(1) gauge transformation implies from (28) that the spinons b_i carry opposite gauge charges on the two sublattices.

As in traditional field-theoretic analyses, (39) imposes the requirement that the long-wavelength action of the a_μ fluctuations must have the form

$$\mathcal{S}_b = \int d^3x \frac{1}{2K'} (\epsilon_{\mu\nu\lambda} \partial_\nu a_\lambda)^2, \quad (40)$$

and this describes a gapless a_μ photon excitation, with a suitable velocity of ‘light’. So, on the square lattice, the spectrum of spin-singlet states includes a linearly-dispersing photon mode. Such a state is a U(1) spin liquid. Actually, the gapless photon of this U(1) spin liquid is ultimately not stable because of monopole tunneling events; this involves a long and interesting story [5, 6, 39, 40] which we will discuss briefly in Section 3.5. For now, in the following subsection, we will consider the case of the triangular lattice, where, the U(1) photon is gapped by the Higgs mechanism to yield a \mathbb{Z}_2 spin liquid.

3.2.2 Triangular lattice

Now we have to consider 3 separate values of \mathcal{Q}_{ij} per site, and so we replace (36) by

$$\mathcal{Q}_{i,i+\hat{e}_p} = \bar{\mathcal{Q}} \exp(i\Theta_{p,i}) \quad (41)$$

where $p = 1, 2, 3$, the vectors \hat{e}_p were defined (33), $\bar{\mathcal{Q}}$ is the mean-field value, and Θ_p is a real phase. The effective action for the $\Theta_{p,i}$ must be invariant under

$$\Theta_{p,i} \rightarrow \Theta_{p,i} - \rho_i - \rho_{i+\hat{e}_p}. \quad (42)$$

Upon performing a Fourier transform, with the link variables Θ_p placed on the center of the links, the gauge invariance takes the form

$$\Theta_p(\mathbf{k}) \rightarrow \Theta_p(\mathbf{k}) - 2\rho(\mathbf{k}) \cos(k_p/2) \quad (43)$$

The momentum \mathbf{k} takes values in the first Brillouin zone of the triangular lattice. This invariance implies that the effective action for the Θ_p can only be a function of the following gauge-invariant combinations:

$$I_{pq}(\mathbf{k}) = 2 \cos(k_q/2) \Theta_p(\mathbf{k}) - 2 \cos(k_p/2) \Theta_q(\mathbf{k}) \quad (44)$$

We now wish to take the continuum limit at points in the Brillouin zone where the action involves only gradients of the Θ_p fields and thus has the possibility of gapless excitations. The same analysis could have been applied to the square lattice, in which case there is only one invariant I_{xy} . In this case, we choose $\mathbf{k} = \mathbf{g} + \mathbf{q}$, with $\mathbf{g} = (\pi, \pi)$ (this corresponds to the choice of η_i above) and \mathbf{q} small; then $I_{xy} = q_x \Theta_y - q_y \Theta_x$ which is clearly the U(1) flux invariant under (39).

The situation is more complex for the case of the triangular lattice [3]. Now there are 3 independent I_{pq} invariants, and it is not difficult to see that only two of the three values of $\cos(k_p/2)$ can vanish at any point of the Brillouin zone. One such point is the wavevector

$$\mathbf{g} = \frac{2\pi}{\sqrt{3}a} (0, 1) \quad (45)$$

where

$$\begin{aligned} \mathbf{g} \cdot \hat{e}_1 &= \pi \\ \mathbf{g} \cdot \hat{e}_2 &= -\pi \\ \mathbf{g} \cdot \hat{e}_3 &= 0. \end{aligned} \quad (46)$$

Taking the continuum limit with the fields varying with momenta with close to \mathbf{g} we find that the I_{pq} depend only upon gradients of Θ_1 and Θ_2 . It is also helpful to parametrize the Θ_p in the following suggestive manner (analogous to (38))

$$\begin{aligned} \Theta_1(\mathbf{r}) &= ia_1(\mathbf{r})e^{i\mathbf{g} \cdot \mathbf{r}} \\ \Theta_2(\mathbf{r}) &= -ia_2(\mathbf{r})e^{i\mathbf{g} \cdot \mathbf{r}} \\ \Theta_3(\mathbf{r}) &= H(\mathbf{r})e^{i\mathbf{g} \cdot \mathbf{r}} \end{aligned} \quad (47)$$

It can be verified that the condition for the reality of Θ_p is equivalent to demanding that a_1, a_2, H be real. We will now take the continuum limit with a_1, a_2, H varying slowly on the scale of the lattice spacing. It is then not difficult to show that the invariants I_{pq} then reduce to (after a Fourier transformation):

$$\begin{aligned} I_{12} &= \partial_2 a_1 - \partial_1 a_2 \\ I_{31} &= \partial_1 H - 2a_1 \\ I_{32} &= \partial_2 H - 2a_2, \end{aligned} \quad (48)$$

where ∂_i is the spatial gradient along the direction \hat{e}_i . Thus the a_1, a_2 are the components of a U(1) gauge field, with the components are taken along an ‘oblique’ co-ordinate system defined by the axes \hat{e}_1, \hat{e}_2 ; this is just as in the square lattice. However, in addition to I_{12} , we also have the invariants I_{31} and I_{32} in the triangular lattice; we observe that this involves the field H

which transforms like the phase of charge ± 2 Higgs field under the $U(1)$ gauge invariance. So the fluctuations of an isotropic triangular lattice will be characterized by an action of the form

$$\mathcal{S}_b = \int d^3x \frac{1}{2K'} [I_{12}^2 + I_{31}^2 + I_{32}^2], \quad (49)$$

which replaces (40). This is the action expected in the *Higgs phase* of a $U(1)$ gauge theory. The Higgs condensate gaps out the $U(1)$ photon, and so there are no gapless singlet excitations on the triangular lattice. This is a necessary condition for mapping the present state onto a \mathbb{Z}_2 spin liquid (the reason for this nomenclature will become clearer in the following subsection).

The presentation so far of the gauge fluctuations described by a charge ± 2 Higgs field coupled to a $U(1)$ gauge field would be appropriate for an anisotropic triangular lattice in which the couplings along the \hat{e}_3 direction are different from those along \hat{e}_1 and \hat{e}_2 . For an isotropic triangular lattice, all three directions must be treated equivalently, and then there is no simple way to take the continuum limit in the gauge sector: we have to work with the action in (49), but with the invariants specified as in (44). Such an action does not have a gapless photon anywhere in the Brillouin zone, and all gauge excitations remain gapped. There are other choices for the wavevector \mathbf{g} in (45) at which the other pairs of values of $\cos(k_p/2)$ vanish; these are the points

$$\frac{2\pi}{\sqrt{3}} \left(\frac{\sqrt{3}}{2}, -\frac{1}{2} \right) \quad , \quad \frac{2\pi}{\sqrt{3}} \left(\frac{-\sqrt{3}}{2}, -\frac{1}{2} \right), \quad (50)$$

which are related to the analysis above by the rotational symmetry of the triangular lattice.

3.3 Topological excitations on the triangular lattice

The analysis in Section 3.2 described small fluctuations in the phases of the Q_{ij} about their saddle-point values \bar{Q} . On the triangular lattice, we found that such fluctuations led only to gapped excitations, which at higher energies become part of the two-spinon continuum.

Now we consider excitations which involve large deviations from the spatially uniform saddle point values, and which turn out to be topologically protected. These excitations are closely connected to the vortices in charged superfluids. Consider a scalar field Ψ with charge q coupled to the electromagnetic $U(1)$ gauge field \mathbf{A} . This has stable vortex-like saddle points with flux $n\Phi_0$, with $\Phi_0 = hc/q$, for all integer n . We have seen above that on the triangular lattice, the Schwinger boson state has fluctuations described by a charge 2 Higgs field H coupled to a $U(1)$ gauge field a_μ . In this case, we are normalizing the gauge field so that $\hbar c \Rightarrow 1$, and so we can expect vortex solutions with a_μ flux $n(2\pi)/2$, for all integer n . However, this is not quite correct. A crucial difference between the present theory and the electromagnetic gauge field is that the a_μ gauge field is ‘compact’: this means that a gauge field $a_{x,y}$ is identical to $a_{x,y} + 2\pi$, and tunneling events which change the total flux by 2π are allowed (these are ‘monopoles’, which will be considered further in Section 3.5). This means that all vortex solutions with even n are identical to each other, as are those with odd n . The $n = 0$ case corresponds to no vortex at all, and so there is only a single non-trivial vortex with $n = 1$ and flux π . This is the sought-after *vison*. Note that because fluxes π and $-\pi$ are identical, the vison saddle point preserves time-reversal symmetry. Similar excitations appear in a \mathbb{Z}_2 gauge theory, and hence the \mathbb{Z}_2 spin liquid nomenclature.

In this section, we will obtain the vison saddle point solution by working with a lattice effective action: this is essential to account for the influence of the monopoles. So we look for spatially non-uniform solutions of the saddle-point equations (31) and (32). In general, solving such equations is a demanding numerical task, and so we will be satisfied with a simplified analysis which is valid when the spin gap is large. In the large spin gap limit, we can

integrate out the Schwinger bosons, and write the energy as a local functional of the \mathcal{Q}_{ij} . This functional is strongly constrained by the gauge transformations in (28): for time-independent \mathcal{Q}_{ij} , this functional takes the form

$$E[\{\mathcal{Q}_{ij}\}] = - \sum_{i < j} \left(\alpha |\mathcal{Q}_{ij}|^2 + \frac{\beta}{2} |\mathcal{Q}_{ij}|^4 \right) - K \sum_{\text{even loops}} \mathcal{Q}_{ij} \mathcal{Q}_{jk}^* \dots \mathcal{Q}_{li}^* \quad (51)$$

Here α , β , and K are coupling constants determined by the parameters in the Hamiltonian of the antiferromagnet. We have shown them to be site-independent, because we have only displayed terms in which all links/loops are equivalent; they can depend upon links/loops for longer range couplings provided the full lattice symmetry is preserved.

We can now search for saddle points of the energy functional in (51). Far from the center of the vison, we have $|\mathcal{Q}_{ij}^v| = \bar{\mathcal{Q}}$, so that the energy differs from the ground state energy only by a finite amount. Closer to the center there are differences in the magnitudes. However, the key difference is in the signs of the link variables, as illustrated in Fig. 11: there is a ‘branch-cut’ emerging from the vison core along which $\text{sgn}(\mathcal{Q}_{ij}^v) = -\text{sgn}(\bar{\mathcal{Q}}_{ij})$. The results of a numerical minimization [41] of $E[\{\mathcal{Q}_{ij}\}]$ on the triangular lattice are shown in Fig. 11. The magnitudes of \mathcal{Q}_{ij}^v are suppressed close to the vison, and converge to $\bar{\mathcal{Q}}_{ij}$ as we move

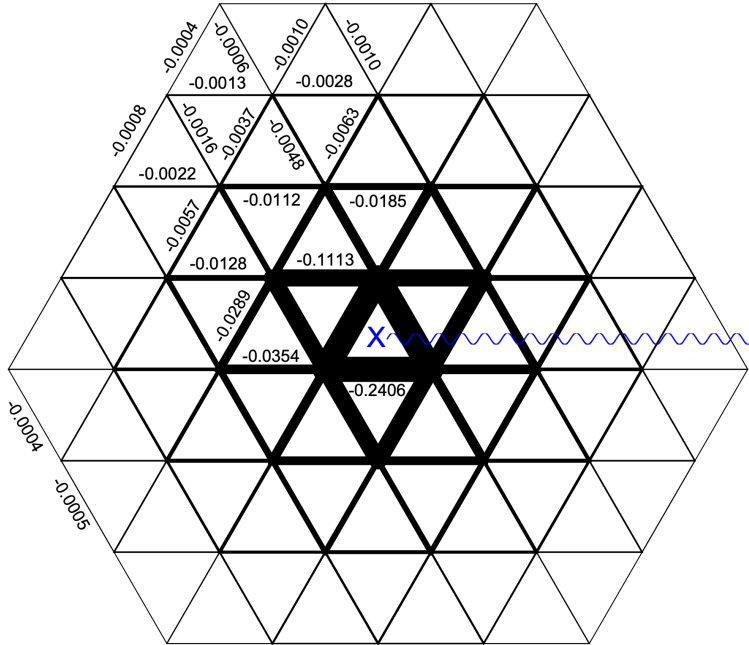


Figure 11: A vison on the triangular lattice [41]. The center of the vison is marked by the X. The wavy line is the ‘branch-cut’ where we have $\text{sgn}(\mathcal{Q}_{ij}^v) = -\text{sgn}(\bar{\mathcal{Q}}_{ij})$ only on the links crossed by the line. Plotted is the minimization result of $E[\{\bar{\mathcal{Q}}_{ij}\}]$ with $\alpha = 1, \beta = -2, K = 0.5$. Minimization is done with the cluster embedded in a vison-free lattice with all nearest neighbor links equal to $\bar{\mathcal{Q}}_{ij}$. The numbers are $(\bar{\mathcal{Q}}_{ij} - \mathcal{Q}_{ij}^v)$ and the thickness of the links are proportional to $(\mathcal{Q}_{ij}^v - \bar{\mathcal{Q}}_{ij})^{1/2}$. Reprinted with permission from APS.

away from the vison (modulo the sign change associated with the branch cut), analogous to those in Abrikosov vortices. Despite the branch-cut breaking the 3-fold rotation symmetry, the gauge-invariant fluxes of \mathcal{Q}_{ij}^v preserve the rotation symmetry.

So we have found a stable real-vortex solution which preserves time-reversal, and has a finite excitation energy. We have also anticipated that this vortex will be identified with the vison particle of the \mathbb{Z}_2 spin liquid: more evidence for this identification will appear in Sections 3.4.2 and 3.4.3.

3.4 Dynamics of excitations on the triangular lattice

For the case of the triangular lattice, Sections 3.1 and 3.3 have identified two types of elementary excitations: bosonic spinons with a 2-fold spin and a 2-fold lattice degeneracy, and a topological excitation which we have anticipated will become with vison particle of a \mathbb{Z}_2 spin liquid. We will now describe the dynamics of the interactions between these excitations, and indeed verify that they reproduce the general structure associated with the \mathbb{Z}_2 spin liquid.

A similar analysis can also be carried for the U(1) spin liquid on the square lattice. However, defer consideration of this case to Section 3.5.

3.4.1 Motion of spinons

The general structure of the theory controlling the low energy spectrum becomes clearer upon taking a suitable continuum limit of the Lagrangian in (27), while replacing $\mathcal{Q}_{ij} = \bar{\mathcal{Q}}_{ij}$ and $i\lambda_i = \bar{\lambda}$. We take the continuum limit after separating 3 sites, u, v, w , in each unit cell (see Fig. 8). We write the boson operators on these sites as $b_u^\alpha = u_\alpha, b_v^\alpha = v_\alpha$ etc. Then to the needed order in spatial gradients, the Lagrangian density becomes [42]

$$\begin{aligned} \mathcal{L} = & u_\alpha^* \frac{\partial u_\alpha}{\partial \tau} + v_\alpha^* \frac{\partial v_\alpha}{\partial \tau} + w_\alpha^* \frac{\partial w_\alpha}{\partial \tau} + \bar{\lambda} (|u_\alpha|^2 + |v_\alpha|^2 + |w_\alpha|^2) \\ & - \frac{3J\bar{\mathcal{Q}}}{2} \mathcal{J}_{\alpha\beta} (u_\alpha v_\beta + v_\alpha w_\beta + w_\alpha u_\beta) + \text{c.c.} \\ & + \frac{3J\bar{\mathcal{Q}}}{8} \mathcal{J}_{\alpha\beta} (\nabla u_\alpha \cdot \nabla v_\beta + \nabla v_\alpha \cdot \nabla w_\beta + \nabla w_\alpha \cdot \nabla u_\beta) + \text{c.c.} \end{aligned} \quad (52)$$

We now perform a unitary transformation to new variables $x_\alpha, y_\alpha, z_\alpha$. These are chosen to diagonalize only the non-gradient terms in \mathcal{L} .

$$\begin{pmatrix} u_\alpha \\ v_\alpha \\ w_\alpha \end{pmatrix} = \frac{z_\alpha}{\sqrt{6}} \begin{pmatrix} 1 \\ \zeta \\ \zeta^2 \end{pmatrix} + \mathcal{J}_{\alpha\beta} \frac{z_\beta^*}{\sqrt{6}} \begin{pmatrix} -i \\ -i\zeta^2 \\ -i\zeta \end{pmatrix} + \frac{y_\alpha}{\sqrt{6}} \begin{pmatrix} 1 \\ \zeta \\ \zeta^2 \end{pmatrix} + \mathcal{J}_{\alpha\beta} \frac{y_\beta^*}{\sqrt{6}} \begin{pmatrix} i \\ i\zeta^2 \\ i\zeta \end{pmatrix} + \frac{x_\alpha}{\sqrt{3}} \begin{pmatrix} 1 \\ 1 \\ 1 \end{pmatrix}. \quad (53)$$

where $\zeta \equiv e^{2\pi i/3}$. The tensor structure above makes it clear that this transformation is rotationally invariant, and that $x_\alpha, y_\alpha, z_\alpha$ transform as spinors under SU(2) spin rotations. Inserting Eq. (53) into \mathcal{L} we find

$$\begin{aligned} \mathcal{L} = & x_\alpha^* \frac{\partial x_\alpha}{\partial \tau} + y_\alpha^* \frac{\partial y_\alpha}{\partial \tau} + z_\alpha^* \frac{\partial z_\alpha}{\partial \tau} + (\bar{\lambda} - 3\sqrt{3}J\bar{\mathcal{Q}}/2)|z_\alpha|^2 \\ & + (\bar{\lambda} + 3\sqrt{3}J\bar{\mathcal{Q}}/2)|y_\alpha|^2 + \bar{\lambda}|x_\alpha|^2 + \frac{3J\bar{\mathcal{Q}}\sqrt{3}}{8} (|\partial_x z_\alpha|^2 + |\partial_y z_\alpha|^2) + \dots \end{aligned} \quad (54)$$

The ellipses indicate omitted terms involving spatial gradients in the x_α and y_α which we will not keep track of. This is because the fields y_α and x_α are massive relative to z_α , and so can

be integrated out. This yields the effective Lagrangian

$$\mathcal{L}_z = \frac{1}{(\bar{\lambda} + 3\sqrt{3}J\bar{Q}/2)} |\partial_\tau z_\alpha|^2 + \frac{3J\bar{Q}\sqrt{3}}{8} (|\partial_x z_\alpha|^2 + |\partial_y z_\alpha|^2) + (\bar{\lambda} - 3\sqrt{3}J\bar{Q}/2) |z_\alpha|^2 + \dots \quad (55)$$

Note that the omitted spatial gradient terms in x_α, y_α do contribute a correction to the spatial gradient term in (55), and we have not accounted for this.

So we reach the important conclusion that the spinons are described by a relativistic complex scalar field z_α . Counting the two values of α , and the particle and anti-pariticle excitations, we have a total of 4 spinons, as expected.

Next, we consider the higher order terms in (55), which will arise from including the fluctuations of the gapped fields Q and λ . Rather than computing these from the microscopic Lagrangian, it is more efficient to deduce their structure from symmetry considerations. The representation in (53), and the connection of the $u_\alpha, v_\alpha, w_\alpha$ to the lattice degrees of freedom, allow us to deduce the following symmetry transformations of the $x_\alpha, y_\alpha, z_\alpha$:

- Under a global spin rotation by the SU(2) matrix $g_{\alpha\beta}$, we have $z_\alpha \rightarrow g_{\alpha\beta} z_\beta$, and similarly for x_α , and y_α .
- Under a 120° lattice rotation, we have $u_\alpha \rightarrow v_\alpha, v_\alpha \rightarrow w_\alpha, w_\alpha \rightarrow u_\alpha$. From (53), we see that this symmetry is realized by

$$z_\alpha \rightarrow \zeta z_\alpha, \quad y_\alpha \rightarrow \zeta y_\alpha, \quad x_\alpha \rightarrow x_\alpha. \quad (56)$$

Note that this is distinct from the SU(2) rotation because $\det(\zeta) \neq 1$.

- Finally, there is a crucial \mathbb{Z}_2 gauge symmetry, which is the remnant of the U(1) gauge symmetry in Eq. (28). This is the transformation

$$z_{i\alpha} \rightarrow \mu_i z_{i\alpha} \quad (57)$$

where $\mu_i = \pm 1$ has an arbitrary site-dependence.

It is easy to verify that Eq. (54) is invariant under all the symmetry operations above. These symmetry operators make it clear that the only allowed quartic term for the Heisenberg Hamiltonian is $(\sum_\alpha |z_\alpha|^2)^2$: this quartic term added to \mathcal{L}_z yields a theory with O(4) symmetry, corresponding to rotations between the 4 real fields that can be extracted from the 2 complex field z_α . We also observe from (55) that the z_α field will condense when

$$r = (\bar{\lambda} - 3\sqrt{3}J\bar{Q}/2) \quad (58)$$

becomes negative as κ is varied across κ_c . This condensation breaks the spin rotation symmetry, and leads to a quantum phase transition to a phase with coplanar antiferromagnetic long-range order, as illustrated in Fig. 12. This order parameter of this coplanar antiferromagnet is related to \mathbb{Z}_2 gauge-invariant bilinears of z_α by

$$S_i \propto \text{Im} [\exp(i\mathbf{Q} \cdot \mathbf{r}) \epsilon_{\alpha\gamma} z_\gamma \sigma_{\alpha\beta} z_\beta], \quad (59)$$

where the wavevector $\mathbf{Q} = (4\pi/a)(1/3, 1/\sqrt{3})$.

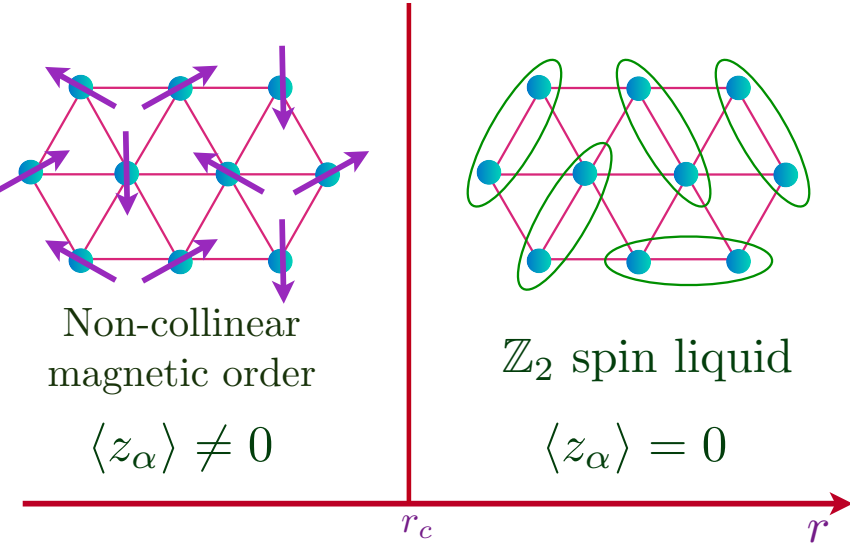


Figure 12: Magnetic ordering transition driven by tuning r in (58). Fractionalized anyonic excitations are present only for $r > r_c$, and so there is a ‘confinement’ transition at $r = r_c$. The critical theory is expressed in terms of bosonic spinons z_α , and is an example of deconfined critical theory. There is evidence for such a transition in KYbSe_2 [43, 44].

3.4.2 Motion of visons

Let us now consider the motion of the vison elementary excitation, which we illustrated earlier in Fig. 13. The vison is located at the center of a triangle, and so can tunnel between neighboring triangular cells. We are interested here in any possible Berry phases the vison could pick up upon tunneling around a closed path.

In Section 3.3, we characterized the vison by the saddle-point configuration \mathcal{Q}_{ij}^v of the bond variables in the Hamiltonian (29). By diagonalizing this Hamiltonian [3, 41], we can show that the wavefunction of the vison can be written as

$$|\Psi^v\rangle = \mathcal{P} \exp \left(\sum_{i < j} f_{ij}^v \mathcal{J}_{\alpha\beta} b_{i\alpha}^\dagger b_{j\beta}^\dagger \right) |0\rangle, \quad (60)$$

where $|0\rangle$ is the boson vacuum, \mathcal{P} is a projection operator which selects only states which obey (19), and the boson pair wavefunction $f_{ij}^v = -f_{ji}^v$ is determined from (29) by a Bogoliubov transformation.

Let us now consider the motion of a single vison [41]. The gauge-invariant Berry phases are those associated with a periodic motion, and so let us consider the motion of a vison along a general closed loop \mathcal{C} . We illustrated the simple case where \mathcal{C} encloses a single site of the triangular lattice in Fig. 13. The wavy lines indicate $\text{sgn}(\mathcal{Q}_{ij}^v) = -\text{sgn}(\bar{\mathcal{Q}}_{ij})$, as in Fig. 11. The last state is gauge-equivalent to the first state, after the gauge transformation $b_i^\alpha \rightarrow -b_i^\alpha$ only for the site i marked by the filled circle. As long as the vison wavefunction can be chosen to be purely real, it is clear that no Berry phase is accumulated from the time-evolution of the wavefunction as the vison tunnels around the path \mathcal{C} . However, there can still be a non-zero Berry phase because a gauge-transformation is required to map the final state to the initial state. The analysis in Fig. 13 shows that the required gauge transformation is

$$\begin{aligned} b_i^\alpha &\rightarrow -b_i^\alpha, & \text{for } i \text{ inside } \mathcal{C} \\ b_i^\alpha &\rightarrow b_i^\alpha, & \text{for } i \text{ outside } \mathcal{C}. \end{aligned} \quad (61)$$

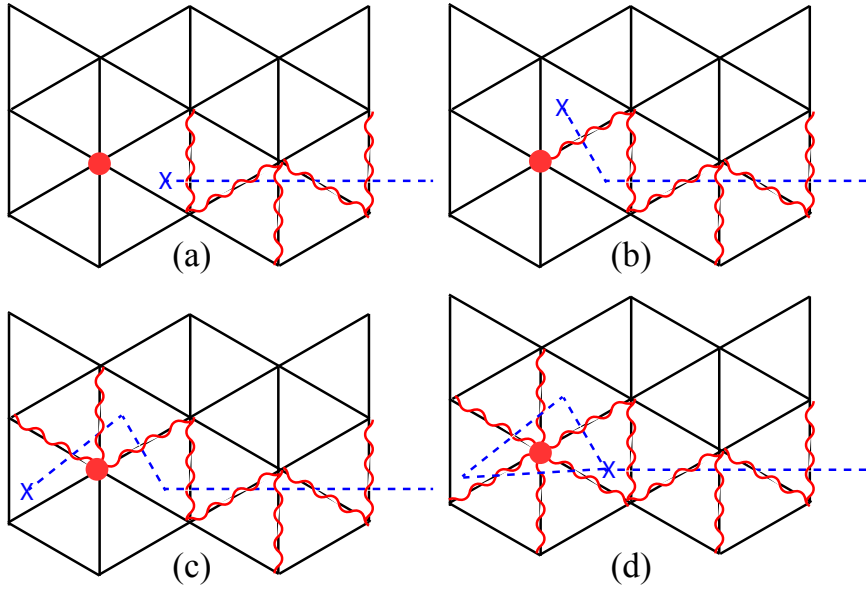


Figure 13: Adiabatic motion of a vison (denoted by the X) around a single site of the triangular lattice (denoted by the filled circle). The wavy line is the vison branch cut, as in Fig. 11. The initial state is in (a), and the final state is in (d), and these differ by a gauge transformation under which $b_{i\alpha} \rightarrow -b_{i\alpha}$ only on the filled circle site.

By Eq. (19), each site has $n_b = 2S$ bosons, and so the total Berry phase accumulated by $|\Psi^v\rangle$ is

$$\pi n_b \times (\text{number of sites enclosed by } \mathcal{C}). \quad (62)$$

For the important case of $S = 1/2$, the vison experiences a flux of π for every site of the triangular lattice. This phase factor of π is related to an ‘anomaly’ associated with the global U(1) boson number symmetry, and translational symmetry [45, 46], and was first noted in Refs. [47, 48] as a feature of \mathbb{Z}_2 spin liquids with half-integer spin. In particular, this result implies the RVB state is an *odd* \mathbb{Z}_2 spin liquid.

A notable feature of (62) is that the quantized integer value of $n_b = 2S$ is important. Memory of this quantization was lost in the mean field theory of Section 3.1, which was sensible also for non-integer values of n_b . So inclusion of the vison fluctuations restores the quantization of spin. A more complete theory for the vison fluctuations appears below in Section 3.4.4.

3.4.3 Semions and fermions

Proceeding the identification of the present Schwinger boson spin liquid with the \mathbb{Z}_2 spin liquid, we need to establish that the spinons and visons are mutual semions. This is immediately apparent from a glance at Figs. 11 and 14.

The Q_{ij}^v transport the spinons from site to site, and for spinon encircling a vison in a large circuit, the only difference between the cases with and without the vison is the branch cut. This branch cut yields an additional phase of π in the vison amplitude, and provides the needed phase for mutual semion statistics [1, 2].

We can now identify the e , ϵ , and m anyons, in the abstract topological characterization of the \mathbb{Z}_2 spin liquid obtained from the toric code [4]. The e anyon is the the Schwinger boson itself, b_α . This is mutual semion with respect to the vison, and so we identify the vison with the m particle. Finally, the ϵ anyon is obtained by the fusion $\epsilon = e \times m$, and so the ϵ

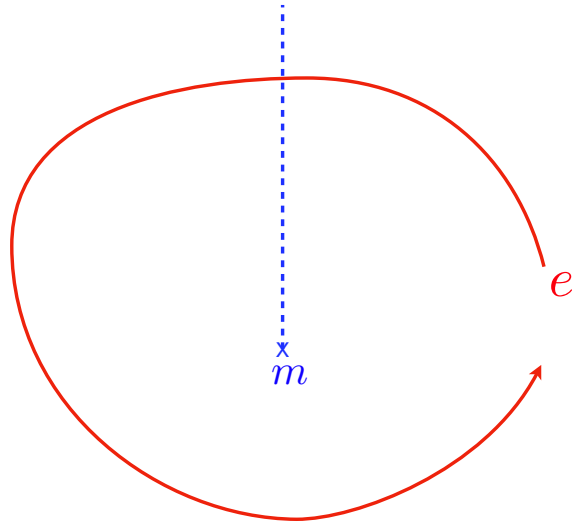


Figure 14: Mutual statistics of e and m particles. This process leads to a Berry phase of -1 , when the e particle crosses the branch cut of the m particle.

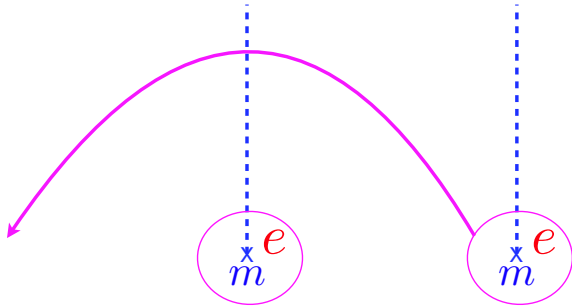


Figure 15: Two e particles undergoing an exchange: after traversing the path shown, a translation returns the e particles to the original state. Each e particle is a bound state of a vison (the m particle) and the s_α bosonic spinon (the e particle). This process leads to a Berry phase of -1 , when the moving e particle crosses the branch cut of the stationary m particle.

anyon is a bound state of e and m . The e anyon is a *fermion* as can be deduced by computing the Berry phase associated with exchanging one bound state of e and m with another bound state, as shown in Fig. 15. (Note that this ‘long-distance’ Berry phase is multiplied by the ‘short-distance’ vison motion phases discussed in Section 3.4.2.) It is quite remarkable that a microscopic theory of bosonic spins S , expressed in terms of fractionalized bosons s_α , yields an excitation which is a fermion: this is one indication of the presence of long-range entanglement and topological order.

An alternative formulation of the \mathbb{Z}_2 spin liquid on the triangular lattice proceeds by expressing the spins S in terms of Schwinger fermions f_α . For the \mathbb{Z}_2 spin liquid, the f_α spinons would become the e particles, and the bosonic e would be the bound state of the f_α and the m vison. So ultimately, independent of whether we choose to fractionalize the S spins in terms of bosonic or fermionic partons, we obtain the same characterization of the observable excitations in the resulting \mathbb{Z}_2 spin liquid. This identity also extends to the symmetry transformations of the anyons, as has been shown in some detail on the triangular [49], square [50, 51] and

kagome [52] lattices.

3.4.4 Complete \mathbb{Z}_2 gauge theory of spinons and visons

We now combine the above results for the dynamics of spinons and visons to write down a \mathbb{Z}_2 gauge theory for the triangular lattice quantum antiferromagnet which couples the $z_{i\alpha}$ to a dynamic \mathbb{Z}_2 gauge field Z_{ij} on the links of a 3-dimensional hexagonal lattice (*i.e.* stacked triangular lattices) [53, 54]:

$$\begin{aligned} \mathcal{Z}_{\mathbb{Z}_2} &= \sum_{Z_{ij}=\pm 1} \prod_i \int dz_{i\alpha} \delta \left(\sum_{\alpha} |z_{i\alpha}|^2 - 1 \right) \left\{ \prod_i Z_{i,i+\hat{\tau}} \right\}^{2S} \exp(-\mathcal{S}_{\mathbb{Z}_2}[z_{\alpha}, Z]) \\ \mathcal{S}_{\mathbb{Z}_2}[z_{\alpha}, Z] &= -J_2 \sum_{\langle ij \rangle} Z_{ij} (z_{i\alpha}^* z_{j\alpha} + \text{c.c.}) - K \sum_{\Delta, \square} \prod_{ij \in \Delta, \square} Z_{ij}. \end{aligned} \quad (63)$$

Here the $z_{i\alpha}$ reside on the sites i of the hexagonal lattice, and the K term acts on the triangular plaquettes of the spatial plane, and the rectangular plaquettes along the temporal direction. Similarly, for quantum antiferromagnets on other two-dimensional lattices, we would work with a three dimensional lattice obtained by stacking the two-dimensional lattice. The Z_{ij} descend from the \mathcal{Q}_{ij} by fixing their magnitudes and allowing their signs to be dynamical via

$$\mathcal{Q}_{ij} \Rightarrow |\mathcal{Q}_{ij}| Z_{ij}. \quad (64)$$

Thus we are approximating the path integral over \mathcal{Q}_{ij} in Eq. (26) by a sum over Z_{ij} ; this is acceptable because the sum is sufficient to allow the vison states to appear. From Eq. (28), the \mathbb{Z}_2 gauge transformation in Eq. (57) acts on the \mathbb{Z}_2 gauge field via

$$Z_{ij} \rightarrow \mu_i Z_{ij} \mu_j. \quad (65)$$

The novel term in Eq. (63), beyond those found in the lattice gauge theory literature, is the prefactor of the exponential in the curly brackets: this is the Berry phase term for half-integer spin S . It is a direct consequence of the presence of a background \mathbb{Z}_2 gauge charge on each site, as implied by Eqs. (19) and (61) [54], and so accounts of the motion of visons in a background π flux.

The partition function in Eq. (63) has been studied by quantum Monte Carlo, and yields the phase diagram in Fig. 16. Apart from the ordered antiferromagnet and the \mathbb{Z}_2 spin liquid in Fig. 12, here we obtain a valence bond solid (VBS) state as a consequence of the Berry phase term [47, 48]. This is gapped state which preserves spin rotation invariance, but breaks lattice translational symmetry.

The transition from the \mathbb{Z}_2 spin liquid to the VBS can be studied by integrating out the z_{α} spinons from Eq. (63). This yields a \mathbb{Z}_2 gauge theory for the visons in terms of the Z_{ij} alone. It is convenient to express this \mathbb{Z}_2 gauge theory in Hamiltonian form on the triangular lattice, which has exactly the form familiar in the lattice gauge theory literature:

$$H_{\mathbb{Z}_2} = -K \sum_{\Delta} \prod_{ij \in \Delta} Z_{ij} - g \sum_{ij} X_{ij}, \quad (66)$$

where X_{ij} are Pauli X operators on the links of the triangular lattice. However, the Berry phase term in Eq. (63) does make a crucial difference in selecting the gauge-invariant sector of the Hilbert space of $H_{\mathbb{Z}_2}$. There are infinite number of \mathbb{Z}_2 gauge charges which commute with $H_{\mathbb{Z}_2}$, one on each site of the triangular lattice:

$$G_i = \prod_{\ell \ni i} X_{\ell}, \quad (67)$$

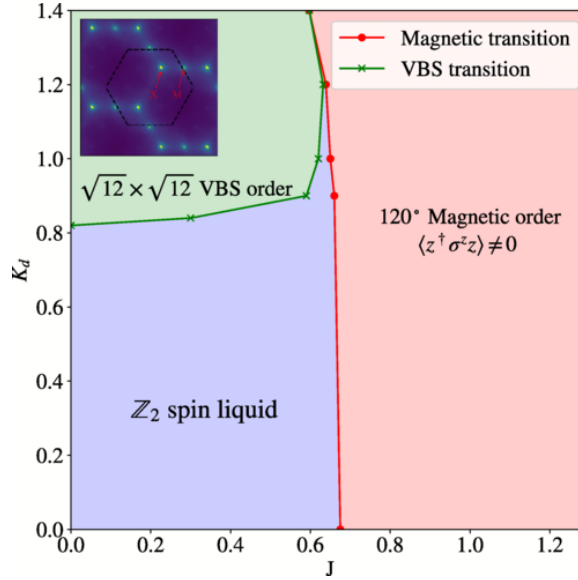


Figure 16: Phase diagram of $\mathcal{Z}_{\mathbb{Z}_2}$ in Eq. (63) obtained via sign-problem-free quantum Monte Carlo in Ref. [54].

where now ℓ labels the links of the triangular lattice. The Berry phase of Eq. (63) implies that we should chose the sector with [47, 48, 55]

$$G_i = (-1)^{2S}. \quad (68)$$

For $(-1)^{2S} = -1$, this term is crucial in ensuring that the confinement transition from the \mathbb{Z}_2 spin liquid leads to a VBS, and there is no trivial ground state at large g .

The transition from the ordered antiferromagnet to the \mathbb{Z}_2 spin liquid is not influenced by the Berry phase term (because the visons remains gapped at this transition), and is described by the O(4) Wilson-Fisher critical theory [56, 57]. However, there is an important difference in the structure of the observable order parameter. Note that z_α was obtained from the continuum limit of the spinon s_α , and so it is fractionalized degree of freedom, carrying a unit \mathbb{Z}_2 charge. Correlators of z_α are therefore not observable, only those of gauge-invariant bilinear combinations. This is denoted by stating the universality class of the transition is actually O(4)*. This critical theory has the same exponents as the O(4) theory, but some observables in a finite geometry are different [58]. As the critical fields of the theory are fractionalized spinons, this is an example of a ‘deconfined critical point’.

Near the multicritical region where the 3 phases meet in Fig. 16, there could be additional deconfined criticality [54] associated with a U(1) gauge theory of fermionic spinons [59–62] which we do not explore here.

3.5 Dynamics of excitations on the square lattice

We now examine the low energy theory on the square lattice in the regime where the energy gap of the spinon excitations is small. Here, we can take a continuum limit for the spinons, and also account for the fluctuations of \mathcal{Q} and λ . For the spinons, we introduce the wavevector at the minimum spinon gap $\mathbf{k}_0 = (\pi/2, \pi/2)$ and parameterize on the checkerboard A and B sublattices (with $i_x + i_y$ even and odd)

$$\begin{aligned} b_{Ai\alpha} &= \psi_{1\alpha}(\mathbf{r}_i) e^{i\mathbf{k}_0 \cdot \mathbf{r}_i} \\ b_{Bi\alpha} &= -i\varepsilon_{\alpha\beta} \psi_{2\beta}(\mathbf{r}_i) e^{i\mathbf{k}_0 \cdot \mathbf{r}_i}. \end{aligned} \quad (69)$$

For \mathcal{Q} and λ , we use the parameterization already discussed in Section 3.2.1.

We insert these parameterizations into the spinon action, perform a gradient expansion, and transform the Lagrangian \mathcal{L}_J into (a is the lattice spacing)

$$\begin{aligned} \mathcal{L}_z = & \int \frac{d^2r}{2a^2} \left[\psi_{1a}^* \left(\frac{d}{d\tau} + ia_\tau \right) \psi_{1a} + \psi_{2a}^* \left(\frac{d}{d\tau} - ia_\tau \right) \psi_{2a} \right. \\ & + \bar{\lambda} (|\psi_{1a}|^2 + |\psi_{2a}|^2) - 2J \bar{\mathcal{Q}} (\psi_{1a} \psi_{2a} + \psi_{1a}^* \psi_{2a}^*) \\ & + (J/2) \bar{\mathcal{Q}} a^2 [(\nabla + ia) \psi_{1a} (\nabla - ia) \psi_{2a} \\ & \left. + (\nabla - ia) \psi_{1a}^* (\nabla + ia) \psi_{2a}^*] \right]. \end{aligned} \quad (70)$$

We now introduce the fields

$$\begin{aligned} z_\alpha &= (\psi_{1a} + \psi_{2a}^*)/\sqrt{2} \\ \pi_\alpha &= (\psi_{1a} - \psi_{2a}^*)/\sqrt{2}, \end{aligned}$$

to map Eq. (70) to

$$\begin{aligned} \mathcal{L}_z = & \int \frac{d^2r}{2a^2} \left[\pi_\alpha^* \left(\frac{d}{d\tau} + ia_\tau \right) z_\alpha - \pi_\alpha \left(\frac{d}{d\tau} - ia_\tau \right) z_\alpha^* \right. \\ & + \bar{\lambda} (|z_\alpha|^2 + |\pi_\alpha|^2) - 2J \bar{\mathcal{Q}} (|z_\alpha|^2 - |\pi_\alpha|^2) \\ & \left. + (J/2) \bar{\mathcal{Q}} a^2 [|(\nabla + ia) z_\alpha|^2 - |(\nabla + ia) \pi_\alpha|^2] \right]. \end{aligned} \quad (71)$$

From Eq. (71), it is clear that the π fields have ‘mass’ $\bar{\lambda} + 2J \bar{\mathcal{Q}}$, while the z fields have a mass $\bar{\lambda} - 2J \bar{\mathcal{Q}}$ which vanishes at a quantum phase transition where the z_α condense, leading to Néel order. The π fields can therefore be safely integrated out, and \mathcal{L}_z yields the following effective action, valid at distances much larger than the lattice spacing [5,6]:

$$S_{\text{eff}} = \int \frac{d^2r}{4\sqrt{2}a} \int d\tau \left\{ |(\partial_\mu - ia_\mu) z_\alpha|^2 + \frac{\Delta^2}{c^2} |z_\alpha|^2 \right\}. \quad (72)$$

Here μ extends over x, y, τ , $c = \sqrt{2J \bar{\mathcal{Q}} a}$ is the spin-wave velocity, we have rescaled $\tau \rightarrow \tau/c$, and $\Delta = (\bar{\lambda}^2 - 4J^2 \bar{\mathcal{Q}}^2)^{1/2}$ is the gap towards spinon excitations. Thus the long-wavelength theory describes a spin liquid with of a massive, spin-1/2, relativistic, boson z_α (spinon) excitation coupled to a U(1) gauge field a_μ .

The continuum theory also makes it easy to determine the fate of the antiferromagnet when the spin energy gap vanishes. We expect that z_α will bose condense, and this will break the spin rotation symmetry; a term quartic in z_α will be needed to stabilize the condensate. But z_α carries a U(1) gauge charge, and so is not directly observable. Following the definitions of the underlying spin operators, it is not difficult to show that the gauge-invariant composite

$$\mathcal{N} = z_\alpha^* \sigma_{\alpha\beta} z_\beta \sim \eta_i S_i \quad (73)$$

is just the Néel order parameter of Fig. 2.

However, there is an important ingredient that our low energy theory has not yet considered. These are non-perturbative fluctuations of a_μ which are Dirac monopoles in 2+1 dimensional spacetime, which carry non-trivial Berry phases. We will not carry out a full analysis here, and only note that these monopole Berry phases are closely connected to the vison Berry phases in Section 3.4.2 [47,48]. An important result is that the spin liquid noted above is ultimately not a spin liquid. It is unstable to proliferation of monopoles, and ultimately confines a valence bond solid. But monopoles do not have a significant effect on the Néel state.

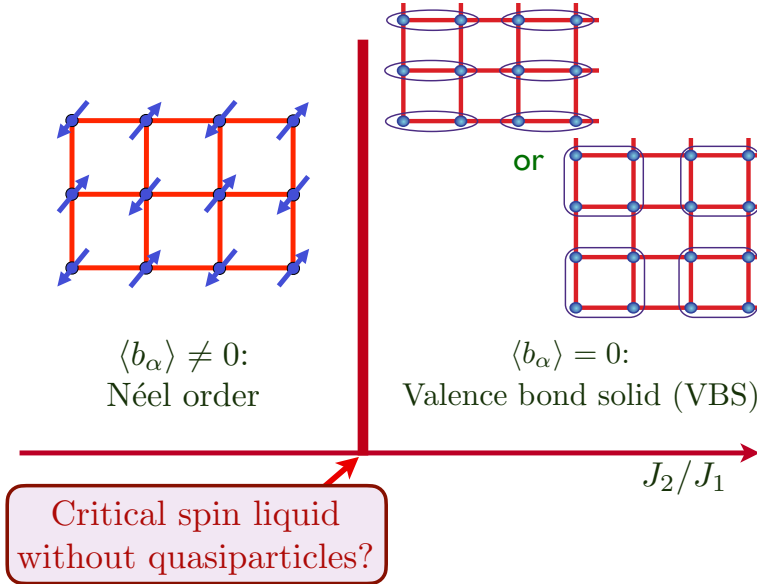


Figure 17: Phase diagram of the $U(1)$ gauge theory with bosonic spinons, Eq. (75). The Néel order appears in a Higgs phase where the bosonic spinons are condensed. The VBS order appears in the confining phase, and is induced by the Berry phases of the confining monopoles. The same phase diagram applies to the fermionic spinon theory in Eq. (97), and the $SO(5)$ σ -model with the WZW term in Eq. (104).

3.5.1 Quantum criticality

On general symmetry grounds, we extend Eq. (72) to a theory for the vicinity of the quantum critical point at which the spinon gap vanishes [63]:

$$\begin{aligned}
 \mathcal{S}_{U(1)} &= \int d^3x (\mathcal{L}_z + \mathcal{L}_{\text{monopole}}) + \mathcal{S}_B \\
 \mathcal{L}_z &= |(\partial_\mu - ia_\mu)z_\alpha|^2 + g|z_\alpha|^2 + u(|z_\alpha|^2)^2 + K(\epsilon_{\mu\nu\lambda}\partial_\nu a_\lambda)^2 \\
 \mathcal{L}_{\text{monopole}} &= -y(\mathcal{M}_a + \mathcal{M}_a^\dagger) \\
 \mathcal{S}_B &= i2S \sum_i \eta_i \int d\tau a_{i\tau}.
 \end{aligned} \tag{74}$$

The theory \mathcal{L}_z is also known as the \mathbb{CP}^1 model. We have included monopoles \mathcal{M}_a in the gauge field a_μ , and also the Berry phase of the spinons in the ground state in \mathcal{S}_B . This Berry phase is closely connected to the vison Berry phase in Section 3.4.2 [47, 48]: note the similarity of \mathcal{S}_B to the Berry phase term in curly brackets of the \mathbb{Z}_2 gauge field in Eq. (63).

As we tune the coupling g in Eq. (74), we can expect the 2 phases shown in Fig. 17:
 (i) Néel phase, $g < g_c$: the spinon z_α condenses in a Higgs phase with $\langle z_\alpha \rangle \neq 0$. The a_μ gauge field is Higgsed, and spin rotation symmetry is broken by opposite polarization of the spins on the two sublattices.

(ii) Valence bond solid (VBS), $g > g_c$: the spinons are gapped. For half-integer spin S , there is broken translational symmetry by the crystallization of valence bonds in the pattern shown in Fig. 17.

We now obtain a potential gapless spin liquid if there is a continuous quantum phase transition at $g = g_c$. For half-integer spin S , the single monopole terms in Eq. (74) average to zero at long wavelengths from the Berry phases, and only quadrupoled monopole terms

survive. So we can simplify the continuum theory for the vicinity of the quantum critical point to [39, 40]

$$\mathcal{L}_z = |(\partial_\mu - ia_\mu)z_\alpha|^2 + g|z_\alpha|^2 + u(|z_\alpha|^2)^2 + K(\epsilon_{\mu\nu\lambda}\partial_\nu a_\lambda)^2 - y_4(\mathcal{M}_a^4 + \mathcal{M}_a^{\dagger 4}), \quad (75)$$

where y_4 is the quadrupoled monopole fugacity. There is ample numerical evidence that y_4 is irrelevant near a possible critical point, and so the question reduces to whether the theory \mathcal{L}_z at $y_4 = 0$ exhibits a critical point which realizes a conformal field theory in 2+1 dimensions. This is a question that has been studied extensively in numerics, and it is clear that a ‘deconfined critical’ description is suitable over a substantial length scale: with fractionalized spinons interacting with a U(1) gauge field in the absence of monopoles [36, 37, 64–67].

4 Fermionic spinon theory of quantum spin liquids

We now present an alternative analysis of the square lattice antiferromagnet in Eq. (17), replacing the bosonic partons in Eq. (21) by fermionic partons. This will ultimately lead to the same phase diagram as in Fig. 17, but with a dual description of the phases and the criticality. This dual fermionic description turns out to be the most efficient way to describe the connection between the critical spin liquid and d -wave superconductivity in the doped antiferromagnet, as we will see in Section 6.

The following *Schwinger fermion* representation applies only for $S = 1/2$

$$\mathbf{S}_i = \frac{1}{2} f_{i\alpha}^\dagger \boldsymbol{\sigma}_{\alpha\beta} f_{i\beta} \quad (76)$$

where $f_{i\alpha}$ are canonical fermions obeying the constraint

$$\sum_\alpha f_{i\alpha}^\dagger f_{i\alpha} = 1 \quad , \quad \text{for all } i. \quad (77)$$

While the bosonic parton representation led to the U(1) gauge symmetry in Eq. (28), it turns out the Eqs. (76) and (77) have a larger SU(2) gauge invariance, and this will be crucial to our results. The analysis is clearest upon introducing a matrix notation for the fermions

$$\mathcal{F}_i \equiv \begin{pmatrix} f_{i\uparrow} & -f_{i\downarrow} \\ f_{i\downarrow}^\dagger & f_{i\uparrow}^\dagger \end{pmatrix} \quad (78)$$

This matrix obeys the ‘reality’ condition

$$\mathcal{F}_i^\dagger = \sigma^y \mathcal{F}_i^T \sigma^y. \quad (79)$$

Now we can write Eq. (76) as

$$\mathbf{S}_i = -\frac{1}{4} \text{Tr}(\mathcal{F}_i \boldsymbol{\sigma}^z \boldsymbol{\sigma}^T \boldsymbol{\sigma}^z \mathcal{F}_i^\dagger). \quad (80)$$

The SU(2) gauge symmetry is now associated with a SU(2) matrix V_i under which [8, 9, 68]

$$\mathcal{F}_i \rightarrow V_i \mathcal{F}_i, \quad (81)$$

which is easily seen to leave the spin operator in Eq. (80) invariant. The global spin rotation symmetry is however

$$\mathcal{F}_i \rightarrow \mathcal{F}_i \boldsymbol{\sigma}^z \Omega^T \boldsymbol{\sigma}^z. \quad (82)$$

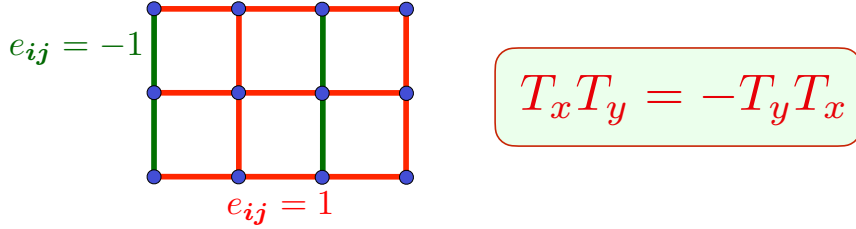


Figure 18: Background π flux acting on the spinons f , and also on the chargons B .

where Ω is the $S = 1/2$ spin rotation matrix defined by

$$\begin{pmatrix} f_{i\uparrow} \\ f_{i\downarrow} \end{pmatrix} \rightarrow \Omega \begin{pmatrix} f_{i\uparrow} \\ f_{i\downarrow} \end{pmatrix}. \quad (83)$$

Next we insert Eq. (80) into Eq. (17), and perform Hubbard-Stratonovich transformation to obtain an effective Hamiltonian for the spinons, following the same procedure as for bosonic spinons. We skip the intermediate steps, and focus directly on the fermion bilinear Hamiltonian on symmetry grounds; we obtain the mean-field nearest-neighbor spin liquid Hamiltonian for the spinons of the π -flux phase [7]:

$$\begin{aligned} \mathcal{H}_{Slf} &= \frac{iJ}{2} \sum_{\langle ij \rangle} e_{ij} [\text{Tr}(\mathcal{F}_i^\dagger \mathcal{F}_j) - \text{Tr}(\mathcal{F}_j^\dagger \mathcal{F}_i)] \\ &= iJ \sum_{\langle ij \rangle} e_{ij} (\Psi_i^\dagger \Psi_j - \Psi_j^\dagger \Psi_i); \quad \Psi_i \equiv \begin{pmatrix} f_{i\uparrow} \\ f_{i\downarrow}^\dagger \end{pmatrix}, \end{aligned} \quad (84)$$

where $e_{ij} = \pm 1$ represents π -flux on the fermions as shown in Fig. 18. We choose $e_{ij} = -e_{ji}$ and

$$e_{i,i+\hat{x}} = 1, \quad e_{i,i+\hat{y}} = (-1)^x, \quad (85)$$

where $i = (x, y)$, $\hat{x} = (1, 0)$, $\hat{y} = (0, 1)$. In the chosen form, it is evident that \mathcal{H}_{Slf} is invariant under the global spin rotation in Eq. (82), and also at least the global gauge transformation associated with Eq. (81). We have chosen the hopping to be pure imaginary because of the identity

$$\text{Tr}(\mathcal{F}_i^\dagger \mathcal{F}_j) = -\text{Tr}(\mathcal{F}_j^\dagger \mathcal{F}_i). \quad (86)$$

We can now easily diagonalize the Hamiltonian in Eq. (84), and obtain the fermionic dispersion spectrum analogous to Eq. (34)

$$\omega_{\mathbf{k}} = \pm 2J (\sin^2 k_x + \sin^2 k_y)^{1/2}. \quad (87)$$

We show a plot of this analogous to Fig. 10 in Fig. 19. Unlike the bosonic spinons, the energy of the fermionic spinons is allowed to be negative, and the negative energy fermion states are occupied in the ground state. The constraint in Eq. (77) is then automatically satisfied. Notice the two independent nodal Dirac points at \mathbf{k}_v , $v = 1, 2$ with

$$\mathbf{k}_1 = (0, 0), \quad \mathbf{k}_2 = (0, \pi). \quad (88)$$

The index v is the ‘valley’.

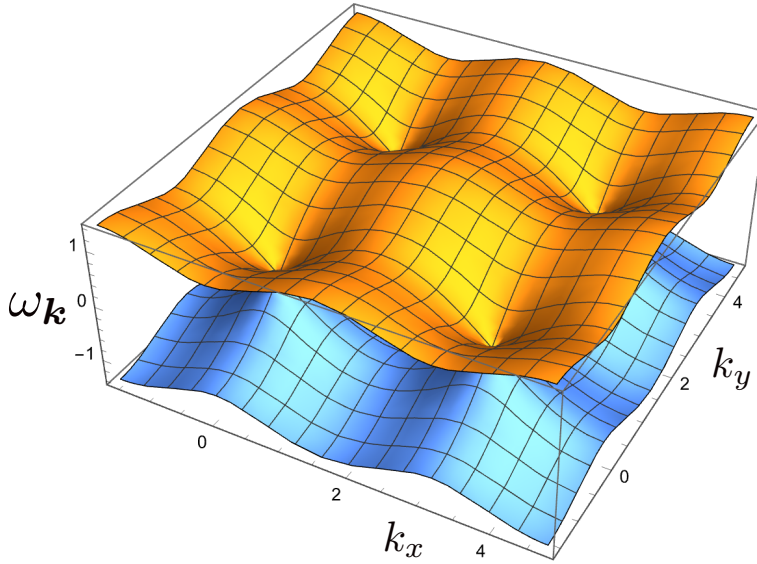


Figure 19: Dispersion of fermionic spinons in Eq. (87).

4.1 Low energy SU(2) gauge theory.

Going beyond mean field theory, while still remaining on the lattice, we extend the mean field Hamiltonian in Eq. (84) to be invariant under space-dependent SU(2) gauge symmetries. To achieve this, we need to introduce a SU(2) gauge field $U_{ij} = U_{ji}^\dagger$ on each lattice link upon which the SU(2) gauge transformation acts as

$$U_{ij} \rightarrow V_i U_{ij} V_j^\dagger. \quad (89)$$

Then, by gauge invariance, we extend Eq. (84) to

$$\begin{aligned} \mathcal{H}_{SLf} &= \frac{iJ}{2} \sum_{\langle ij \rangle} e_{ij} \left[\text{Tr}(\mathcal{F}_i^\dagger U_{ij} \mathcal{F}_j) - \text{Tr}(\mathcal{F}_j^\dagger U_{ji} \mathcal{F}_i) \right] \\ &= iJ \sum_{\langle ij \rangle} e_{ij} (\Psi_i^\dagger U_{ij} \Psi_j - \Psi_j^\dagger U_{ji} \Psi_i); \quad \Psi_i \equiv \begin{pmatrix} f_{i\uparrow} \\ f_{i\downarrow}^\dagger \end{pmatrix}, \end{aligned} \quad (90)$$

The first form in terms of \mathcal{F} makes both the SU(2) gauge invariance and the SU(2) spin rotation invariance explicit, while in the second form in terms of Ψ only the gauge invariance is explicit.

If we had not used the pure imaginary hopping in Eq. (84), then the mean-field Hamiltonian would break ('Higgs') the SU(2) gauge symmetry to a smaller symmetry. A 'staggered flux' ansatz which breaks the SU(2) down to U(1) has commonly been used in the literature [69]. However, it is now known that this U(1) spin liquid allows single monopole perturbations [70, 71] (unlike the quadrupole monopole perturbations in Eq. (75)), and such single monopole terms are expected to drive a strong instability to confinement. So we don't consider the staggered-flux U(1) spin liquid.

The continuum formulation of this theory can be obtained by following the same procedure as in Section 3.5, but we have to carefully account for the SU(2) gauge symmetry. First, neglecting gauge fluctuations of U_{ij} for now, let us write Eq. (84) in momentum space, in terms of the fermions $\mathcal{F}_s(\mathbf{k})$, where $s = A, B$ is a sublattice index. Now the sublattices refer to sites with i_x even and odd, which are the two sites in the unit cell. We obtain

$$\mathcal{H}_{SLf} = -J \sum_{\mathbf{k}} \text{Tr}(\mathcal{F}^\dagger(\mathbf{k}) [\rho^x \sin(k_x) + \rho^z \sin(k_y)] \mathcal{F}^\dagger(\mathbf{k})), \quad (91)$$

where ρ^ℓ , with $\ell = x, y, z$, are Pauli matrices in sublattice space. Next, analogous to Eq. (69), we take the continuum limit near the valley momenta in terms of $\mathcal{X}_{sv}(\mathbf{r}, \tau)$

$$\begin{aligned}\mathcal{F}_{Ai} &= \sum_v \mathcal{X}_{Av}(\mathbf{r}, \tau) e^{i\mathbf{k}_v \cdot \mathbf{r}_i} \\ \mathcal{F}_{Bi} &= \sum_v \mathcal{X}_{Bv}(\mathbf{r}, \tau) e^{i\mathbf{k}_v \cdot \mathbf{r}_i}\end{aligned}\quad (92)$$

for i on the A and B sublattices respectively. This yields the imaginary time Lagrangian density

$$\mathcal{L}_{\mathcal{X}} = \frac{1}{2} \text{Tr} \left(\mathcal{X}^\dagger \left[\partial_\tau + 2Ji\rho^x \partial_x + 2Ji\rho^z \mu^z \partial_y \right] \mathcal{X} \right), \quad (93)$$

where μ^ℓ are the Pauli matrices in valley space. We recall that the fermion \mathcal{X}_{sv} has four-components, and each component is a 2×2 matrix which obeys the reality condition in Eq. (79). We can write this in a relativistic Dirac form

$$\mathcal{L}_{\mathcal{X}} = \frac{i}{2} \text{Tr} \left(\bar{\mathcal{X}} \gamma^\mu \partial_\mu \mathcal{X} \right), \quad (94)$$

with the definitions

$$\bar{\mathcal{X}} = -i\mathcal{X}^\dagger \gamma^0, \quad \gamma^0 = \rho^y \mu^z, \quad \gamma^x = \rho^z \mu^z, \quad \gamma^y = -\rho^x, \quad (95)$$

where we have absorbed factor of $c = 2J$ for the velocity of light. Finally, it is a simple matter to include the SU(2) gauge field by taking the continuum limit by writing

$$U_{ij} = \exp \left(-iA_{ij}^\ell \sigma^\ell \right) \quad (96)$$

(where σ^ℓ are the Pauli matrices in SU(2) gauge space) and expanding the exponential. We then obtain

$$\mathcal{L}_{\mathcal{X}} = \frac{i}{2} \text{Tr} \left(\bar{\mathcal{X}} \gamma^\mu \left[\partial_\mu - iA_\mu^\ell \sigma^\ell \right] \mathcal{X} \right). \quad (97)$$

The theory in Eq. (97) is the analog of the \mathcal{L}_z in Eq. (74) for bosonic spinons. The latter theory was a U(1) gauge theory with two relativistic complex scalars z_α . In the present case, we have a SU(2) gauge theory with $N_f = 2$ massless Dirac fermions, associated with valley index v . The global symmetry of z_α was just spin rotations $z \rightarrow Rz$. In contrast, here we have emergent global symmetry which combines spin and valley rotations. A first guess is a SU(4) symmetry generalizing Eq. (82)

$$\mathcal{X} \rightarrow \mathcal{X}L, \quad (98)$$

where L acts on spin and valley space with $L^\dagger L = 1$. However, imposition of the reality condition Eq. (79) shows that we also need

$$L^T = \sigma^y L^\dagger \sigma^y, \quad (99)$$

and so the symmetry is only $\text{Sp}(4) = \text{SO}(5)/\mathbb{Z}_2$ [11, 72]. In terms of the Hermitian Lie algebra elements M , with $L = e^{iM}$, the reality condition is

$$M^T = -\sigma^y M \sigma^y. \quad (100)$$

Requiring that M commute with the γ^μ , we can now write down the 10 elements of the Lie algebra of $\text{Sp}(4) = \text{SO}(5)/\mathbb{Z}_2$

$$M = \{\sigma^x, \sigma^y, \sigma^z, \mu^z \sigma^x, \mu^z \sigma^y, \mu^z \sigma^z, \rho^x \mu^y, \rho^x \mu^x \sigma^x, \rho^x \mu^x \sigma^y, \rho^x \mu^x \sigma^z\}. \quad (101)$$

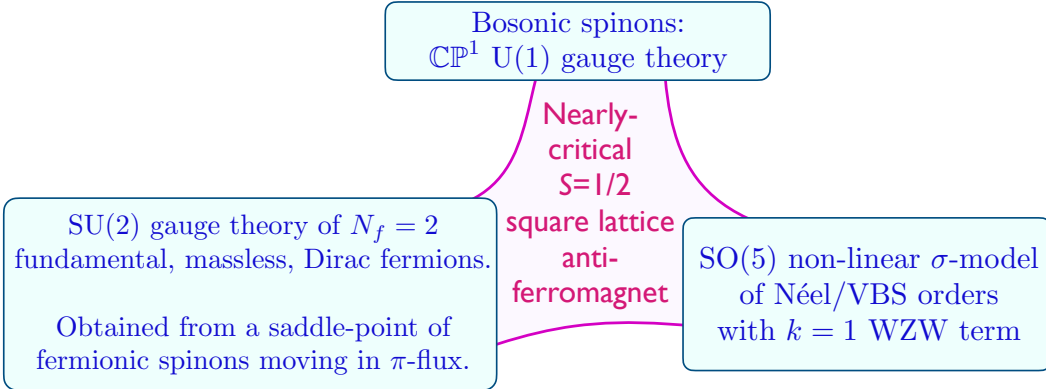


Figure 20: Three field-theoretical formulations of the $S = 1/2$ square lattice antiferromagnet near the Néel-VBS transition in Fig. 17. All three are valid descriptions [11], but the SU(2) gauge theory of Dirac fermions is the most convenient starting point to describe the connection to d -wave superconductivity.

The remaining 5 SU(4) generators which commute with the γ^μ are ($t = 1 \dots 5$)

$$\Gamma^t = \{\mu^z, \rho^x \mu^x, \rho^x \mu^y \sigma^x, \rho^x \mu^y \sigma^y, \rho^x \mu^y \sigma^z\}. \quad (102)$$

The Γ^t all anti-commute with each other, and transform as a SO(5) vector under the generators in Eq. (101). It is now straightforward to check by working back to the lattice operators from the information above that the vector $i\text{Tr}(\bar{\mathcal{X}}\Gamma^t \mathcal{X})$ corresponds precisely to the 5 components of the order parameters shown in Fig. 17: the first two components are the VBS order, and the last 3 components are the Néel order \mathcal{N} in Eq. (73) [11, 72].

Wang *et al.* [11] have argued that the likely fate of the SU(2) gauge theory upon confinement is a state which the SO(5) symmetry is spontaneously broken with $\langle i\text{Tr}(\bar{\mathcal{X}}\Gamma^t \mathcal{X}) \rangle \neq 0$. The lattice model does not have exact SO(5) symmetry, and the choice between the Néel and VBS components of Γ^t is made by additional 4-fermi terms that can be added to Eq. (97). So the ultimate fate of the theory is essentially identical to the fate of the bosonic spinon theory in Section 3.5.1, as illustrated in Fig. 17. This is essentially the reason for the duality between the theories in Section 3.5.1 and 4.1, and Wang *et al.* have provided additional topological arguments.

4.2 SO(5) non-linear σ -model

There is a third formulation of the theories in Section 3.5.1 and 4.1 which is useful for some purposes, as we illustrate in Fig. 20. This is obtained most simply by coupling Eq. (97) to the SO(5) vector order parameter, and integrating out the fermions. Introducing the SO(5) fundamental unit length field n_t , $n_t n_t = 1$ to Eq. (97)

$$\mathcal{L}_{\mathcal{X}n} = \frac{i}{2} \text{Tr} \left(\bar{\mathcal{X}} \gamma^\mu \left[\partial_\mu - i A_\mu^\ell \sigma^\ell \right] \mathcal{X} \right) - i n_t \text{Tr} \left(\bar{\mathcal{X}} \Gamma^t \mathcal{X} \right), \quad (103)$$

we integrate out the Dirac fermions following the analysis of Ref. [73] and obtain

$$\mathcal{L}_n = \frac{1}{2g} (\partial_\mu n_t)^2 + 2\pi i \Gamma[n_t] \quad (104)$$

The last term is the Wess-Zumino-Witten (WZW) term at level 1: it is a Berry phase associated with spacetime textures of n_t , a higher dimensional analog of the Berry phase of a single spin which is proportional to area enclosed by a spherical path [11, 74]: an explicit expression

of $\Gamma[n_t]$ requires 4+1 dimensions with an emergent spatial direction. Upon reduction to a $O(3)$ non-linear sigma model for the Néel order parameter \mathcal{N} in Eq. (73), the WZW term reduces [75] to the Berry phases of the monopoles noted near Eq. (75).

Also, note that while the $SO(5)$ symmetry is explicit in the fermionic spinon theory in Eq. (97), it is not explicit in the bosonic spinon theory in Eq. (75), but expected to be emergent [76].

The form in Eq. (104) has been exploited in recent numerical work on the fuzzy sphere [67]. Their results, and those of a number of other numerical works [34–37, 64–66, 77] show that the critical spin liquid defined by Eq. (75), Eq. (97), or (104) is stable over a substantial intermediate energy and length scales, before ultimately confining into a Néel or VBS state. This intermediate range stability is not a bug, but a feature ideal for our purpose in Section 7 of defining a FL^* state at intermediate temperatures, which ultimately confines to variety of other states at low temperatures.

5 Holon metal from a quantum spin liquid with bosonic spinons

This section dopes the spin liquid state of Section 3.1 with holes of density p . We already discussed the fate of the ordered antiferromagnet upon doping in Section 2, and here we will discuss the fate of the spin liquid.

For the Néel state in Section 2 we obtained a Fermi liquid metal with hole pockets of spin-1/2, charge e quasiparticles. After accounting for the doubling of the unit cell, there are 2 independent pockets in Fig. 6, and so the fractional area of each pocket is $p/4$.

In the present section, doping the spin liquid will yield a *holon metal*, which has Fermi pockets of *spinless*, charge e quasiparticles, *i.e.* holons. There is no doubling of the unit cell here, and we will see that there are 4 independent pockets. So the area of each holon pocket is again $p/4$. But such pockets are not directly observable in photoemission, as the electron operator is a composite of a holon and a spinon. However the holon pockets will contribute to magnetotransport observables restricted to motion within each square lattice plane.

We will argue in Section 7 that the holon metal does not provide a satisfactory description of the cuprate pseudogap. However, recent work [78, 79] has argued that the holon metal descending from a \mathbb{Z}_2 spin liquid is indeed appropriate for the Hubbard model on the Lieb lattice.

A popular way to dope a spin liquid is to introduce a fermionic holon h , so that the electron operator can be written as

$$c_{i\alpha} = h_i^\dagger b_{i\alpha}. \quad (105)$$

However, this approach runs into complications associated with the sublattice assignment of opposite $U(1)$ gauge charges in Eq. (69). We shall instead follow a simpler approach which is ultimately equivalent to Eq. (105), but is applicable more broadly. The central idea here is to transform the electron operator into a rotating reference frame in spin space [79–91]

$$\begin{pmatrix} c_{i,\uparrow} \\ c_{i,\downarrow} \end{pmatrix} = R_i \begin{pmatrix} \psi_{i,+} \\ \psi_{i,-} \end{pmatrix}, \quad R_i^\dagger R_i = R_i R_i^\dagger = \mathbb{1}. \quad (106)$$

The fermions in the rotating reference frame are spinless ‘chargons’ ψ_s , with $s = \pm$, carrying the electromagnetic charge. The $SU(2)$ rotation matrix R_i is represented by two complex numbers

$$R_i = \begin{pmatrix} z_{i,\uparrow} & -z_{i,\downarrow}^* \\ z_{i,\downarrow} & z_{i,\uparrow}^* \end{pmatrix}, \quad |z_{i,\uparrow}|^2 + |z_{i,\downarrow}|^2 = 1. \quad (107)$$

Indeed, we identify z_α with the spinons of the spin liquid described by the complex scalars of the \mathbb{CP}^1 field theory in Eq. (74). Note that $\sum_{p=\pm} \psi_{i,p}^\dagger \psi_{i,p} = \sum_{\alpha=\uparrow,\downarrow} c_{i,\alpha}^\dagger c_{i,\alpha}$, so the density of the chargons is the same as that of the electrons.

A key property of the decomposition in Eq. (106) is that it introduces a SU(2) gauge invariance [84].

$$\begin{aligned} R_i &\rightarrow R_i W_i^\dagger \\ \begin{pmatrix} \psi_{i,+} \\ \psi_{i,-} \end{pmatrix} &\rightarrow W_i \begin{pmatrix} \psi_{i,+} \\ \psi_{i,-} \end{pmatrix}, \end{aligned} \quad (108)$$

where W_i is the SU(2) matrix generating the gauge transformation. This gauge invariance is distinct from the SU(2) gauge invariance of the fermionic spinons in Section 4, which is instead associated with a transformation in pseudospin space.

We now apply this transformation to the paramagnon theory in Eq. (4). Then, we write the Yukawa coupling between the paramagnon P_i and the electrons as

$$P_i \cdot c_{i\alpha}^\dagger \frac{\sigma_{\alpha\beta}}{2} c_{i\beta} \Rightarrow H_i \cdot \psi_{i,s}^\dagger \frac{\sigma_{ss'}}{2} \psi_{i,s'}. \quad (109)$$

We have now introduced a ‘Higgs’ field H_i [84] given by

$$\sigma \cdot H_i = R_i^\dagger \sigma \cdot P_i R_i. \quad (110)$$

It is easy to deduce from Eq. (110) that H transforms as an adjoint under the SU(2) gauge transformation

$$\sigma \cdot H_i \rightarrow W_i \sigma \cdot H_i W_i^\dagger \quad (111)$$

The action of the SU(2) gauge transformation W_i , should be distinguished from the action of global SU(2) spin rotations Ω under which

$$\begin{aligned} R_i &\rightarrow \Omega R_i \\ \begin{pmatrix} c_{i\uparrow} \\ c_{i\downarrow} \end{pmatrix} &\rightarrow \Omega \begin{pmatrix} c_{i\uparrow} \\ c_{i\downarrow} \end{pmatrix} \\ \psi_{i,s} &\rightarrow \psi_{i,s} \\ H_i &\rightarrow H_i. \end{aligned} \quad (112)$$

Note that R carries global spin, and so describes spinons. On the other hand H and ψ are spinless.

We can now use the SU(2) gauge theory of ψ , R , and H to describe the phases of the Hubbard model. The many possibilities are discussed at some length in Refs. [79, 84, 87–91]. We limit ourselves here to the simplest case of the state obtained by rotationally averaging the Néel state of Section 2. The doped spin liquid so obtained, the holon metal, corresponds to condensing the Higgs field as

$$\langle H_i \rangle = \eta_i (0, 0, H_0) \quad (113)$$

where η_i is the sublattice staggering of Eq. (11). Such a condensate preserves spin rotation invariance, but breaks the SU(2) gauge invariance down to U(1). So the low energy theory of the holon metal is a U(1) gauge theory, with a gauge field a_μ which is the same as that introduced in Eq. (38), and which also appears in the \mathbb{CP}^1 theory of R in Eq. (74). The effective theory for the chargons ψ can be obtained from Eq. (4) after (i) replacing the electrons $c_{i\alpha}$ by the chargon $\psi_{i,s}$, (ii) replacing the paramagnon P_i by the Higgs condensate in Eq. (113), and

(iii) minimally coupling the ψ to the U(1) gauge field a_μ . So we obtain the effective chargon action

$$\mathcal{S}_\psi = \int_0^\beta d\tau \left[\sum_{i,s} \psi_{i,s}^\dagger (\partial_\tau - \mu - ia_\tau) \psi_{i,s} - \sum_{i,j,s,s'} t_{ij} e^{ia_{ij}} \psi_{i,s}^\dagger \psi_{j,s} \right. \\ \left. + \sum_{i,s,s'} H_0 \cdot \psi_{i,s}^\dagger \frac{\sigma_{ss'}^z}{2} \psi_{i,s'} \right], \quad (114)$$

where t_{ij} are the hoppings corresponding to the dispersion ε_k in Eq. (4). At leading order, this yields chargon pockets of spinless fermions which are the same as the pockets of electrons in the ordered Néel state presented in Section 2. At higher order, the gauge field will renormalize the dispersion so that the pockets lose the reflection symmetry about the magnetic Brillouin zone boundary present in the Néel state: the Brillouin zone of the holon metal is the same as that of underlying antiferromagnet without symmetry breaking.

The holon metal in Eq. (114) is associated with a U(1) spin liquid. If we replace Eq. (113) by a non-collinear configuration, then we obtain a \mathbb{Z}_2 spin liquid, as is argued to be the case on the Lieb lattice [79].

6 *d*-wave superconductor and charge orders from a quantum spin liquid with fermionic spinons

We now turn to the fermionic spinon theory of an insulating square lattice spin liquid in Section 4. We wish to consider a more general situation in which the gap to charged excitations can vanish [21]. In the cuprates, gapless charged excitations appear when we dope the antiferromagnet. But we can also consider the case where the charge gap vanishes while the electronic density remains the same as in an insulator. In the latter case, there can be an emergent particle-hole symmetry, which simplifies considerations of quantum criticality. We can decrease the charge gap by describing the insulator by an underlying Hubbard model with on-site repulsion U , and reducing the value of U , or by adding additional off-site interactions. Such models have been considered in numerical studies [92–103]. We will now show that the SU(2) gauge theory of Eq. (90) has fates other than those in Fig. 17 once charged excitations are included, the most interesting of which is a *d*-wave superconductor with gapless nodal quasiparticles.

In terms of adiabatic continuity, this *d*-wave superconductor is precisely the BCS superconductor observed in the cuprates. However, the *d*-wave superconductor obtained in this section has one significant quantitative difference from the observations: it has a Lorentz-invariant form of its dispersion, with the two velocities only the square lattice diagonals, v_F and v_Δ , being equal to each other (see Fig. 32B). The cuprates instead have $v_F \gg v_\Delta$. We will resolve this problem in an interesting manner in Section 7.6 when we consider the transition from FL* to a *d*-wave superconductor in the doped case.

The only matter field in Section 4 is the fermion \mathcal{F} , which has electrical charge 0, spin 1/2, and is a gauge SU(2) fundamental. As we are allowing for charged fluctuations, we need to define an electron operator, which has charge $-e$, spin 1/2, and is a gauge SU(2) singlet. This directly leads us to introducing a boson B , first introduced in Ref. [9], which has charge $+e$, spin 0, and is a gauge SU(2) fundamental, so that a composite of \mathcal{F} and B will have the same quantum numbers as the electron. We now show that this information is sufficient to deduce an effective action for B , and to reach our main conclusions. We will give a more microscopic definition of the field B in the doped case later near Eq. (134).

First, similar to Eq. (78), we introduce a matrix notation for the electron \mathcal{C} and the boson B :

$$\mathcal{C}_i \equiv \begin{pmatrix} c_{i\uparrow} & -c_{i\downarrow} \\ c_{i\downarrow}^\dagger & c_{i\uparrow}^\dagger \end{pmatrix}, \quad B_i \equiv \begin{pmatrix} B_{1i} \\ B_{2i} \end{pmatrix}, \quad \mathcal{B}_i \equiv \begin{pmatrix} B_{1i} & -B_{2i}^* \\ B_{2i} & B_{1i}^* \end{pmatrix}, \quad (115)$$

all of which obey the reality condition analogous to Eq. (79). Then we write the fact that the electron operator is a composite of the boson B (the ‘chargon’) and the spinon \mathcal{F} by

$$\mathcal{C}_i \sim \mathcal{B}_i^\dagger \mathcal{F}_i. \quad (116)$$

In terms of the matrix components, we can write Eq. (116) as

$$c_{ia}^\dagger \sim B_{1i} f_{ia}^\dagger + B_{2i} \varepsilon_{\alpha\beta} f_{i\beta}, \quad (117)$$

where $\varepsilon_{\alpha\beta}$ is the unit antisymmetric tensor for spin SU(2) in Eq. (24). Comparing to the transformation to a rotating reference frame in spin space in Eq. (106) in Section 5, we see that Eq. (116) corresponds to a transformation to a rotating reference frame in Nambu pseudospin space, with \mathcal{B}_i serving as the rotation matrix [88].

Now we can use Eq. (116) to determine the symmetry transformations of \mathcal{B} from those of \mathcal{F} , using the fact the \mathcal{C} is gauge invariant and transforms trivially under all symmetries. A boson with the same quantum numbers as our B was introduced in earlier work [9, 10, 68], but with an important difference. In the earlier work, the expectation value of $B^\dagger B$ was set to be equal to the doping density. That is not the case here, as we also include second order time derivatives in B (see Eq. (125)), and the doping density also includes the density of fermionic holes (see Section 7.5).

The generalization of the SU(2) gauge transformation in Eq. (81) is

$$\begin{aligned} \mathcal{C}_i &\rightarrow \mathcal{C}_i & \mathcal{F}_i &\rightarrow V_i \mathcal{F}_i \\ \mathcal{B}_i &\rightarrow V_i \mathcal{B}_i & U_{ij} &\rightarrow V_i U_{ij} V_j^\dagger, \end{aligned} \quad (118)$$

while the generalization of the global SU(2) spin rotation in Eq. (82) is

$$\begin{aligned} \mathcal{C}_i &\rightarrow \mathcal{C}_i \sigma^z R^T \sigma^z & \mathcal{F}_i &\rightarrow \mathcal{F}_i \sigma^z R^T \sigma^z \\ \mathcal{B}_i &\rightarrow \mathcal{B}_i & U_{ij} &\rightarrow U_{ij}. \end{aligned} \quad (119)$$

Finally, the U(1) charge conservation symmetry acts as

$$\begin{aligned} \mathcal{C}_i &\rightarrow \Theta \mathcal{C}_i & \mathcal{F}_i &\rightarrow \mathcal{F}_i \\ \mathcal{B}_i &\rightarrow \mathcal{B}_i \Theta^\dagger & U_{ij} &\rightarrow U_{ij}, \end{aligned} \quad (120)$$

where

$$\Theta = \begin{pmatrix} e^{i\theta} & 0 \\ 0 & e^{-i\theta} \end{pmatrix}. \quad (121)$$

See also Table 2 later for a summary of these gauge and symmetry transformations.

We now obtain an energy functional for B in a Landau-type expansion [19]. Such a functional must also involve the gauge field U_{ij} of Section 4 to maintain gauge invariance. The fermion f experiences a π flux with pure imaginary hopping, while the electron c has purely real hopping with zero flux (in the absence of an applied physical magnetic field). From these facts and Eq. (116) we reach the important conclusion that the boson B must also have purely imaginary hopping with π -flux (the iw term in Eq. (123) below). So the relation

$$T_x T_y = -T_y T_x, \quad (122)$$

Symmetry	f_α	B_a
T_x	$(-1)^y f_\alpha$	$(-1)^y B_a$
T_y	f_α	B_a
P_x	$(-1)^x f_\alpha$	$(-1)^x B_a$
P_y	$(-1)^y f_\alpha$	$(-1)^y B_a$
P_{xy}	$(-1)^{xy} f_\alpha$	$(-1)^{xy} B_a$
\mathcal{T}	$(-1)^{x+y} \epsilon_{\alpha\beta} f_\beta$	$(-1)^{x+y} B_a$

Table 1: Projective transformations of the f spinons and B chargons on lattice sites $\mathbf{i} = (x, y)$ under the symmetries $T_x : (x, y) \rightarrow (x + 1, y)$; $T_y : (x, y) \rightarrow (x, y + 1)$; $P_x : (x, y) \rightarrow (-x, y)$; $P_y : (x, y) \rightarrow (x, -y)$; $P_{xy} : (x, y) \rightarrow (y, x)$; and time-reversal \mathcal{T} . The indices α, β refer to global SU(2) spin, while the index $a = 1, 2$ refers to gauge SU(2).

realizing the π -flux applies both to the spinons and to B . We can also reach these conclusions, and obtain other constraints, by examining the action of all symmetry operators of f , and use Eq. (116) to deduce the action of symmetry operations on B : the results are summarized in Table 1. These considerations lead to the energy functional $\mathcal{E}_2[B, U] + \mathcal{E}_4[B, U]$ with terms quadratic and quartic in B respectively:

$$\begin{aligned}
 \mathcal{E}_2[B, U] &= (r + 2\sqrt{2}w) \sum_i B_i^\dagger B_i + iw \sum_{\langle ij \rangle} e_{ij} (B_i^\dagger U_{ij} B_j - B_j^\dagger U_{ji} B_i) \\
 &\quad + \kappa \sum_{\square} \left\{ 1 - \frac{1}{2} \text{ReTr} \prod_{ij \in \square} U_{ij} \right\} \\
 \mathcal{E}_4[B, U] &= \frac{u}{2} \sum_i \rho_i^2 + V_1 \sum_i \rho_i (\rho_{i+\hat{x}} + \rho_{i+\hat{y}}) + g \sum_{\langle ij \rangle} |\Delta_{ij}|^2 + J_1 \sum_{\langle ij \rangle} Q_{ij}^2 \\
 &\quad + K_1 \sum_{\langle ij \rangle} J_{ij}^2 + V_{11} \sum_i \rho_i (\rho_{i+\hat{x}+\hat{y}} + \rho_{i+\hat{x}-\hat{y}}) \\
 &\quad + V_{22} \sum_i \rho_i (\rho_{i+2\hat{x}+2\hat{y}} + \rho_{i+2\hat{x}-2\hat{y}}). \tag{123}
 \end{aligned}$$

The quartic terms are expressed as products of bilinears of B which are associated with various gauge-invariant observables as identified below

$$\begin{aligned}
 \text{site charge density: } & \langle c_{i\alpha}^\dagger c_{i\alpha} \rangle \sim \rho_i = B_i^\dagger B_i \\
 \text{bond density: } & \langle c_{i\alpha}^\dagger c_{j\alpha} + c_{j\alpha}^\dagger c_{i\alpha} \rangle \sim Q_{ij} = Q_{ji} = \text{Im}(B_i^\dagger e_{ij} U_{ij} B_j) \\
 \text{bond current: } & i \langle c_{i\alpha}^\dagger c_{j\alpha} - c_{j\alpha}^\dagger c_{i\alpha} \rangle \sim J_{ij} = -J_{ji} = \text{Re}(B_i^\dagger e_{ij} U_{ij} B_j) \\
 \text{Pairing: } & \langle \epsilon_{\alpha\beta} c_{i\alpha} c_{j\beta} \rangle \sim \Delta_{ij} = \Delta_{ji} = \epsilon_{ab} B_{ai} e_{ij} U_{ij} B_{bj}. \tag{124}
 \end{aligned}$$

We have retained terms involving nearest neighbor sites, and a few terms with longer-range density-density interactions.

A schematic global phase diagram is shown in Fig. 21, as a function of the tuning parameter r , which is the ‘mass’ of B .

- When r is large and positive, then we can ignore the B sector, and revert to the spinon only theory of Section 4. The low energy theory is Eq. (97), and we expect a confining insulator with either Néel or VBS order as the ground state.

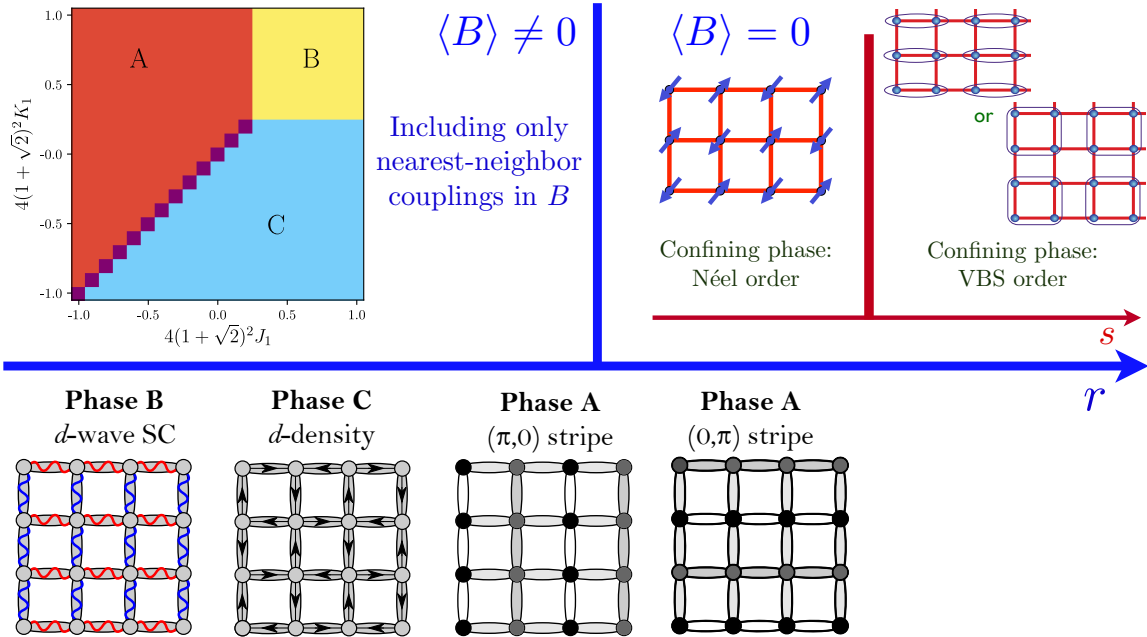


Figure 21: Mean field phase diagram obtained by minimization of the Higgs potential of B , $\mathcal{E}_2 + \mathcal{E}_4$ (from Ref. [19]). For $r > 0$, there is no Higgs condensate $\langle B \rangle = 0$, and we obtain the same phases as in the insulator from the confinement of the fermionic spinons described by Eq. (90). For $r < 0$, $\langle B \rangle \neq 0$, and we minimized the Higgs potential with only nearest neighbor interactions by setting $V_{11} = V_{22} = 0$.

- When r is negative, B condenses, and this has the salutary effect of making the gauge field A massive, as in the Higgs phenomenon. In this case, a mean-field treatment of interactions in the bosonic sector by minimizing $\mathcal{E}_2[B, U] + \mathcal{E}_4[B, U]$ is qualitatively valid.

For negative r , Fig. 21 shows the phases obtained by minimizing the energy functional with nearest-neighbor interactions only, $V_{11} = V_{22} = 0$. Three phases are found:

- This state has charge stripe order with period 2, centered on the sites.
- A d -wave superconductor, with $\Delta_{i,i+\hat{x}} = -\Delta_{i,i+\hat{y}}$.
- A “ d -density wave” state which has a staggered pattern of spontaneous current.

Including further neighbor interactions can induce other phases, including period-4 charge order and pair density waves [19, 22, 23]), as shown in Fig. 22.

The present theory of multiple orders should be contrasted from more conventional Landau theory approaches [104–110]. In our case, we employ a fractionalized order parameter B , whose gauge-invariant composites can represent multiple ordering patterns and broken symmetries. Upon integrating strong gauge fluctuations of U , the fractionalized approach will yield an effective action which is essentially the same as in the Landau theory. But an important advantage of the fractionalized approach is that allows a local description of the fermionic spectrum in the pseudogap metal at non-zero temperatures [23]. Moreover, an interesting feature of the fractionalized approach is that the gauge-invariant orders are degenerate in the quadratic energy functional \mathcal{E}_2 , and the degeneracy is broken only at quartic order in \mathcal{E}_4 . The fact that the leading term is degenerate provides a rationale for nearly-degenerate multiple competing or ‘intertwined’ orders [19]; Landau theory approaches [104–110] do not have any term in which the degeneracy is exact without fine-tuning.

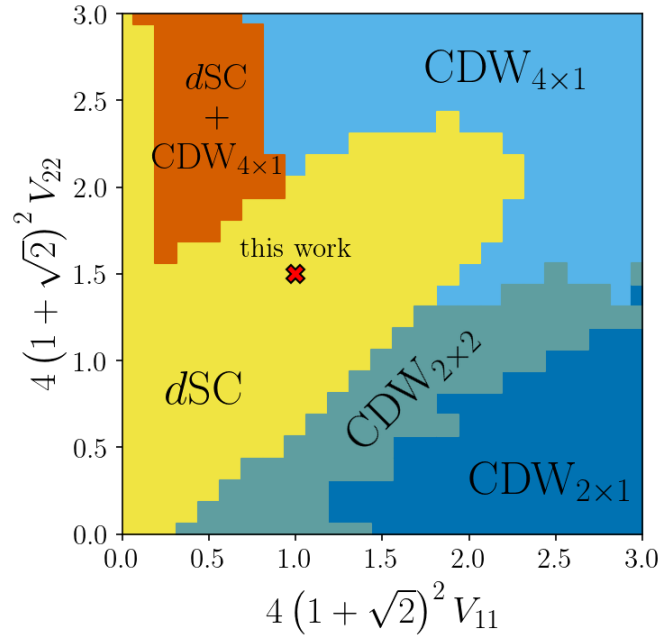


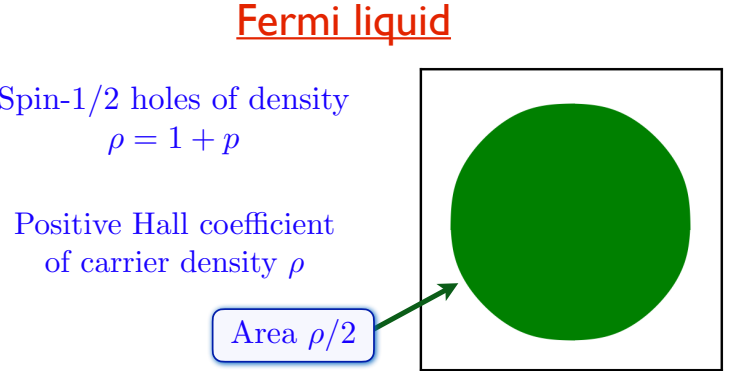
Figure 22: From Ref. [23]. Mean-Field phase diagram of Eq. (123) a function of the further neighbor interactions V_{11} and V_{22} , extending that in Fig. 21. The other parameters are $r = -0.732$, $w = 0.40$, $u = 0$, $V_1 = 0$, $g = 0.021446$, $J_1 = K_1 = 2/(4(1 + \sqrt{2})^2)$. dSC is d -wave superconductivity, $CDW_{n \times m}$ is a charge density wave with a supercell with $n \times m$ lattice sites. The red cross marks the parameter values chosen for the Monte Carlo simulations in Ref. [23].

Our primary interest for now is the d -wave superconductor, phase B. Remarkably, the structure of the π -flux spin liquid, and consequently the π -flux on B leads to d -wave pairing, and not s -wave pairing. Also, once B is condensed, we can identify $c \sim f$ via Eq. (116), and so the electron spectral function will inherit nodal Bogoliubov quasiparticles from the massless Dirac spinons [10, 69, 111–113]. The main phenomenological difficulty is that the Bogoliubov quasiparticles will have isotropic dispersion, as in Eq. (87) and Fig. 19, in contrast to observations [14]; we will address this difficulty in Section 7. However, other features of the d -wave state obtained from the energy functional in Eq. (123) do match observations, including vortices with flux $h/(2e)$ (despite the boson B having charge e), and competing charge order halos of vortex cores.

Going beyond a classical treatment of B and U , we can consider a quantum lattice model to study the interplay of the full array of competing order parameters and deconfined criticality at half-filling. This is obtained by extending the energy functionals in Eq. (123) and the lattice fermion theory in Eq. (90) to

$$\mathcal{L} = \sum_i |D_\tau B_i|^2 + \mathcal{E}_2[B, U] + \mathcal{E}_4[B, U] + \sum_i \Psi_i^\dagger D_\tau \Psi_i + \mathcal{H}_{SLf} + \mathcal{L}_{YM}[U]. \quad (125)$$

Here D_τ represents a covariant time derivative with the SU(2) gauge field U , and \mathcal{L}_{YM} is the lattice Yang-Mills Lagrangian for U . We have added only a relativistic time derivative term for \hat{B} , which is the allowed term at half-filling with particle-hole symmetry. Away from half-filling, we will also have to include the hole pockets to be discussed in Section 7, and that will likely lead to difficulties with the sign problem.



Luttinger, 1960: Area enclosed by the Fermi surface is the same as that for free fermions *with the same symmetry*.

Oshikawa, 2000: Area constrained by a 't Hooft anomaly of global U(1) and translations

Figure 23: Properties of the Fermi liquid (FL) state.

7 Fractionalized Fermi liquids (FL*)

Our motivation for studying quantum spin liquids has been to find a basis for a theory of the cuprate phase diagram. Christos *et al.* proposed [19] that the appropriate spin liquid was precisely that observed in various numerical studies of square lattice antiferromagnets: this is the spin liquid described by the \mathbb{CP}^1 theory of Section 3.5.1, which is dual to the SU(2) gauge theory of fermionic spinons in Section 4. The previous sections have shown that the theories of directly doping such spin liquids run into difficulties:

- Doping the \mathbb{CP}^1 spin liquid yields a holon metal state described in Section 5, which is a candidate for the pseudogap metal. However, as we discuss in Section 7.1.1, the holon metal is incompatible with recent angle-dependent magnetoresistance (ADMR) experiments [12, 13].
- Doping the fermionic spin liquid can lead to a *d*-wave superconductor, as described in Section 6. However, the velocities of the nodal quasiparticles are nearly isotropic, with $v_F \sim v_\Delta$ [14].

We now show that replacing the holon metal with another doped spin liquid phase, the fractionalized Fermi liquid (FL*), resolves both (and other) difficulties above. It agrees with the ADMR measurements in the pseudogap, and a confinement transition from FL* yields a *d*-wave superconductor with anisotropic nodal velocities.

We begin by presenting the basic definition of the FL* state. Consider any system of $S = 1/2$ fermions of density ρ , with spin rotation invariance preserved. In the Fermi liquid (FL) state, Luttinger's argument [114] states that the fractional volume of the Brillouin zone enclosed by the Fermi surface should be $\rho/2$, modulo integers to account for filled bands. Oshikawa [115] placed Luttinger's argument on a non-perturbative basis by relating to an anomaly associated with translations and charge conservation; see Ref. [116] for a review. This is summarized in Fig. 23.

The idea of a 'fractionalized Fermi liquid' (FL*) was introduced in Refs. [15, 16], as a metallic state in which the Fermi surface did *not* obey the Luttinger constraint. In the simplest case, the fractional volume enclosed by the Fermi surface in FL* is $(\rho - 1)/2$. The central point [16, 17, 45, 116–121] was that it was possible to satisfy Oshikawa's anomaly by combining

Fractionalized Fermi liquid (FL*)

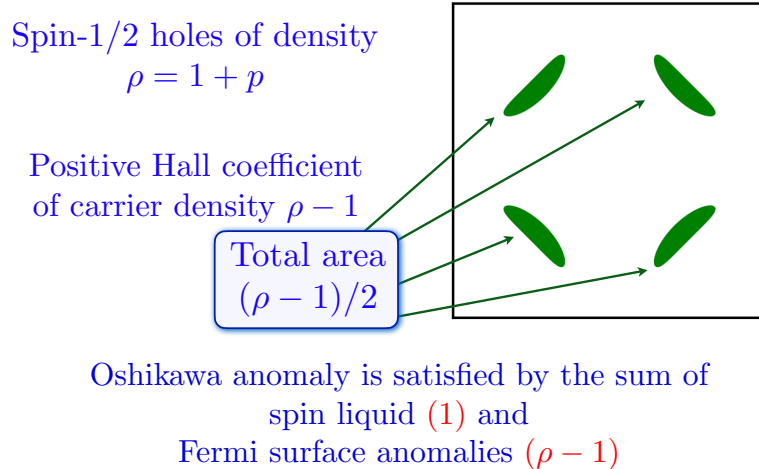


Figure 24: Properties of the fractionalized Fermi liquid (FL*) state.

the anomaly of a Fermi surface (which contributes an amount equivalent to a density $\rho - 1$) with that of a fractionalized spin liquid (which contributes an amount equivalent to a density 1). It is trivially possible to shift ρ by an even integer by adding and removing filled bands, and the novelty is the shift in FL* by an odd integer. This is summarized in Fig. 24.

7.1 FL* in single band models

We describe here construction of the FL* phase in a single band model, such as the square lattice Hubbard model (possibly with additional short-range interactions) of interest for the cuprates. At the level of cartoon pictures, we illustrate the structure of the FL* and other states in Fig. 25 [122]. This figure describes three distinct metallic phases in a Hubbard time model with electron density $1 - p$. Recall that in the absence of a broken symmetry, the Luttinger constraint on hole Fermi surfaces is that they have a fractional area per spin of $(1 + p)/2$, relative to the area of the full square lattice Brillouin zone.

- *AF Metal.* This is a state with antiferromagnetic long-range order, which we described in Section 2. We can understand the Fermi surface by considering free electrons moving in a background with the same symmetry *i.e.* in a background spin-dependent potential which has a modulation at the wavevector (π, π) . This leads to the magnetic Brillouin zone boundary shown by the dashed line, and 4 hole pocket Fermi surfaces. Only two of these pockets are independent within the magnetic Brillouin zone. After accounting for a factor of 2 from spin, we conclude that the fractional area of each pocket is $p/4$. This Fermi surface area obeys the Luttinger constraint. Thermal fluctuations do not move Fermi surfaces, only broaden them, and so we expect that a fluctuating spin density wave state will also have pockets of area $p/4$ [123–126].
- *Holon metal.* This is a state with no broken symmetry, in which the electrons have paired up in singlet bonds which resonate with each other. The dopants are realized by spinless mobile vacancies of charge $+e$, known as holons. The density of holons is p , and if the holons are fermions, they will form Fermi surfaces corresponding to spinless free fermions of density p . If there are four distinct Fermi surfaces in the Brillouin zone (as is the case in many computations), then the fractional area of each pocket will be $p/4$. Although this area is the same as that for the AF metal, the reason is very different. Now

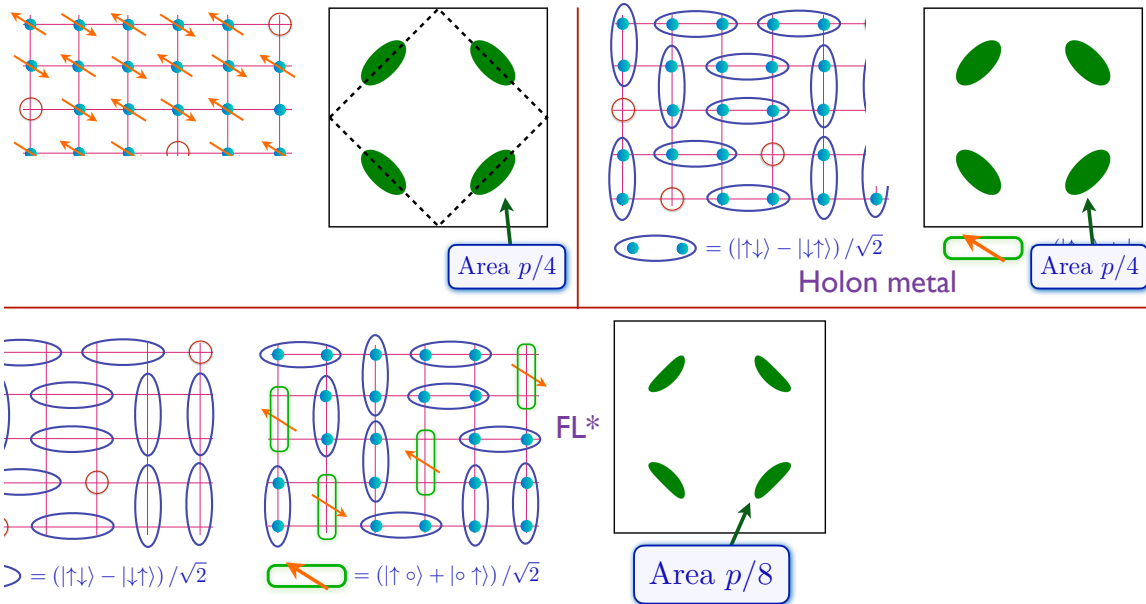


Figure 25: Cartoon pictures of different states of doped antiferromagnets; adapted from Ref. [122]. The areas are those that would be measured by a probe such as quantum oscillation. The AF metal has long-range antiferromagnetic order, and the reduced Brillouin zone is shown with the dashed line. The other phases do not break any symmetries. The open circles are holons, and these are assumed fermionic in the holon metal. The green dimers represent bound states of holons and spinons. Note that all 3 states would show a Hall co-efficient of density p positively charged carries.

there is no broken symmetry, and the fermionic quasiparticles are spinless holons. This Fermi surface area does *not* obey the Luttinger constraint, and this is permitted because of the presence of the spin liquid. A systematic, gauge theoretic treatment of the holon metal state was presented in Section 5 [85–87, 89–91, 127–131], and it is relevant to ultracold studies of the Hubbard model on the Lieb lattice [78, 79]. The discussion below Eq. (114) explains the equality of pocket areas between the AF metal and the holon metal.

- FL^* . Finally, we turn to the metallic state of interest. The holon metal state also has spinon excitations, which can be created out of the ground state. Now imagine a situation in which each holons gains energy by binding with a spinon, so that the system can pay the price for creating the spinons. In a t - J model with electron hopping t , and exchange energy J , the cost for creating a spinon is order J , and the energy gain from the formation of the holon-spinon bound state is of order t , and so this bound state formation is very likely in the natural situation with $t \gg J$. Then the ground state will change into one in which the mobile charge carriers are holon-spinon bound states [120, 122, 132–145]. These bound states are always fermions with charge $+e$, spin $S = 1/2$, just like a hole. Treating these holes as free fermions, we conclude that the total area of the Fermi surface should be $p/2$. If there are 4 distinct pockets (as there in the computation below), then each pocket will have the distinctive area of $p/8$. This Fermi surface area also does *not* obey the Luttinger constraint.

We highlight key features of the single-band FL^* state [122] in Fig. 25. We will see that these features will also play a key role in the Ancilla Layer Model of Section 7.2, as we illustrate later in Fig. 30.

- The electron quasiparticle of FL^* is a (green) “dimer” in Fig. 25, a bound state of a spin and vacancy.
- FL^* has a background of spinon excitations obtained by breaking singlet bonds (the blue dimers) in Fig. 25.

7.1.1 ADMR

Recent ADMR observations [12, 13] in the pseudogap metal are well modeled by hole pockets containing quasiparticles which can tunnel coherently between layers. This is not possible for holon metals, as the holons carry charges of distinct emergent gauge fields within each layer. In the AF metal, coherent tunneling requires significant interlayer spin correlations, which are not observed [146, 147], but could perhaps be induced by the applied magnetic field. The FL^* quasiparticles are gauge neutral and can indeed tunnel coherently between layers. So even at the outset, before any quantitative comparisons, these observations strongly favor a FL^* description of the pseudogap phase of the cuprates [148].

Moreover, the observations [13] also provide a quantitative correspondence with the FL^* theory. Their observation of the Yamaji effect in the cuprate $\text{HgBa}_2\text{CuO}_{4+\delta}$ show pockets of a fractional area of ‘approximately 1.3%’ at a doping $p = 0.1$, close to the value $p/8 = 1.25\%$ predicted for FL^* [15, 16, 120, 133, 148–150].

7.2 Layer construction with ancilla qubits

While much insight can be gained from the methods above, they fall short of providing a mean-field theory for the FL^* phase, which could be used to study quantum phase transitions out of it. A suitable mean field theory can also lead to a trial wavefunction for the FL^* state, which can be used for variational numerical computations and compared to cold atom observations [151–153], as discussed in Section 7.4. To these ends, we now describe the Ancilla Layer Model (ALM) [154, 155], which also easily ensures consistency with anomaly arguments.

We wish to have a mean-field theory which changes a large hole-like Fermi surface of area $(1+p)/2$ to small hole-like Fermi surfaces of total area $p/2$. The simplest way to achieve this in mean-field theory is to hybridize the large Fermi surface with another band at half-filling (as in the Kondo lattice, and was done by Yang-Rice-Zhang (YRZ) [150, 156])—this leads to a Fermi surface of the needed area $(1+p+1)/2 \pmod{1} = p/2$. But we are *not allowed* to add a single band at half-filling because it is not ‘trivial’ *i.e.* it is not anomaly-free, and its excitations cannot be integrated out because the extra band can only acquire a gap with a broken symmetry. On the other hand, we are *allowed* to add two bands at half filling each (or any even number of bands), because they can form a trivial insulator with a gap. After the first added band hybridizes with the physical electrons to yield the small Fermi surfaces, the second added band is left decoupled, and it can form the spin liquid needed to satisfy the Oshikawa anomaly. This is the essence of the ALM.

We begin with a constructive derivation of the ALM starting from the familiar Hubbard model in Eq. (1), and returning to the paramagnon representation in Eq. (4). After some renormalization of the high energy states we give the paramagnon \mathbf{P} some independent dynamics with a non-zero mass $m_{\mathbf{P}}$, and obtain its effective Lagrangian

$$\mathcal{L}[\mathbf{P}] = \sum_i \left[\frac{m_{\mathbf{P}}}{2} (\partial_{\tau} \mathbf{P}_i)^2 + \frac{3U}{8} \mathbf{P}_i^2 \right], \quad (126)$$

where the \mathbf{P}^2 term is as in Eq. (4). This is a paramagnon theory with 3 local harmonic oscillators of frequency $(3U/(4m_{\mathbf{P}}))^{1/2}$ on each site, which are coupled to the electrons with a

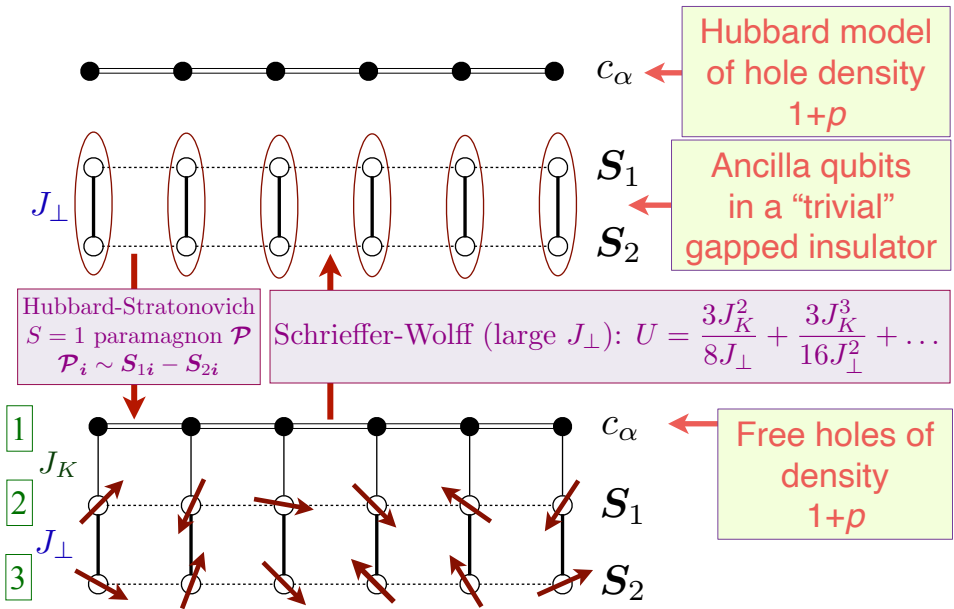


Figure 26: Illustration of the mapping from a single-band Hubbard model with decoupled ancilla qubits, to a single band with free fermions coupled to a bilayer antiferromagnet. The Schrieffer-Wolff transformation is derived in Ref. [157], and the Hubbard-Stratonovich transformation is derived in Ref. [158]. The layer numbers of the layer construction with ancilla qubits are indicated in the bottom picture.

Yukawa coupling of strength U in Eq. (4). Now we take steps different from conventional paramagnon approaches. The ground state of the paramagnon theory is obtained when all three oscillators are in the $n = 0$ state: $|0, 0, 0\rangle$. There is a triplet of first excited states:

$$|1, 0, 0\rangle \sim \mathbf{P}_{ix} |0, 0, 0\rangle; |0, 1, 0\rangle \sim \mathbf{P}_{iy} |0, 0, 0\rangle; |0, 0, 1\rangle \sim \mathbf{P}_{iz} |0, 0, 0\rangle.$$

We can map this low energy spectrum to that of a pair of $S = 1/2$ ancilla spins with a mutual interaction $J_{\perp} \mathbf{S}_{1i} \cdot \mathbf{S}_{2i}$. By comparing the above matrix elements to those that couple the singlet and triplet spin states states, we obtain the operator identification

$$\mathbf{P}_i \sim \mathbf{S}_{1i} - \mathbf{S}_{2i}. \quad (127)$$

Inserting Eq. (127) into Eq. (4), we obtain the Hamiltonian of the ALM, \mathcal{H}_{ALM} . This has a Kondo lattice Hamiltonian \mathcal{H}_{KL} with couples the electrons c_{α} to the \mathbf{S}_1 spins by an antiferromagnetic Kondo coupling $J_K \sim U$, and a second layer of \mathbf{S}_2 spins which have a rung coupling $J_{\perp} = (3U/(4m_P))^{1/2}$ to the \mathbf{S}_1 spins:

$$\begin{aligned} \mathcal{H}_{\text{ALM}} &= \mathcal{H}_{\text{KL}} + J_{\perp} \sum_i \mathbf{S}_{1i} \cdot \mathbf{S}_{2i} + \sum_{i < j} J_{ij} \mathbf{S}_{2i} \cdot \mathbf{S}_{2j} \\ \mathcal{H}_{\text{KL}} &= \sum_{i < j} J_{1,ij} \mathbf{S}_{1i} \cdot \mathbf{S}_{1j} - \sum_{i,j} t_{ij} c_{i\alpha}^{\dagger} c_{j\alpha} + \sum_i \frac{J_K}{2} \mathbf{S}_{1i} \cdot c_{i\alpha}^{\dagger} \boldsymbol{\sigma}_{\alpha\beta} c_{i\beta}. \end{aligned} \quad (128)$$

This Hamiltonian is illustrated in the bottom half of Fig. 26.

So we see that the ancilla spins are simply the fractionalization of the familiar $S = 1$ paramagnon into a pair of $S = 1/2$ spins [158]. The above derivation of the mapping to the ALM yields an additional ferromagnetic Kondo interaction between the electrons $c_{i\alpha}$ and spins \mathbf{S}_{2i} . Ferromagnetic Kondo couplings are expected to be irrelevant, and we will note this coupling

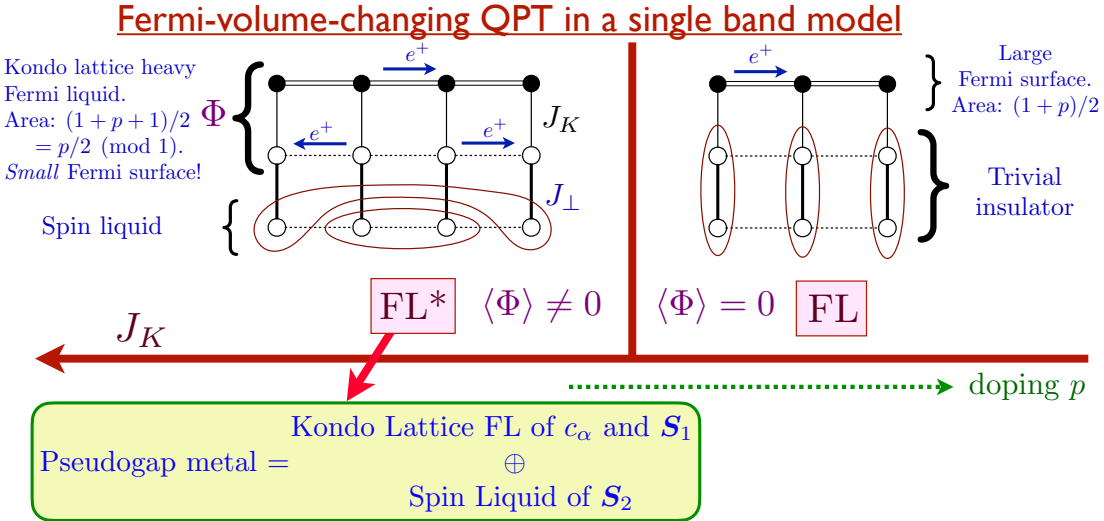


Figure 27: Phases of the Ancilla Layer Model. The noted areas are per spin. The phases are distinguished by the condensation of the boson Φ , which hybridizes the conduction electrons in the top layer with the fermionic spinons in the middle layer.

again in Eq. (134). Note that it is Eq. (127) which breaks the symmetry between S_1 and S_2 , and we *choose* the spins in the middle layer to be the ones which have the antiferromagnetic Kondo coupling with the electrons. We have also explicitly included a direct exchange interaction between the S_{2i} spins, as it will be important for our purposes below. Note also that there is no Hubbard interaction U in \mathcal{H}_{ALM} , and it has been replaced by the Kondo interaction J_K in \mathcal{H}_{ALM} .

We discuss the phase diagram of \mathcal{H}_{ALM} shown in Fig. 27.

At small J_K , the ancilla spins decouple into rung singlets, and we are back to a c_α state adiabatically connected to free electrons, which is the conventional Fermi liquid with a large hole pocket of area $(1+p)/2$.

At large J_K , we assume that the c_α electrons and S_1 spins realize the commonly observed heavy Fermi liquid (FL) phase of \mathcal{H}_{KL} . With the density of c_α equal to $1+p$, the total density of the ‘large’ Fermi surface is $2+p$. As a trivial filled band with density 2 can always be removed, we obtain ‘small’ Fermi surface associated with density p in the FL phase of \mathcal{H}_{KL} . So the total area of hole pockets is $p/2$. While this is the Luttinger value for \mathcal{H}_{KL} , it is *not* for \mathcal{H}_{ALM} . The S_{2i} have an effective ferromagnetic Kondo coupling to the conduction electrons c_α (mediated by the antiferromagnetic J_\perp and the antiferromagnetic J_K), and so we can expect them to decouple from the top two layers. Indeed, we obtain a FL* phase for \mathcal{H}_{ALM} if the S_{2i} layer forms a spin liquid, and the effects of J_\perp in Eq. (128) can be treated perturbatively. This leads the identification in Fig. 27 of the FL* pseudogap metal with the combination of a Kondo lattice FL state of c_α and S_1 , and a spin liquid of S_2 .

We can now summarize the FL* construction of the Hubbard model in the following simple terms. We express the Hubbard model as a theory of antiferromagnetic paramagnons, and then fractionalize the $S = 1$ paramagnon into two $S = 1/2$ spins, S_1 and S_2 . The S_1 spins form a Kondo lattice heavy Fermi liquid with the electrons c_α to yield the hole pockets. The S_2 spins form the spin liquid needed to satisfy the Oshikawa anomaly.

7.3 Mean field theory of the cuprate pseudogap.

We can now obtain a mean-field theory of the pseudogap by extending the Kondo lattice mean-field theory to the Hamiltonian \mathcal{H}_{ALM} in Eq. (128).

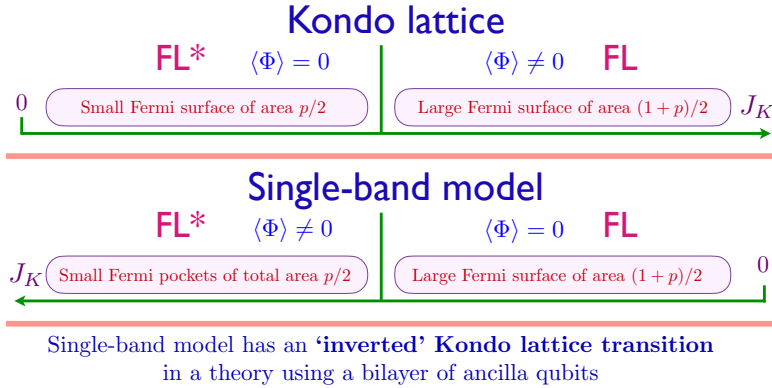


Figure 28: Comparison of the phases of the Kondo lattice model and the Ancilla Layer Model of the single band Hubbard model in Fig. 27. There is an inversion in the phase in which Φ is condensed.

We begin with the top two layers of electrons c_α and spins S_1 in the ALM in Fig. 26. We proceed with parton decomposition of S_1 in terms of the fermionic spinons $f_{1\alpha}$ as in Eq. (76)

$$S_{1i} = \frac{1}{2} f_{1i\alpha}^\dagger \sigma_{\alpha\beta} f_{1i\beta}, \quad (129)$$

and obtain the mean-field fermion Kondo lattice Hamiltonian for the c_α and $f_{1\alpha}$:

$$\mathcal{H}_{\text{KLmf}} = \sum_{i,j} [-t_{ij} c_{i\alpha}^\dagger c_{j\alpha} - t_{1,ij} f_{1i\alpha}^\dagger f_{1j\alpha}] - \sum_i (\Phi c_{i\alpha}^\dagger f_{1i\alpha} + \Phi^* f_{1i\alpha}^\dagger c_{i\alpha}). \quad (130)$$

Here Φ is decoupling field of the J_K exchange interaction in Eq. (128), and is illustrated in Fig. 31. At the mean-field level, we can assume the S_2 spin liquid remains decoupled, and important effects of this spin liquid will be discussed in Section 7.5.

When considered as a theory of the Kondo lattice model \mathcal{H}_{KL} , the FL state corresponds to the condensation of the decoupling field Φ . On the other hand, on the Hilbert space of the full \mathcal{H}_{ALM} , this same Φ condensed phase is the FL* state. This interesting inversion is highlighted in Fig. 28: the single band model has an ‘inverted’ Kondo lattice transition. The magnitude of Φ determines the value of the electronic gap in the anti-nodal region of the Brillouin zone (near momenta $(\pi, 0), (0, \pi)$).

Fig 29 shows the electron spectral density (as measured by photoemission) at zero frequency for both the electron and hole pockets, computed by diagonalizing Eq. (130).

We can now present in Fig. 30 the close analogy between the FL* state obtained in the ALM and the state presented in Fig. 25 as highlighted in the box before the beginning of Section 7.2

- The electron quasiparticle of FL* is the hybridization of c_α and $f_{1\alpha}$ induced by Φ , which creates the bound state $\sim c_{i\alpha} f_{1i\alpha}^\dagger$ between a vacancy and a spin, analogous to the green dimers in Fig. 25.
- The background of spinons in FL* are obtained from the spin liquid of S_2 spinons in the bottom layer, analogous to the spinons obtained by breaking the blue dimers in Fig. 25. We will later represent these spinons by f_α via Eq. (132).

A key observation is that the number of spin-singlet blue dimers in the ALM is exactly N more than in the dimer model of Fig. 25, while the number of green dimers is the same. This is acceptable because N spin singlets is precisely the number that can be accommodated in a trivial rung-singlet state of a bilayer antiferromagnet.

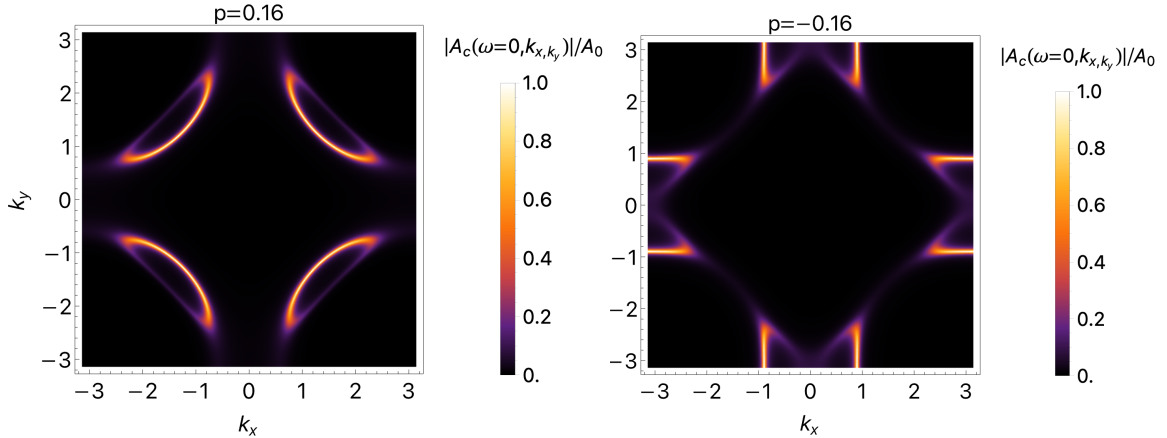


Figure 29: Spectral density of hole (left) and electron (right) pockets at $p = 0.16$ and $p = -0.16$ respectively in the FL^* state. The fractional area of each hole pocket is $p/8$, and the fractional area of the electron pocket is $|p|/4$. Compared to Fig. 7 for the SDW state, the pocket areas have been halved in the FL^* state. Figure by A. Nikolaenko.

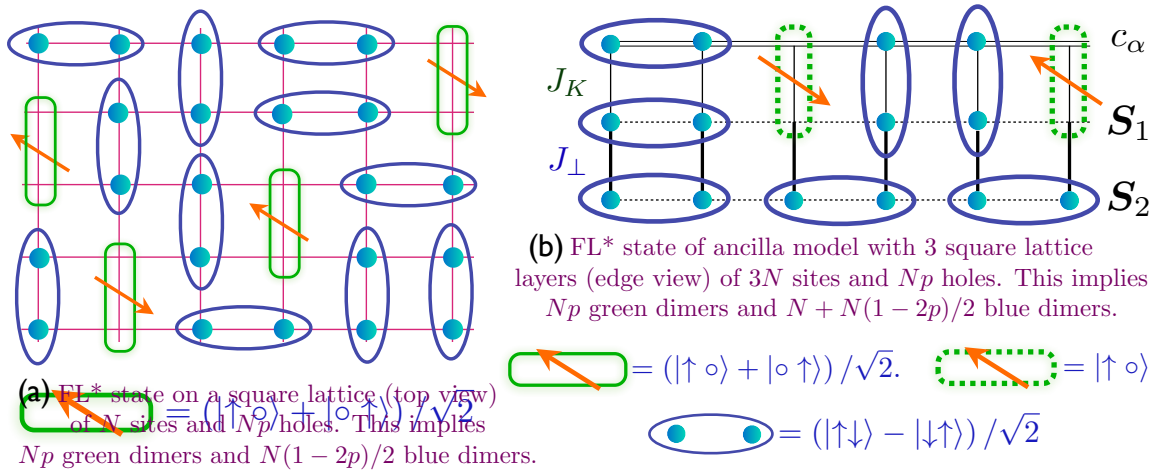


Figure 30: Comparison between (a) the quantum dimer theory of the square lattice FL^* state [122] and the (b) ALM. The dashed green dimer is the state $c_{i\alpha}f_{1i\alpha}^\dagger$ created by the hybridization Φ in the ALM. Note that the ALM has exactly N blue dimers more than the dimer model, and these extra dimers are the number in a trivial rung-singlet bilayer antiferromagnet.

The connection in Fig. 30 shows that the ALM is, in a sense, ‘minimal’. For a FL^* mean field theory with both a small Fermi surface and spinons, we need the middle and bottom ancilla layers to provide the vacancy-spin and singlet valence bonds respectively. And a bonus, not available in the quantum dimer analysis of Ref. [122, 140] or other approaches [132, 138, 139], is that it also provides a mean-field theory which captures the FL^* large Fermi when the bottom two layers are in a rung-singlet state.

7.4 Wavefunction for FL^* and cold atom observations.

A separate mean-field approach is to work with variational wavefunctions. The ancilla layer method was the first to provide a variational wavefunction for the FL^* phase of the single-band Hubbard model. This approach couples all three layers together in the proposed wavefunction [154]

$$\begin{aligned} |\text{FL}^*\rangle &= [\text{Projection onto rung singlets of } \mathbf{S}_1, \mathbf{S}_2] \\ &\bowtie |\text{Slater determinant of } (c, f_1)\rangle \\ &\otimes |\text{Spin liquid of } \mathbf{S}_2\rangle. \end{aligned} \quad (131)$$

Here f_1 is obtained from the parton decomposition of \mathbf{S}_1 in Eq. (129). Note that this wavefunction depends only upon the co-ordinates of the c electrons alone, as the co-ordinates of the f, f_1 fermions have been projected out. This wavefunction replaces the ‘vanilla’ Gutzwiller projected wavefunctions of the c electrons alone [159] in the underdoped region. We see rather explicitly in Eq. (131) the expressivity of the layered construction [160], allowing us to include both a small Fermi surface and a spin liquid in the same state.

The wavefunction Eq. (131) has been studied numerically in Refs. [152, 153, 161], with the couplings in $\mathcal{H}_{\text{KLmf}}$ treated as variational parameters. The results of Refs. [152, 153] successfully capture the evolution of local, multi-point spin and charge correlations with doping as measured in cold atom experiments on the square lattice fermionic Hubbard model [151, 162, 163]. The results of Ref. [161] compare well with the exact diagonalization of Hubbard models in one and two dimensions.

7.5 $\text{SU}(2)$ gauge theory of the onset of nodal d -wave superconductivity from FL^*

This section addresses the fate of the FL^* pseudogap as the temperature is lowered, upon including the coupling to the \mathbf{S}_2 spin liquid in $\mathcal{H}_{\text{pseudogap}}$ in Eq. (135). This Hamiltonian specifically chooses the π -flux spin liquid of Section 4 for the \mathbf{S}_2 layer. We will show that for this spin liquid there is a transition to a conventional BCS-type d -wave superconductor, with anisotropic nodal velocities for the Boboliubov quasiparticles, and $h/(2e)$ vortices. Nevertheless the transition itself is not of the BCS type with a Cooper-pairing instability of a Fermi surface. Instead, the transition is driven by the confinement of the fractionalized excitations of the \mathbf{S}_2 spin liquid. We also find nearby instabilities to charge ordering, consistent with observations—see the review in Ref. [18] for more information.

We note here recent numerics which support the idea of the d -wave superconductor emerging from the doping-induced confinement of the π -flux spin liquid. As we have discussed in Section 4, the π -flux spin liquid is one description of the quantum-criticality between the Néel and VBS states. The numerical studies of Refs. [164, 165] examined the J_1 - J_2 square lattice antiferromagnet near the Néel-VBS transition, and indeed found d -wave superconductivity upon doping.

Now we return to the analysis of the pseudogap using the ALM in Eq. (128). In Section 7.3, we presented a mean field analysis in terms of decoupled Kondo lattice and spin liquid models. This section will couple them using the methods developed in Sections 3 and 6.

Field	Layer	Gauge	Global	
		SU(2)	SU(2)	U(1)
c or \mathcal{C}	1	1	2_R	-1
f_1 or \mathcal{F}_1	2	1	2_R	-1
f or \mathcal{F}	3	2_L	2_R	0
B or \mathcal{B}	$2 \leftrightarrow 3$	2_L	1	1

Table 2: Summary of gauge and global symmetry transformations for the fields of the ALM in the FL^* phase. The representations of the $SU(2)$ are indicated by their dimension; the subscripts L/R indicate whether the $SU(2)$ acts by left/right multiplication in the matrix form of the field. The representations of the global $U(1)$ is the electrical charge in units of e . For the fermions, the layer column indicates the layer number is Fig. 26. For the bosons, the layer column indicates the layers between which there is a Yukawa coupling to the fermions.

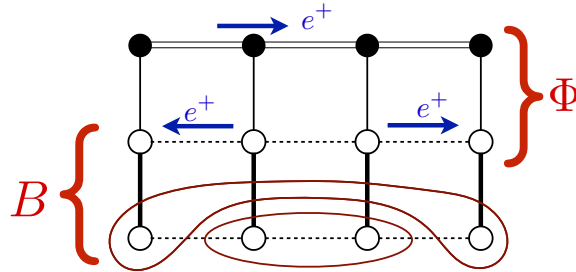


Figure 31: The two distinct Higgs fields in the ancilla layer theory of the single band Hubbard model. Φ hybridizes conduction electrons in the top layer with spinons in the middle layer. B couples the spinons of the bottom layer to the upper layers.

On the spin liquid layer of S_2 spins we write a parton decomposition which parallels that in Eq. (76) and (129)

$$S_{2i} = \frac{1}{2} f_{i\alpha}^\dagger \boldsymbol{\sigma}_{\alpha\beta} f_{i\beta}. \quad (132)$$

Then the analysis of the exchange interactions within the S_2 layer is precisely that in Section 4. We decouple the J_{ij} term in Eq. (128) to \mathcal{H}_{SLf} in Eq. (90) realizing a π -flux state of the S_2 spins with a $SU(2)$ gauge field.

To couple this spin liquid to the Kondo lattice, we have to decouple the J_\perp term coupling the f_1 and f spinons in Eq. (128). Given the $SU(2)$ gauge structure of the S_2 layer, it pays to decouple the J_\perp term in a manner which keeps the $SU(2)$ gauge invariance explicit. In fact, the needed decoupling field is precisely the boson \mathcal{B}_i introduced in Eq. (115). We also introduce a matrix fermion operator \mathcal{F}_{1i}

$$\mathcal{F}_{1i} \equiv \begin{pmatrix} f_{1i\uparrow} & -f_{1i\downarrow} \\ f_{1i\downarrow}^\dagger & f_{1i\uparrow}^\dagger \end{pmatrix}, \quad (133)$$

whose transformations under the symmetries in Eqs. (118,119,120) are the same as those of \mathcal{C}_i . We summarize the gauge and symmetry properties in Table 2.

Then, from the J_\perp term, symmetry considerations are sufficient to constrain the structure of the Yukawa term between B and the fermions [19], which follows from Eq. (116) and is illustrated in Fig. 31:

$$\begin{aligned}
 \mathcal{H}_Y &= -\frac{1}{2} \sum_i [i \text{Tr}(\mathcal{F}_{1i}^\dagger \mathcal{B}_i^\dagger \mathcal{F}_i) + ig \text{Tr}(\mathcal{C}_i^\dagger \mathcal{B}_i^\dagger \mathcal{F}_i) + \text{H.c.}] \\
 &= \sum_i [i(B_{1i} f_{i\alpha}^\dagger f_{1i\alpha} - B_{2i} \varepsilon_{\alpha\beta} f_{i\alpha} f_{1i\beta}) + \text{H.c.}] \\
 &\quad + ig(B_{1i} f_{i\alpha}^\dagger c_{i\alpha} - B_{2i} \varepsilon_{\alpha\beta} f_{i\alpha} c_{i\beta}) + \text{H.c.}
 \end{aligned} \tag{134}$$

We have also included a Yukawa coupling to c_α from an allowed term $\sim \mathbf{S}_{2i} \cdot \mathbf{c}_{i\alpha}^\dagger \boldsymbol{\sigma}_{\alpha\beta} \mathbf{c}_{i\beta}$, which descends from the Kondo coupling noted below Eq. (127).

We can now collect all terms to write down the complete Hamiltonian needed for our analysis of the pseudogap metal, and its low temperature instabilities.

$$\mathcal{H}_{\text{pseudogap}} = \mathcal{H}_{\text{KLmf}} + \mathcal{H}_{SLf} + \mathcal{H}_Y + \mathcal{E}_2[B, U] + \mathcal{E}_4[B, U] \tag{135}$$

specified in Eqs. (130), (90), (134), (123). This Hamiltonian has 3 fermions $c_\alpha, f_{1\alpha}, f_\alpha$ whose transformations under SU(2) gauge, spin rotation, and electromagnetic charge symmetries are in Eqs. (118), (119), (120), with $f_{1\alpha}$ transforming just like c_α .

The boson B couples the Kondo Lattice to the spin liquid on the bottom layer, with SU(2) gauge field U_{ij} .

There is a remarkable similarity between Eq. (135), and the Weinberg-Salam theory of weak interactions [19]. Although the dispersions of the fermions and bosons have a lattice structure, the $\text{SU}(2) \times \text{U}(1)$ gauge structure (we treat the electromagnetic $\text{U}(1)$ as global), and the Yukawa couplings between the Higgs and the fermions are similar, with the spinons mapping to neutrinos, and the electrons mapping to electrons.

7.6 Anisotropic velocities in the d -wave superconductor

We now show how the problem of isotropic quasiparticle velocities (in contrast to observations in Ref. [14]), noted in Section 6, is resolved by the presence of the pocket Fermi surfaces described by $\mathcal{H}_{\text{KLmf}}$ in Eq. (130). The discussion below is based on the detailed computations presented in Refs. [20, 166].

Given the pocket Fermi surfaces and spinons in the FL^* normal state, we imagine imposing a BCS type pairing on the Fermi surface excitations. If the pairing is d -wave, it would lead to 8 nodal Bogoliubov points as shown in Fig. 32A. However this state also has the 4 nodal quasiparticles of the \mathbf{S}_2 spin liquid, associated with the dispersion in Fig. 19. So strictly speaking, this state remains fractionalized, and is *not* a conventional d -wave superconductor. It would be appropriate to call it $d\text{-SC}^*$.

However, if we induce the pairing by the B condensate in Eq. (134), the SU(2) gauge field is higgsed. Moreover, the Yukawa coupling allows the nodal quasiparticles of the \mathbf{S}_2 spin liquid to hybridize with the Bogoliubov quasiparticles of the pocket Fermi surfaces. The net result, sketched in Fig. 32B, is that the B condensate can enable the nodal points on the ‘backsides’ of the pocket Fermi surfaces to mutually annihilate with the spinons of the \mathbf{S}_2 spin liquid. We are then left with the 4 nodal quasiparticles on front sides of the pocket Fermi surfaces. The number of nodal points are the same as those obtained in conventional BCS theory from d -wave pairing of a Fermi liquid. These remaining nodal points are associated with pairing on the pocket Fermi surfaces, and these is no reason for their velocity to be isotropic (unlike the spinons).

The annihilation of the extra nodal points occurs via hybridization between the electrons and spinons within a mean-field band structure of $\mathcal{H}_{\text{KLmf}} + \mathcal{H}_{SLf} + \mathcal{H}_Y$ in Eqs. (130), (84), and (134). Furthermore, computations which diagonalize this Hamiltonian with B fixed and $U = 1$ do indeed yield anisotropic velocities similar to those observed. Unlike the situation in

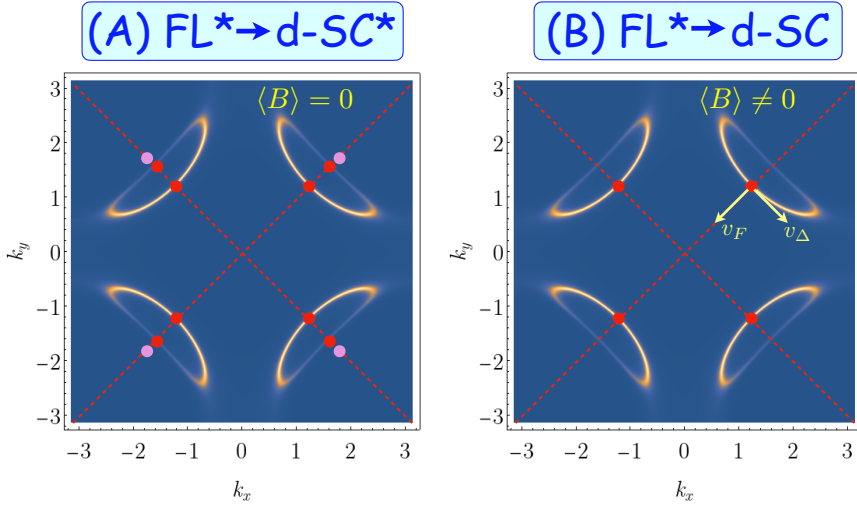


Figure 32: (A) Cooper pairing the Fermi surface quasiparticles in FL^* leads to $d\text{-}SC^*$ state, with 8 nodal Bogoliubov quasiparticles (red), and 4 nodal spinons (pink). (B) Upon condensing B , the spinons mutually annihilate 4 of the Bogoliubov quasiparticles, leaving 4 Bogoliubov quasiparticles with $v_F \gg v_\Delta$.

Section 6, the spinons do *not* become the Bogoliubov quasiparticles in the doped case; instead the spinons are needed to annihilate the extraneous Bogoliubov quasiparticles.

An interesting prediction can be made in the particular case of the electron-doped cuprates. In these materials, photoemission experiments have observed a normal state to superconductivity which is gapped near $(\pi/2, \pi/2)$ and has spectral weight only near electron pockets at the antinode [167]. If d -wave superconductivity were to emerge as a BCS instability from such a normal state, the resulting superconductor should be gapped. However, the FL^* theory yields a different prediction. Similar to how the spinon degrees of freedom emerge to annihilate with the backside pocket when B Higgs condenses in the hole-doped case, the Dirac node of the spin liquid will appear with a finite spectral weight near $(\pi/2, \pi/2)$ when B condenses, leading to a nodal superconductor. Such a prediction can be explored in future photoemission experiments in the electron doped cuprates [168] and could serve as an experimental test of the FL^* theory.

Acknowledgements

I thank Pietro Bonetti, Shubhayu Chatterjee, Maine Christos, Markus Greiner, Yasir Iqbal, Anant Kale, Martin Lebrat, Zhu-Xi Luo, Eric Mascot, Dirk Morr, Tobias Müller, Alexander Nikolaenko, Harshit Pandey, Matthias Scheurer, Leyna Shackleton, Ravi Shanker, Sayantan Sharma, Ronny Thomale, Maria Tikhonovskaya, Ya-Hui Zhang, and Jing-Yu Zhao for recent collaborations [19–21, 23, 54, 79, 148, 152, 154, 157, 158] on the work reviewed here. I thank my co-authors of the review in Ref. [18], from which some of the text is drawn, and A. Nikolaenko for assistance with Figs. 7 and 29. I thank Henning Schlömer for valuable comments on the manuscript. This research was supported by NSF Grant DMR-2245246 and by the Simons Collaboration on Ultra-Quantum Matter which is a grant from the Simons Foundation (651440, S. S.).

References

- [1] N. Read and S. Sachdev, *Large N expansion for frustrated quantum antiferromagnets*, Phys. Rev. Lett. **66**, 1773 (1991), doi:[10.1103/PhysRevLett.66.1773](https://doi.org/10.1103/PhysRevLett.66.1773).
- [2] X. G. Wen, *Mean-field theory of spin-liquid states with finite energy gap and topological orders*, Phys. Rev. B **44**, 2664 (1991), doi:[10.1103/PhysRevB.44.2664](https://doi.org/10.1103/PhysRevB.44.2664).
- [3] S. Sachdev, *Kagome and triangular-lattice Heisenberg antiferromagnets: Ordering from quantum fluctuations and quantum-disordered ground states with unconfined bosonic spinons*, Phys. Rev. B **45**, 12377 (1992), doi:[10.1103/PhysRevB.45.12377](https://doi.org/10.1103/PhysRevB.45.12377).
- [4] A. Y. Kitaev, *Fault-tolerant quantum computation by anyons*, Annals of Physics **303**(1), 2 (2003), doi:[10.1016/S0003-4916\(02\)00018-0](https://doi.org/10.1016/S0003-4916(02)00018-0), [quant-ph/9707021](https://arxiv.org/abs/quant-ph/9707021).
- [5] N. Read and S. Sachdev, *Valence-bond and spin-Peierls ground states of low-dimensional quantum antiferromagnets*, Phys. Rev. Lett. **62**, 1694 (1989), doi:[10.1103/PhysRevLett.62.1694](https://doi.org/10.1103/PhysRevLett.62.1694).
- [6] N. Read and S. Sachdev, *Spin-Peierls, valence-bond solid, and Néel ground states of low-dimensional quantum antiferromagnets*, Phys. Rev. B **42**, 4568 (1990), doi:[10.1103/PhysRevB.42.4568](https://doi.org/10.1103/PhysRevB.42.4568).
- [7] I. Affleck and J. B. Marston, *Large- n limit of the Heisenberg-Hubbard model: Implications for high- T_c superconductors*, Phys. Rev. B **37**, 3774 (1988), doi:[10.1103/PhysRevB.37.3774](https://doi.org/10.1103/PhysRevB.37.3774).
- [8] I. Affleck, Z. Zou, T. Hsu and P. W. Anderson, *$SU(2)$ gauge symmetry of the large- U limit of the Hubbard model*, Phys. Rev. B **38**, 745 (1988), doi:[10.1103/PhysRevB.38.745](https://doi.org/10.1103/PhysRevB.38.745).
- [9] E. Dagotto, E. Fradkin and A. Moreo, *$SU(2)$ gauge invariance and order parameters in strongly coupled electronic systems*, Phys. Rev. B **38**, 2926 (1988), doi:[10.1103/PhysRevB.38.2926](https://doi.org/10.1103/PhysRevB.38.2926).
- [10] X.-G. Wen and P. A. Lee, *Theory of Underdoped Cuprates*, Phys. Rev. Lett. **76**(3), 503 (1996), doi:[10.1103/PhysRevLett.76.503](https://doi.org/10.1103/PhysRevLett.76.503), [cond-mat/9506065](https://arxiv.org/abs/cond-mat/9506065).
- [11] C. Wang, A. Nahum, M. A. Metlitski, C. Xu and T. Senthil, *Deconfined quantum critical points: symmetries and dualities*, Phys. Rev. X **7**(3), 031051 (2017), doi:[10.1103/PhysRevX.7.031051](https://doi.org/10.1103/PhysRevX.7.031051), [1703.02426](https://arxiv.org/abs/1703.02426).
- [12] Y. Fang, G. Grissonnanche, A. Legros, S. Verret, F. Laliberté, C. Collignon, A. Ataei, M. Dion, J. Zhou, D. Graf, M. J. Lawler, P. A. Goddard *et al.*, *Fermi surface transformation at the pseudogap critical point of a cuprate superconductor*, Nature Physics **18**(5), 558 (2022), doi:[10.1038/s41567-022-01514-1](https://doi.org/10.1038/s41567-022-01514-1), [2004.01725](https://arxiv.org/abs/2004.01725).
- [13] M. K. Chan, K. A. Schreiber, O. E. Ayala-Valenzuela, E. D. Bauer, A. Shekhter and N. Harrison, *Observation of the Yamaji effect in a cuprate superconductor*, Nature Physics **21**(11), 1753 (2025), doi:[10.1038/s41567-025-03032-2](https://doi.org/10.1038/s41567-025-03032-2), [2411.10631](https://arxiv.org/abs/2411.10631).
- [14] M. Chiao, R. W. Hill, C. Lupien, L. Taillefer, P. Lambert, R. Gagnon and P. Fournier, *Low-energy quasiparticles in cuprate superconductors: A quantitative analysis*, Phys. Rev. B **62**(5), 3554 (2000), doi:[10.1103/PhysRevB.62.3554](https://doi.org/10.1103/PhysRevB.62.3554), [cond-mat/9910367](https://arxiv.org/abs/cond-mat/9910367).
- [15] T. Senthil, S. Sachdev and M. Vojta, *Fractionalized Fermi Liquids*, Phys. Rev. Lett. **90**(21), 216403 (2003), doi:[10.1103/PhysRevLett.90.216403](https://doi.org/10.1103/PhysRevLett.90.216403), [cond-mat/0209144](https://arxiv.org/abs/cond-mat/0209144).

[16] T. Senthil, M. Vojta and S. Sachdev, *Weak magnetism and non-Fermi liquids near heavy-fermion critical points*, Phys. Rev. B **69**(3), 035111 (2004), doi:[10.1103/PhysRevB.69.035111](https://doi.org/10.1103/PhysRevB.69.035111), [cond-mat/0305193](https://arxiv.org/abs/cond-mat/0305193).

[17] S. Sachdev, M. A. Metlitski and M. Punk, *Antiferromagnetism in metals: from the cuprate superconductors to the heavy fermion materials*, Journal of Physics Condensed Matter **24**(29), 294205 (2012), doi:[10.1088/0953-8984/24/29/294205](https://doi.org/10.1088/0953-8984/24/29/294205), [1202.4760](https://arxiv.org/abs/1202.4760).

[18] P. M. Bonetti, M. Christos, A. Nikolaenko, A. A. Patel and S. Sachdev, *Fractionalized Fermi liquids and the cuprate phase diagram*, arXiv e-prints arXiv:2508.20164 (2025), doi:[10.48550/arXiv.2508.20164](https://doi.org/10.48550/arXiv.2508.20164), [2508.20164](https://arxiv.org/abs/2508.20164).

[19] M. Christos, Z.-X. Luo, L. Shackleton, Y.-H. Zhang, M. S. Scheurer and S. Sachdev, *A model of d-wave superconductivity, antiferromagnetism, and charge order on the square lattice*, Proc. Nat. Acad. Sci. **120**(21), e2302701120 (2023), doi:[10.1073/pnas.2302701120](https://doi.org/10.1073/pnas.2302701120), [2302.07885](https://arxiv.org/abs/2302.07885).

[20] M. Christos and S. Sachdev, *Emergence of nodal Bogoliubov quasiparticles across the transition from the pseudogap metal to the d-wave superconductor*, npj Quantum Materials **9**(1), 4 (2024), doi:[10.1038/s41535-023-00608-0](https://doi.org/10.1038/s41535-023-00608-0), [2308.03835](https://arxiv.org/abs/2308.03835).

[21] M. Christos, L. Shackleton, S. Sachdev and Z.-X. Luo, *Deconfined quantum criticality of nodal d-wave superconductivity, Néel order, and charge order on the square lattice at half-filling*, Physical Review Research **6**(3), 033018 (2024), doi:[10.1103/PhysRevResearch.6.033018](https://doi.org/10.1103/PhysRevResearch.6.033018), [2402.09502](https://arxiv.org/abs/2402.09502).

[22] P. M. Bonetti, M. Christos and S. Sachdev, *Quantum oscillations in the hole-doped cuprates and the confinement of spinons*, Proceedings of the National Academy of Sciences **121**, e2418633121 (2024), doi:[10.1073/pnas.2418633121](https://doi.org/10.1073/pnas.2418633121), [2405.08817](https://arxiv.org/abs/2405.08817).

[23] H. Pandey, M. Christos, P. M. Bonetti, R. Shanker, A. Nikolaenko, S. Sharma and S. Sachdev, *Thermal SU(2) lattice gauge theory of the cuprate pseudogap: reconciling Fermi arcs and hole pockets*, arXiv e-prints arXiv:2507.05336 (2025), doi:[10.48550/arXiv.2507.05336](https://doi.org/10.48550/arXiv.2507.05336), [2507.05336](https://arxiv.org/abs/2507.05336).

[24] J.-X. Zhang and S. Sachdev, *Vortex structure in a d-wave superconductor obtained by a confinement transition from the pseudogap metal*, Phys. Rev. B **110**(23), 235120 (2024), doi:[10.1103/PhysRevB.110.235120](https://doi.org/10.1103/PhysRevB.110.235120), [2406.12964](https://arxiv.org/abs/2406.12964).

[25] T. Gazdić, I. Maggio-Aprile, G. Gu and C. Renner, *Wang-MacDonald d-Wave Vortex Cores Observed in Heavily Overdoped $Bi_2Sr_2CaCu_2O_{8+\delta}$* , Physical Review X **11**(3), 031040 (2021), doi:[10.1103/PhysRevX.11.031040](https://doi.org/10.1103/PhysRevX.11.031040), [2103.05994](https://arxiv.org/abs/2103.05994).

[26] Y. Wang and A. H. MacDonald, *Mixed-state quasiparticle spectrum for d-wave superconductors*, Phys. Rev. B **52**(6), R3876 (1995), doi:[10.1103/PhysRevB.52.R3876](https://doi.org/10.1103/PhysRevB.52.R3876), [cond-mat/9505142](https://arxiv.org/abs/cond-mat/9505142).

[27] J. E. Hoffman, E. W. Hudson, K. M. Lang, V. Madhavan, H. Eisaki, S. Uchida and J. C. Davis, *A Four Unit Cell Periodic Pattern of Quasi-Particle States Surrounding Vortex Cores in $Bi_2Sr_2CaCu_2O_{8+\delta}$* , Science **295**(5554), 466 (2002), doi:[10.1126/science.1066974](https://doi.org/10.1126/science.1066974), [cond-mat/0201348](https://arxiv.org/abs/cond-mat/0201348).

[28] A. A. Patel, H. Guo, I. Esterlis and S. Sachdev, *Universal theory of strange metals from spatially random interactions*, Science **381**, 790 (2023), doi:[10.1126/science.abq6011](https://doi.org/10.1126/science.abq6011), [2203.04990](https://arxiv.org/abs/2203.04990).

[29] C. Li, D. Valentinis, A. A. Patel, H. Guo, J. Schmalian, S. Sachdev and I. Esterlis, *Strange Metal and Superconductor in the Two-Dimensional Yukawa-Sachdev-Ye-Kitaev Model*, Phys. Rev. Lett. **133**(18), 186502 (2024), doi:[10.1103/PhysRevLett.133.186502](https://doi.org/10.1103/PhysRevLett.133.186502), [2406.07608](https://arxiv.org/abs/2406.07608).

[30] P. Lunts, A. A. Patel and S. Sachdev, *Thermopower across Fermi-volume-changing quantum phase transitions without translational symmetry breaking*, Phys. Rev. B **111**(24), 245151 (2025), doi:[10.1103/3639-byq1](https://doi.org/10.1103/3639-byq1), [2412.15330](https://arxiv.org/abs/2412.15330).

[31] D. Valentinis, J. Schmalian, S. Sachdev and A. A. Patel, *Superlinear Hall angle and carrier mobility from non-Boltzmann magnetotransport in the spatially disordered Yukawa-SYK model on a square lattice*, arXiv e-prints arXiv:2511.01030 (2025), doi:[10.48550/arXiv.2511.01030](https://doi.org/10.48550/arXiv.2511.01030), [2511.01030](https://arxiv.org/abs/2511.01030).

[32] S. Sachdev and J. Ye, *Gapless spin-fluid ground state in a random quantum Heisenberg magnet*, Phys. Rev. Lett. **70**(21), 3339 (1993), doi:[10.1103/PhysRevLett.70.3339](https://doi.org/10.1103/PhysRevLett.70.3339), [cond-mat/9212030](https://arxiv.org/abs/cond-mat/9212030).

[33] A. Kitaev, *A simple model of quantum holography, talk given at KITP program: entanglement in Strongly-Correlated Quantum Matter*, University of California, Santa Barbara (2015).

[34] F. Ferrari and F. Becca, *Gapless spin liquid and valence-bond solid in the J_1 - J_2 Heisenberg model on the square lattice: Insights from singlet and triplet excitations*, Phys. Rev. B **102**(1), 014417 (2020), doi:[10.1103/PhysRevB.102.014417](https://doi.org/10.1103/PhysRevB.102.014417), [2005.12941](https://arxiv.org/abs/2005.12941).

[35] Y. Nomura and M. Imada, *Dirac-Type Nodal Spin Liquid Revealed by Refined Quantum Many-Body Solver Using Neural-Network Wave Function, Correlation Ratio, and Level Spectroscopy*, Physical Review X **11**(3), 031034 (2021), doi:[10.1103/PhysRevX.11.031034](https://doi.org/10.1103/PhysRevX.11.031034), [2005.14142](https://arxiv.org/abs/2005.14142).

[36] W.-Y. Liu, D. Poilblanc, S.-S. Gong, W.-Q. Chen and Z.-C. Gu, *Tensor network study of the spin-1/2 square-lattice J_1 - J_2 - J_3 model: Incommensurate spiral order, mixed valence-bond solids, and multicritical points*, Phys. Rev. B **109**(23), 235116 (2024), doi:[10.1103/PhysRevB.109.235116](https://doi.org/10.1103/PhysRevB.109.235116), [2309.13301](https://arxiv.org/abs/2309.13301).

[37] J. Takahashi, H. Shao, B. Zhao, W. Guo and A. W. Sandvik, *$SO(5)$ multicriticality in two-dimensional quantum magnets*, arXiv e-prints (2024), [2405.06607](https://arxiv.org/abs/2405.06607).

[38] D. P. Arovas and A. Auerbach, *Functional integral theories of low-dimensional quantum Heisenberg models*, Phys. Rev. B **38**, 316 (1988), doi:[10.1103/PhysRevB.38.316](https://doi.org/10.1103/PhysRevB.38.316).

[39] T. Senthil, A. Vishwanath, L. Balents, S. Sachdev and M. P. A. Fisher, *Deconfined Quantum Critical Points*, Science **303**, 1490 (2004), doi:[10.1126/science.1091806](https://doi.org/10.1126/science.1091806), [cond-mat/0311326](https://arxiv.org/abs/cond-mat/0311326).

[40] T. Senthil, L. Balents, S. Sachdev, A. Vishwanath and M. P. A. Fisher, *Quantum criticality beyond the Landau-Ginzburg-Wilson paradigm*, Phys. Rev. B **70**(14), 144407 (2004), doi:[10.1103/PhysRevB.70.144407](https://doi.org/10.1103/PhysRevB.70.144407), [cond-mat/0312617](https://arxiv.org/abs/cond-mat/0312617).

[41] Y. Huh, M. Punk and S. Sachdev, *Vison states and confinement transitions of \mathbb{Z}_2 spin liquids on the kagome lattice*, Phys. Rev. B **84**(9), 094419 (2011), doi:[10.1103/PhysRevB.84.094419](https://doi.org/10.1103/PhysRevB.84.094419), [1106.3330](https://arxiv.org/abs/1106.3330).

[42] Y. Huh, L. Fritz and S. Sachdev, *Quantum criticality of the kagome antiferromagnet with Dzyaloshinskii-Moriya interactions*, Phys. Rev. B **81**(14), 144432 (2010), doi:[10.1103/PhysRevB.81.144432](https://doi.org/10.1103/PhysRevB.81.144432), [1003.0891](https://arxiv.org/abs/1003.0891).

[43] A. O. Scheie, E. A. Ghioldi, J. Xing, J. A. M. Paddison, N. E. Sherman, M. Dupont, L. D. Sanjeeewa, S. Lee, A. J. Woods, D. Abernathy, D. M. Pajerowski, T. J. Williams *et al.*, *Proximate spin liquid and fractionalization in the triangular antiferromagnet KYbSe₂*, Nature Physics **20**(1), 74 (2024), doi:[10.1038/s41567-023-02259-1](https://doi.org/10.1038/s41567-023-02259-1), [2109.11527](https://arxiv.org/abs/2109.11527).

[44] A. O. Scheie, M. Lee, K. Wang, P. Laurell, E. S. Choi, D. Pajerowski, Q. Zhang, J. Ma, H. D. Zhou, S. Lee, S. M. Thomas, M. O. Ajeesh *et al.*, *Spectrum and low-energy gap in triangular quantum spin liquid NaYbSe₂*, arXiv e-prints arXiv:2406.17773 (2024), doi:[10.48550/arXiv.2406.17773](https://doi.org/10.48550/arXiv.2406.17773), [2406.17773](https://arxiv.org/abs/2406.17773).

[45] P. Bonderson, M. Cheng, K. Patel and E. Plamadeala, *Topological Enrichment of Luttinger's Theorem*, arXiv e-prints arXiv:1601.07902 (2016), doi:[10.48550/arXiv.1601.07902](https://doi.org/10.48550/arXiv.1601.07902), [1601.07902](https://arxiv.org/abs/1601.07902).

[46] D. V. Else and T. Senthil, *Strange Metals as Ersatz Fermi Liquids*, Phys. Rev. Lett. **127**(8), 086601 (2021), doi:[10.1103/PhysRevLett.127.086601](https://doi.org/10.1103/PhysRevLett.127.086601), [2010.10523](https://arxiv.org/abs/2010.10523).

[47] R. A. Jalabert and S. Sachdev, *Spontaneous alignment of frustrated bonds in an anisotropic, three-dimensional Ising model*, Phys. Rev. B **44**, 686 (1991), doi:[10.1103/PhysRevB.44.686](https://doi.org/10.1103/PhysRevB.44.686).

[48] S. Sachdev and M. Vojta, *Translational symmetry breaking in two-dimensional antiferromagnets and superconductors*, J. Phys. Soc. Jpn **69**, Supp. B, 1 (1999), [cond-mat/9910231](https://arxiv.org/abs/cond-mat/9910231).

[49] Y.-M. Lu, *Symmetric Z₂ spin liquids and their neighboring phases on triangular lattice*, Phys. Rev. B **93**(16), 165113 (2016), doi:[10.1103/PhysRevB.93.165113](https://doi.org/10.1103/PhysRevB.93.165113), [1505.06495](https://arxiv.org/abs/1505.06495).

[50] X. Yang and F. Wang, *Schwinger boson spin-liquid states on square lattice*, Phys. Rev. B **94**(3), 035160 (2016), doi:[10.1103/PhysRevB.94.035160](https://doi.org/10.1103/PhysRevB.94.035160), [1507.07621](https://arxiv.org/abs/1507.07621).

[51] A. Thomson and S. Sachdev, *Fermionic Spinon Theory of Square Lattice Spin Liquids near the Néel State*, Physical Review X **8**(1), 011012 (2018), doi:[10.1103/PhysRevX.8.011012](https://doi.org/10.1103/PhysRevX.8.011012), [1708.04626](https://arxiv.org/abs/1708.04626).

[52] Y.-M. Lu, G. Y. Cho and A. Vishwanath, *Unification of bosonic and fermionic theories of spin liquids on the kagome lattice*, Phys. Rev. B **96**, 205150 (2017), doi:[10.1103/PhysRevB.96.205150](https://doi.org/10.1103/PhysRevB.96.205150), [1403.0575](https://arxiv.org/abs/1403.0575).

[53] K. Park and S. Sachdev, *Bond and Néel order and fractionalization in ground states of easy-plane antiferromagnets in two dimensions*, Phys. Rev. B **65**(22), 220405 (2002), doi:[10.1103/PhysRevB.65.220405](https://doi.org/10.1103/PhysRevB.65.220405), [cond-mat/0112003](https://arxiv.org/abs/cond-mat/0112003).

[54] L. Shackleton and S. Sachdev, *Sign-problem-free effective models of triangular lattice quantum antiferromagnets*, Phys. Rev. B **111**(7), 075101 (2025), doi:[10.1103/PhysRevB.111.075101](https://doi.org/10.1103/PhysRevB.111.075101), [2311.01572](https://arxiv.org/abs/2311.01572).

[55] T. Senthil and M. P. A. Fisher, *Z₂ gauge theory of electron fractionalization in strongly correlated systems*, Phys. Rev. B **62**(12), 7850 (2000), doi:[10.1103/PhysRevB.62.7850](https://doi.org/10.1103/PhysRevB.62.7850), [cond-mat/9910224](https://arxiv.org/abs/cond-mat/9910224).

[56] A. V. Chubukov, T. Senthil and S. Sachdev, *Universal magnetic properties of frustrated quantum antiferromagnets in two dimensions*, Phys. Rev. Lett. **72**, 2089 (1994), doi:[10.1103/PhysRevLett.72.2089](https://doi.org/10.1103/PhysRevLett.72.2089), [cond-mat/9311045](https://arxiv.org/abs/cond-mat/9311045).

[57] A. V. Chubukov, S. Sachdev and T. Senthil, *Quantum phase transitions in frustrated quantum antiferromagnets*, Nucl. Phys. B **426**, 601 (1994), doi:[10.1016/0550-3213\(94\)90023-X](https://doi.org/10.1016/0550-3213(94)90023-X), [cond-mat/9402006](https://arxiv.org/abs/cond-mat/9402006).

[58] S. Whitsitt and S. Sachdev, *Transition from the Z_2 spin liquid to antiferromagnetic order: Spectrum on the torus*, Phys. Rev. B **94**(8), 085134 (2016), doi:[10.1103/PhysRevB.94.085134](https://doi.org/10.1103/PhysRevB.94.085134), [1603.05652](https://arxiv.org/abs/1603.05652).

[59] X.-Y. Song, Y.-C. He, A. Vishwanath and C. Wang, *From spinon band topology to the symmetry quantum numbers of monopoles in Dirac spin liquids*, Phys. Rev. X **10**(1), 011033 (2020), doi:[10.1103/PhysRevX.10.011033](https://doi.org/10.1103/PhysRevX.10.011033), [1811.11182](https://arxiv.org/abs/1811.11182).

[60] X.-Y. Song, C. Wang, A. Vishwanath and Y.-C. He, *Unifying description of competing orders in two-dimensional quantum magnets*, Nature Communications **10**, 4254 (2019), doi:[10.1038/s41467-019-11727-3](https://doi.org/10.1038/s41467-019-11727-3), [1811.11186](https://arxiv.org/abs/1811.11186).

[61] A. Wietek, S. Capponi and A. M. Läuchli, *Quantum Electrodynamics in 2 +1 Dimensions as the Organizing Principle of a Triangular Lattice Antiferromagnet*, Physical Review X **14**(2), 021010 (2024), doi:[10.1103/PhysRevX.14.021010](https://doi.org/10.1103/PhysRevX.14.021010), [2303.01585](https://arxiv.org/abs/2303.01585).

[62] J. Willsher and J. Knolle, *Dynamics and stability of $U(1)$ spin liquids beyond mean-field theory: Triangular-lattice J_1 - J_2 Heisenberg model*, arXiv e-prints arXiv:2503.13831 (2025), doi:[10.48550/arXiv.2503.13831](https://doi.org/10.48550/arXiv.2503.13831), [2503.13831](https://arxiv.org/abs/2503.13831).

[63] S. Sachdev and R. Jalabert, *Effective lattice models for two-dimensional antiferromagnets*, Modern Physics Letters B **04**(16), 1043 (1990), doi:[10.1142/S0217984990001318](https://doi.org/10.1142/S0217984990001318).

[64] A. Nahum, P. Serna, J. T. Chalker, M. Ortúñoz and A. M. Somoza, *Emergent $SO(5)$ Symmetry at the Néel to Valence-Bond-Solid Transition*, Phys. Rev. Lett. **115**(26), 267203 (2015), doi:[10.1103/PhysRevLett.115.267203](https://doi.org/10.1103/PhysRevLett.115.267203), [1508.06668](https://arxiv.org/abs/1508.06668).

[65] B.-B. Chen, X. Zhang, Y. Wang, K. Sun and Z. Y. Meng, *Phases of (2+1)D $SO(5)$ Nonlinear Sigma Model with a Topological Term on a Sphere: Multicritical Point and Disorder Phase*, Phys. Rev. Lett. **132**(24), 246503 (2024), doi:[10.1103/PhysRevLett.132.246503](https://doi.org/10.1103/PhysRevLett.132.246503), [2307.05307](https://arxiv.org/abs/2307.05307).

[66] S. M. Chester and N. Su, *Bootstrapping Deconfined Quantum Tricriticality*, Phys. Rev. Lett. **132**(11), 111601 (2024), doi:[10.1103/PhysRevLett.132.111601](https://doi.org/10.1103/PhysRevLett.132.111601), [2310.08343](https://arxiv.org/abs/2310.08343).

[67] Z. Zhou, L. Hu, W. Zhu and Y.-C. He, *$SO(5)$ Deconfined Phase Transition under the Fuzzy-Sphere Microscope: Approximate Conformal Symmetry, Pseudo-Criticality, and Operator Spectrum*, Physical Review X **14**(2), 021044 (2024), doi:[10.1103/PhysRevX.14.021044](https://doi.org/10.1103/PhysRevX.14.021044), [2306.16435](https://arxiv.org/abs/2306.16435).

[68] P. Coleman and N. Andrei, *Kondo-stabilised spin liquids and heavy fermion superconductivity*, Journal of Physics: Condensed Matter **1**(26), 4057 (1989), doi:[10.1088/0953-8984/1/26/003](https://doi.org/10.1088/0953-8984/1/26/003).

[69] P. A. Lee, N. Nagaosa and X.-G. Wen, *Doping a Mott insulator: Physics of high-temperature superconductivity*, Rev. Mod. Phys. **78**, 17 (2006), doi:[10.1103/RevModPhys.78.17](https://doi.org/10.1103/RevModPhys.78.17), [cond-mat/0410445](https://arxiv.org/abs/cond-mat/0410445).

[70] J. Alicea, *Monopole quantum numbers in the staggered flux spin liquid*, Phys. Rev. B **78**(3), 035126 (2008), doi:[10.1103/PhysRevB.78.035126](https://doi.org/10.1103/PhysRevB.78.035126), [0804.0786](https://arxiv.org/abs/0804.0786).

[71] X.-Y. Song, Y.-C. He, A. Vishwanath and C. Wang, *From spinon band topology to the symmetry quantum numbers of monopoles in Dirac spin liquids*, Phys. Rev. X **10**(1), 011033 (2020), doi:[10.1103/PhysRevX.10.011033](https://doi.org/10.1103/PhysRevX.10.011033), [1811.11182](https://arxiv.org/abs/1811.11182).

[72] Y. Ran and X.-g. Wen, *Continuous quantum phase transitions beyond Landau's paradigm in a large- N spin model*, arXiv e-prints cond-mat/0609620 (2006), doi:[10.48550/arXiv.cond-mat/0609620](https://doi.org/10.48550/arXiv.cond-mat/0609620), cond-mat/0609620.

[73] A. G. Abanov and P. B. Wiegmann, *Theta terms in nonlinear sigma models*, Nucl. Phys. B **570**, 685 (2000), doi:[10.1016/S0550-3213\(99\)00820-2](https://doi.org/10.1016/S0550-3213(99)00820-2), hep-th/9911025.

[74] J. Lee and S. Sachdev, *Wess-Zumino-Witten Terms in Graphene Landau Levels*, Phys. Rev. Lett. **114**(22), 226801 (2015), doi:[10.1103/PhysRevLett.114.226801](https://doi.org/10.1103/PhysRevLett.114.226801), [1411.5684](https://arxiv.org/abs/1411.5684).

[75] A. Tanaka and X. Hu, *Many-Body Spin Berry Phases Emerging from the π -Flux State: Competition between Antiferromagnetism and the Valence-Bond-Solid State*, Phys. Rev. Lett. **95**(3), 036402 (2005), doi:[10.1103/PhysRevLett.95.036402](https://doi.org/10.1103/PhysRevLett.95.036402), cond-mat/0501365.

[76] T. Senthil and M. P. A. Fisher, *Competing orders, nonlinear sigma models, and topological terms in quantum magnets*, Phys. Rev. B **74**(6), 064405 (2006), doi:[10.1103/PhysRevB.74.064405](https://doi.org/10.1103/PhysRevB.74.064405), cond-mat/0510459.

[77] M. Hering, J. Sonnenschein, Y. Iqbal and J. Reuther, *Characterization of quantum spin liquids and their spinon band structures via functional renormalization*, Phys. Rev. B **99**(10), 100405 (2019), doi:[10.1103/PhysRevB.99.100405](https://doi.org/10.1103/PhysRevB.99.100405), [1806.05021](https://arxiv.org/abs/1806.05021).

[78] M. Lebrat, A. Kale, L. Haldar Kendrick, M. Xu, Y. Gang, A. Nikolaenko, P. M. Bonetti, S. Sachdev and M. Greiner, *Ferrimagnetism of ultracold fermions in a multi-band Hubbard system*, arXiv e-prints arXiv:2404.17555 (2024), doi:[10.48550/arXiv.2404.17555](https://doi.org/10.48550/arXiv.2404.17555), [2404.17555](https://arxiv.org/abs/2404.17555).

[79] A. Nikolaenko, P. M. Bonetti, A. Kale, M. Lebrat, M. Greiner and S. Sachdev, *Canted magnetism and Z_2 fractionalization in metallic states of the Lieb lattice Hubbard model near quarter filling*, Phys. Rev. B **112**(4), 045129 (2025), doi:[10.1103/19xn-h95s.2502.12235](https://doi.org/10.1103/19xn-h95s.2502.12235).

[80] B. I. Shraiman and E. D. Siggia, *Mobile Vacancies in a Quantum Heisenberg Antiferromagnet*, Phys. Rev. Lett. **61**, 467 (1988), doi:[10.1103/PhysRevLett.61.467](https://doi.org/10.1103/PhysRevLett.61.467).

[81] H. J. Schulz, *Effective action for strongly correlated fermions from functional integrals*, Phys. Rev. Lett. **65**, 2462 (1990), doi:[10.1103/PhysRevLett.65.2462](https://doi.org/10.1103/PhysRevLett.65.2462).

[82] N. Dupuis, *Spin fluctuations and pseudogap in the two-dimensional half-filled Hubbard model at weak coupling*, Phys. Rev. B **65**(24), 245118 (2002), doi:[10.1103/PhysRevB.65.245118](https://doi.org/10.1103/PhysRevB.65.245118), cond-mat/0110138.

[83] K. Borejsza and N. Dupuis, *Antiferromagnetism and single-particle properties in the two-dimensional half-filled Hubbard model: A nonlinear sigma model approach*, Phys. Rev. B **69**(8), 085119 (2004), doi:[10.1103/PhysRevB.69.085119](https://doi.org/10.1103/PhysRevB.69.085119), cond-mat/0307238.

[84] S. Sachdev, M. A. Metlitski, Y. Qi and C. Xu, *Fluctuating spin density waves in metals*, Phys. Rev. B **80**(15), 155129 (2009), doi:[10.1103/PhysRevB.80.155129](https://doi.org/10.1103/PhysRevB.80.155129), [0907.3732](https://arxiv.org/abs/0907.3732).

[85] D. Chowdhury and S. Sachdev, *Higgs criticality in a two-dimensional metal*, Phys. Rev. B **91**(11), 115123 (2015), doi:[10.1103/PhysRevB.91.115123](https://doi.org/10.1103/PhysRevB.91.115123), [1412.1086](https://arxiv.org/abs/1412.1086).

[86] D. Chowdhury and S. Sachdev, *The Enigma of the Pseudogap Phase of the Cuprate Superconductors*, In J. Jedrzejewski, ed., *Quantum criticality in condensed matter*, 50th Karpacz Winter School of Theoretical Physics, pp. 1–43. World Scientific, doi:[10.1142/9789814704090_0001](https://doi.org/10.1142/9789814704090_0001) (2015), [1501.00002](https://arxiv.org/abs/1501.00002).

[87] S. Chatterjee, S. Sachdev and M. Scheurer, *Intertwining topological order and broken symmetry in a theory of fluctuating spin density waves*, Phys. Rev. Lett. **119**(22), 227002 (2017), doi:[10.1103/PhysRevLett.119.227002](https://doi.org/10.1103/PhysRevLett.119.227002), [1705.06289](https://arxiv.org/abs/1705.06289).

[88] M. S. Scheurer and S. Sachdev, *Orbital currents in insulating and doped antiferromagnets*, Phys. Rev. B **98**(23), 235126 (2018), doi:[10.1103/PhysRevB.98.235126](https://doi.org/10.1103/PhysRevB.98.235126), [1808.04826](https://arxiv.org/abs/1808.04826).

[89] S. Sachdev, H. D. Scammell, M. S. Scheurer and G. Tarnopolsky, *Gauge theory for the cuprates near optimal doping*, Phys. Rev. B **99**(5), 054516 (2019), doi:[10.1103/PhysRevB.99.054516](https://doi.org/10.1103/PhysRevB.99.054516), [1811.04930](https://arxiv.org/abs/1811.04930).

[90] P. M. Bonetti and W. Metzner, *SU(2) gauge theory of the pseudogap phase in the two-dimensional Hubbard model*, Phys. Rev. B **106**(20), 205152 (2022), doi:[10.1103/PhysRevB.106.205152](https://doi.org/10.1103/PhysRevB.106.205152), [2207.00829](https://arxiv.org/abs/2207.00829).

[91] R. Scholle, P. M. Bonetti, D. Vilardi and W. Metzner, *Comprehensive mean-field analysis of magnetic and charge orders in the two-dimensional Hubbard model*, Phys. Rev. B **108**(3), 035139 (2023), doi:[10.1103/PhysRevB.108.035139](https://doi.org/10.1103/PhysRevB.108.035139), [2303.15358](https://arxiv.org/abs/2303.15358).

[92] F. F. Assaad, M. Imada and D. J. Scalapino, *Quantum Transition between an Antiferromagnetic Mott Insulator and $d_{x^2-y^2}$ Superconductor in Two Dimensions*, Phys. Rev. Lett. **77**(22), 4592 (1996), doi:[10.1103/PhysRevLett.77.4592](https://doi.org/10.1103/PhysRevLett.77.4592), [cond-mat/9609034](https://arxiv.org/abs/cond-mat/9609034).

[93] A. Götz, S. Beyl, M. Hohenadler and F. F. Assaad, *Valence-bond solid to antiferromagnet transition in the two-dimensional Su-Schrieffer-Heeger model by Langevin dynamics*, Phys. Rev. B **105**(8), 085151 (2022), doi:[10.1103/PhysRevB.105.085151](https://doi.org/10.1103/PhysRevB.105.085151), [2102.08899](https://arxiv.org/abs/2102.08899).

[94] A. Götz, M. Hohenadler and F. F. Assaad, *Phases and exotic phase transitions of a two-dimensional Su-Schrieffer-Heeger model*, Phys. Rev. B **109**(19), 195154 (2024), doi:[10.1103/PhysRevB.109.195154](https://doi.org/10.1103/PhysRevB.109.195154), [2307.07613](https://arxiv.org/abs/2307.07613).

[95] A. Götz, F. F. Assaad and N. C. Costa, *Tuning the order of a deconfined quantum critical point*, arXiv e-prints arXiv:2412.17215 (2024), doi:[10.48550/arXiv.2412.17215](https://doi.org/10.48550/arXiv.2412.17215), [2412.17215](https://arxiv.org/abs/2412.17215).

[96] X. Y. Xu and T. Grover, *Competing Nodal d -Wave Superconductivity and Antiferromagnetism*, Phys. Rev. Lett. **126**(21), 217002 (2021), doi:[10.1103/PhysRevLett.126.217002](https://doi.org/10.1103/PhysRevLett.126.217002), [2009.06644](https://arxiv.org/abs/2009.06644).

[97] B. Xing, W. Chiu, D. Poletti, R. T. Scalettar and G. G. Batrouni, *Quantum Monte Carlo Simulations of the 2D Su-Schrieffer-Heeger Model*, Physical Review Letters **126**(1), 017601 (2021), doi:[10.1103/PhysRevLett.126.017601](https://doi.org/10.1103/PhysRevLett.126.017601), [2005.09673](https://arxiv.org/abs/2005.09673).

[98] C. Feng, B. Xing, D. Poletti, R. T. Scalettar and G. G. Batrouni, *Phase Diagram of the Su-Schrieffer-Heeger-Hubbard model on a square lattice*, Physical Review B **106**(8), L081114 (2022), doi:[10.1103/PhysRevB.106.L081114](https://doi.org/10.1103/PhysRevB.106.L081114), [2109.09206](https://arxiv.org/abs/2109.09206).

[99] X. Cai, Z.-X. Li and H. Yao, *Antiferromagnetism Induced by Bond Su-Schrieffer-Heeger Electron-Phonon Coupling: A Quantum Monte Carlo Study*, Phys. Rev. Lett. **127**(24), 247203 (2021), doi:[10.1103/PhysRevLett.127.247203](https://doi.org/10.1103/PhysRevLett.127.247203), [2102.05060](https://arxiv.org/abs/2102.05060).

[100] X. Cai, Z.-X. Li and H. Yao, *Robustness of antiferromagnetism in the Su-Schrieffer-Heeger Hubbard model*, Phys. Rev. B **106**(8), L081115 (2022), doi:[10.1103/PhysRevB.106.L081115](https://doi.org/10.1103/PhysRevB.106.L081115), [2112.14744](https://arxiv.org/abs/2112.14744).

[101] H.-X. Wang, Y.-F. Jiang and H. Yao, *Robust d-wave superconductivity from the Su-Schrieffer-Heeger-Hubbard model: Possible route to high-temperature superconductivity*, Science Bulletin **70**(14), 2260 (2025), doi:<https://doi.org/10.1016/j.scib.2025.04.055>, [2211.09143](https://arxiv.org/abs/2211.09143).

[102] Z. Han and S. A. Kivelson, *Resonating Valence Bond States in an Electron-Phonon System*, Phys. Rev. Lett. **130**(18), 186404 (2023), doi:[10.1103/PhysRevLett.130.186404](https://doi.org/10.1103/PhysRevLett.130.186404), [2210.16321](https://arxiv.org/abs/2210.16321).

[103] X. Cai, Z. Han, Z.-X. Li, S. A. Kivelson and H. Yao, *Quantum spin liquid from electron-phonon coupling*, Proceedings of the National Academy of Science **122**(33), e2426111122 (2025), doi:[10.1073/pnas.2426111122](https://doi.org/10.1073/pnas.2426111122), [2408.04002](https://arxiv.org/abs/2408.04002).

[104] A. Jaafari, S. Lal and E. Fradkin, *Charge-density wave and superconductor competition in stripe phases of high-temperature superconductors*, Phys. Rev. B **82**(14), 144531 (2010), doi:[10.1103/PhysRevB.82.144531](https://doi.org/10.1103/PhysRevB.82.144531), [1007.2187](https://arxiv.org/abs/1007.2187).

[105] L. E. Hayward, D. G. Hawthorn, R. G. Melko and S. Sachdev, *Angular fluctuations of a multi-component order describe the pseudogap regime of the cuprate superconductors*, Science **343**, 1336 (2014), doi:[10.1126/science.1246310](https://doi.org/10.1126/science.1246310), [1309.6639](https://arxiv.org/abs/1309.6639).

[106] P. A. Lee, *Amperean Pairing and the Pseudogap Phase of Cuprate Superconductors*, Physical Review X **4**(3), 031017 (2014), doi:[10.1103/PhysRevX.4.031017](https://doi.org/10.1103/PhysRevX.4.031017), [1401.0519](https://arxiv.org/abs/1401.0519).

[107] L. Nie, L. E. H. Sierens, R. G. Melko, S. Sachdev and S. A. Kivelson, *Fluctuating orders and quenched randomness in the cuprates*, Phys. Rev. B **92**(17), 174505 (2015), doi:[10.1103/PhysRevB.92.174505](https://doi.org/10.1103/PhysRevB.92.174505), [1505.06206](https://arxiv.org/abs/1505.06206).

[108] E. Fradkin, S. A. Kivelson and J. M. Tranquada, *Colloquium: Theory of intertwined orders in high temperature superconductors*, Reviews of Modern Physics **87**(2), 457 (2015), doi:[10.1103/RevModPhys.87.457](https://doi.org/10.1103/RevModPhys.87.457), [1407.4480](https://arxiv.org/abs/1407.4480).

[109] C. Pépin and H. Freire, *Charge order and emergent symmetries in cuprate superconductors*, Annals of Physics **456**, 169233 (2023), doi:[10.1016/j.aop.2023.169233](https://doi.org/10.1016/j.aop.2023.169233), [2210.04046](https://arxiv.org/abs/2210.04046).

[110] E. Fradkin, *Intertwined Orders and the Physics of High Temperature Superconductors*, Particles **8**(3) (2025), doi:[10.3390/particles8030070](https://doi.org/10.3390/particles8030070), [2506.21673](https://arxiv.org/abs/2506.21673).

[111] F. C. Zhang, C. Gros, T. M. Rice and H. Shiba, *A renormalised Hamiltonian approach for a resonant valence bond wavefunction*, Superconductor Science and Technology **1**, 36 (1988), doi:[10.1088/0953-2048/1/1/009](https://doi.org/10.1088/0953-2048/1/1/009), [cond-mat/0311604](https://arxiv.org/abs/cond-mat/0311604).

[112] G. Kotliar and J. Liu, *Superechange mechanism and d-wave superconductivity*, Phys. Rev. B **38**, 5142 (1988), doi:[10.1103/PhysRevB.38.5142](https://doi.org/10.1103/PhysRevB.38.5142).

[113] D. A. Ivanov and T. Senthil, *Projected wave functions for fractionalized phases of quantum spin systems*, Phys. Rev. B **66**(11), 115111 (2002), doi:[10.1103/PhysRevB.66.115111](https://doi.org/10.1103/PhysRevB.66.115111), cond-mat/0204043.

[114] J. M. Luttinger, *Fermi Surface and Some Simple Equilibrium Properties of a System of Interacting Fermions*, Phys. Rev. **119**, 1153 (1960), doi:[10.1103/PhysRev.119.1153](https://doi.org/10.1103/PhysRev.119.1153).

[115] M. Oshikawa, *Topological Approach to Luttinger's Theorem and the Fermi Surface of a Kondo Lattice*, Phys. Rev. Lett. **84**, 3370 (2000), doi:[10.1103/PhysRevLett.84.3370](https://doi.org/10.1103/PhysRevLett.84.3370), cond-mat/0002392.

[116] S. Sachdev, *Quantum Phases of Matter*, Cambridge University Press, Cambridge, UK, 1 edn. (2023).

[117] A. Paramekanti and A. Vishwanath, *Extending Luttinger's theorem to \mathbb{Z}_2 fractionalized phases of matter*, Phys. Rev. B **70**(24), 245118 (2004), doi:[10.1103/PhysRevB.70.245118](https://doi.org/10.1103/PhysRevB.70.245118), cond-mat/0406619.

[118] S. Powell, S. Sachdev and H. P. Büchler, *Depletion of the Bose-Einstein condensate in Bose-Fermi mixtures*, Phys. Rev. B **72**(2), 024534 (2005), doi:[10.1103/PhysRevB.72.024534](https://doi.org/10.1103/PhysRevB.72.024534), cond-mat/0502299.

[119] P. Coleman, I. Paul and J. Rech, *Sum rules and Ward identities in the Kondo lattice*, Phys. Rev. B **72**(9), 094430 (2005), doi:[10.1103/PhysRevB.72.094430](https://doi.org/10.1103/PhysRevB.72.094430), cond-mat/0503001.

[120] Y. Qi and S. Sachdev, *Effective theory of Fermi pockets in fluctuating antiferromagnets*, Phys. Rev. B **81**(11), 115129 (2010), doi:[10.1103/PhysRevB.81.115129](https://doi.org/10.1103/PhysRevB.81.115129), 0912.0943.

[121] D. V. Else, R. Thorngren and T. Senthil, *Non-Fermi Liquids as Ersatz Fermi Liquids: General Constraints on Compressible Metals*, Physical Review X **11**(2), 021005 (2021), doi:[10.1103/PhysRevX.11.021005](https://doi.org/10.1103/PhysRevX.11.021005), 2007.07896.

[122] M. Punk, A. Allais and S. Sachdev, *A quantum dimer model for the pseudogap metal*, Proc. Nat. Acad. Sci. **112**, 9552 (2015), doi:[10.1073/pnas.1512206112](https://doi.org/10.1073/pnas.1512206112), 1501.00978.

[123] J. Schmalian, D. Pines and B. Stojković, *Weak Pseudogap Behavior in the Underdoped Cuprate Superconductors*, Phys. Rev. Lett. **80**(17), 3839 (1998), doi:[10.1103/PhysRevLett.80.3839](https://doi.org/10.1103/PhysRevLett.80.3839), cond-mat/9708238.

[124] J. Schmalian, D. Pines and B. Stojković, *Microscopic theory of weak pseudogap behavior in the underdoped cuprate superconductors: General theory and quasiparticle properties*, Phys. Rev. B **60**(1), 667 (1999), doi:[10.1103/PhysRevB.60.667](https://doi.org/10.1103/PhysRevB.60.667), cond-mat/9804129.

[125] M. Ye and A. V. Chubukov, *Crucial role of thermal fluctuations and vertex corrections for the magnetic pseudogap*, Phys. Rev. B **108**(8), L081118 (2023), doi:[10.1103/PhysRevB.108.L081118](https://doi.org/10.1103/PhysRevB.108.L081118), 2306.05489.

[126] E. K. Kokkinis and A. V. Chubukov, *Pseudogap in electron-doped cuprates: thermal precursor to magnetism*, arXiv e-prints arXiv:2505.11727 (2025), doi:[10.48550/arXiv.2505.11727](https://doi.org/10.48550/arXiv.2505.11727), 2505.11727.

[127] S. Sachdev, M. A. Metlitski, Y. Qi and C. Xu, *Fluctuating spin density waves in metals*, Phys. Rev. B **80**, 155129 (2009), doi:[10.1103/PhysRevB.80.155129](https://doi.org/10.1103/PhysRevB.80.155129), 0907.3732.

[128] W. Wu, M. S. Scheurer, S. Chatterjee, S. Sachdev, A. Georges and M. Ferrero, *Pseudogap and Fermi-Surface Topology in the Two-Dimensional Hubbard Model*, Phys. Rev. X **8**(2), 021048 (2018), doi:[10.1103/PhysRevX.8.021048](https://doi.org/10.1103/PhysRevX.8.021048), 1707.06602.

[129] M. S. Scheurer, S. Chatterjee, W. Wu, M. Ferrero, A. Georges and S. Sachdev, *Topological order in the pseudogap metal*, Proc. Nat. Acad. Sci. **115**(16), E3665 (2018), doi:[10.1073/pnas.1720580115](https://doi.org/10.1073/pnas.1720580115), [1711.09925](https://arxiv.org/abs/1711.09925).

[130] S. Sachdev, *Topological order, emergent gauge fields, and Fermi surface reconstruction*, Rept. Prog. Phys. **82**(1), 014001 (2019), doi:[10.1088/1361-6633/aae110](https://doi.org/10.1088/1361-6633/aae110), [1801.01125](https://arxiv.org/abs/1801.01125).

[131] W. Wu, M. S. Scheurer, M. Ferrero and A. Georges, *Effect of van Hove singularities in the onset of pseudogap states in Mott insulators*, Phys. Rev. Res. **2**, 033067 (2020), doi:[10.1103/PhysRevResearch.2.033067](https://doi.org/10.1103/PhysRevResearch.2.033067), [2001.00019](https://arxiv.org/abs/2001.00019).

[132] T. C. Ribeiro and X.-G. Wen, *New Mean-Field Theory of the $tt't''J$ Model Applied to High- T_c Superconductors*, Phys. Rev. Lett. **95**(5), 057001 (2005), doi:[10.1103/PhysRevLett.95.057001](https://doi.org/10.1103/PhysRevLett.95.057001), [cond-mat/0410750](https://arxiv.org/abs/cond-mat/0410750).

[133] R. K. Kaul, A. Kolezhuk, M. Levin, S. Sachdev and T. Senthil, *Hole dynamics in an antiferromagnet across a deconfined quantum critical point*, Phys. Rev. B **75**(23), 235122 (2007), doi:[10.1103/PhysRevB.75.235122](https://doi.org/10.1103/PhysRevB.75.235122), [cond-mat/0702119](https://arxiv.org/abs/cond-mat/0702119).

[134] R. K. Kaul, Y. B. Kim, S. Sachdev and T. Senthil, *Algebraic charge liquids*, Nature Physics **4**, 28 (2008), doi:[10.1038/nphys790](https://doi.org/10.1038/nphys790), [0706.2187](https://arxiv.org/abs/0706.2187).

[135] B. Lau, M. Berciu and G. A. Sawatzky, *High-Spin Polaron in Lightly Doped CuO_2 Planes*, Phys. Rev. Lett. **106**(3), 036401 (2011), doi:[10.1103/PhysRevLett.106.036401](https://doi.org/10.1103/PhysRevLett.106.036401), [1010.1867](https://arxiv.org/abs/1010.1867).

[136] E. G. Moon and S. Sachdev, *Underdoped cuprates as fractionalized Fermi liquids: Transition to superconductivity*, Phys. Rev. B **83**(22), 224508 (2011), doi:[10.1103/PhysRevB.83.224508](https://doi.org/10.1103/PhysRevB.83.224508), [1010.4567](https://arxiv.org/abs/1010.4567).

[137] B. Lau, M. Berciu and G. A. Sawatzky, *Computational approach to a doped antiferromagnet: Correlations between two spin polarons in the lightly doped CuO_2 plane*, Phys. Rev. B **84**(16), 165102 (2011), doi:[10.1103/PhysRevB.84.165102](https://doi.org/10.1103/PhysRevB.84.165102), [1107.4141](https://arxiv.org/abs/1107.4141).

[138] J.-W. Mei, S. Kawasaki, G.-Q. Zheng, Z.-Y. Weng and X.-G. Wen, *Luttinger-volume violating Fermi liquid in the pseudogap phase of the cuprate superconductors*, Phys. Rev. B **85**(13), 134519 (2012), doi:[10.1103/PhysRevB.85.134519](https://doi.org/10.1103/PhysRevB.85.134519), [1109.0406](https://arxiv.org/abs/1109.0406).

[139] M. Punk and S. Sachdev, *Fermi surface reconstruction in hole-doped t - J models without long-range antiferromagnetic order*, Phys. Rev. B **85**(19), 195123 (2012), doi:[10.1103/PhysRevB.85.195123](https://doi.org/10.1103/PhysRevB.85.195123), [1202.4023](https://arxiv.org/abs/1202.4023).

[140] J. Feldmeier, S. Huber and M. Punk, *Exact Solution of a Two-Species Quantum Dimer Model for Pseudogap Metals*, Phys. Rev. Lett. **120**, 187001 (2018), doi:[10.1103/PhysRevLett.120.187001](https://doi.org/10.1103/PhysRevLett.120.187001), [1712.01854](https://arxiv.org/abs/1712.01854).

[141] F. Grusdt, M. Kánsz-Nagy, A. Bohrdt, C. S. Chiu, G. Ji, M. Greiner, D. Greif and E. Demler, *Parton Theory of Magnetic Polarons: Mesonic Resonances and Signatures in Dynamics*, Physical Review X **8**(1), 011046 (2018), doi:[10.1103/PhysRevX.8.011046](https://doi.org/10.1103/PhysRevX.8.011046), [1712.01874](https://arxiv.org/abs/1712.01874).

[142] C. S. Chiu, G. Ji, A. Bohrdt, M. Xu, M. Knap, E. Demler, F. Grusdt, M. Greiner and D. Greif, *String patterns in the doped Hubbard model*, Science **365**(6450), 251 (2019), doi:[10.1126/science.aav3587](https://doi.org/10.1126/science.aav3587), [1810.03584](https://arxiv.org/abs/1810.03584).

[143] F. Grusdt, E. Demler and A. Bohrdt, *Pairing of holes by confining strings in antiferromagnets*, SciPost Physics **14**(5), 090 (2023), doi:[10.21468/SciPostPhys.14.5.090](https://doi.org/10.21468/SciPostPhys.14.5.090), [2210.02321](https://arxiv.org/abs/2210.02321).

[144] H. Schrömer, U. Schollwöck, A. Bohrdt and F. Grusdt, *Kinetic-to-magnetic frustration crossover and linear confinement in the doped triangular $t-J$ model*, Phys. Rev. B **110**(4), L041117 (2024), doi:[10.1103/PhysRevB.110.L041117](https://doi.org/10.1103/PhysRevB.110.L041117), [2305.02342](https://arxiv.org/abs/2305.02342).

[145] J. H. Nyhegn, K. K. Nielsen, L. Balents and G. M. Bruun, *Spin-Charge Bound States and Emerging Fermions in a Quantum Spin Liquid*, PRX Quantum **6**(4), 040347 (2025), doi:[10.1103/w23h-dhrk](https://doi.org/10.1103/w23h-dhrk), [2507.02508](https://arxiv.org/abs/2507.02508).

[146] W. Tabis, Y. Li, M. L. Tacon, L. Braicovich, A. Kreyssig, M. Minola, G. Dellea, E. Weschke, M. J. Veit, M. Ramazanoglu, A. I. Goldman, T. Schmitt *et al.*, *Charge order and its connection with Fermi-liquid charge transport in a pristine high- T_c cuprate*, Nature Communications **5**, 5875 (2014), doi:[10.1038/ncomms6875](https://doi.org/10.1038/ncomms6875), [1404.7658](https://arxiv.org/abs/1404.7658).

[147] Z. W. Anderson, Y. Tang, V. Nagarajan, M. K. Chan, C. J. Dorow, G. Yu, D. L. Abernathy, A. D. Christianson, L. Mangin-Thro, P. Steffens, T. Sterling, D. Reznik *et al.*, *Gapped commensurate antiferromagnetic response in a strongly underdoped model cuprate superconductor*, npj Quantum Materials **10**(1), 93 (2025), doi:[10.1038/s41535-025-00804-0](https://doi.org/10.1038/s41535-025-00804-0), [2412.03524](https://arxiv.org/abs/2412.03524).

[148] J.-Y. Zhao, S. Chatterjee, S. Sachdev and Y.-H. Zhang, *Yamaji effect in models of underdoped cuprates*, arXiv e-prints arXiv:2510.13943 (2025), doi:[10.48550/arXiv.2510.13943](https://doi.org/10.48550/arXiv.2510.13943), [2510.13943](https://arxiv.org/abs/2510.13943).

[149] A. Nikolaenko, J. von Milczewski, D. G. Joshi and S. Sachdev, *Spin density wave, Fermi liquid, and fractionalized phases in a theory of antiferromagnetic metals using paramagnons and bosonic spinons*, Phys. Rev. B **108**(4), 045123 (2023), doi:[10.1103/PhysRevB.108.045123](https://doi.org/10.1103/PhysRevB.108.045123), [2211.10452](https://arxiv.org/abs/2211.10452).

[150] Y. Zhong, F.-C. Zhang and K. Jiang, *Yamaji effect and quantum oscillation in Yang-Rice-Zhang model of underdoped cuprates*, arXiv e-prints arXiv:2512.10475 (2025), doi:[10.48550/arXiv.2512.10475](https://doi.org/10.48550/arXiv.2512.10475), [2512.10475](https://arxiv.org/abs/2512.10475).

[151] J. Koepsell, D. Bourgund, P. Sompé, S. Hirthe, A. Bohrdt, Y. Wang, F. Grusdt, E. Demler, G. Salomon, C. Gross and I. Bloch, *Microscopic evolution of doped Mott insulators from polaronic metal to Fermi liquid*, Science **374**(6563), 82 (2021), doi:[10.1126/science.abe7165](https://doi.org/10.1126/science.abe7165), [2009.04440](https://arxiv.org/abs/2009.04440).

[152] T. Müller, R. Thomale, S. Sachdev and Y. Iqbal, *Polaronic correlations from optimized ancilla wave functions for the Fermi-Hubbard model*, Proceedings of the National Academy of Science **122**(20), e2504261122 (2025), doi:[10.1073/pnas.2504261122](https://doi.org/10.1073/pnas.2504261122), [2408.01492](https://arxiv.org/abs/2408.01492).

[153] L. Shackleton and S. Zhang, *Emergent polaronic correlations in doped spin liquids*, arXiv e-prints arXiv:2408.02190 (2024), doi:[10.48550/arXiv.2408.02190](https://doi.org/10.48550/arXiv.2408.02190), [2408.02190](https://arxiv.org/abs/2408.02190).

[154] Y.-H. Zhang and S. Sachdev, *From the pseudogap metal to the Fermi liquid using ancilla qubits*, Physical Review Research **2**(2), 023172 (2020), doi:[10.1103/PhysRevResearch.2.023172](https://doi.org/10.1103/PhysRevResearch.2.023172), [arXiv.2001.09159](https://arxiv.org/abs/2001.09159), [2001.09159](https://arxiv.org/abs/2001.09159).

[155] Y.-H. Zhang and S. Sachdev, *Deconfined criticality and ghost Fermi surfaces at the onset of antiferromagnetism in a metal*, Phys. Rev. B **102**(15), 155124 (2020), doi:[10.1103/PhysRevB.102.155124](https://doi.org/10.1103/PhysRevB.102.155124), [arXiv.2006.01140](https://arxiv.org/abs/2006.01140), [2006.01140](https://arxiv.org/abs/2006.01140).

[156] K.-Y. Yang, T. M. Rice and F.-C. Zhang, *Phenomenological theory of the pseudogap state*, Phys. Rev. B **73**(17), 174501 (2006), doi:[10.1103/PhysRevB.73.174501](https://doi.org/10.1103/PhysRevB.73.174501), cond-mat/[0602164](https://arxiv.org/abs/0602164).

[157] A. Nikolaenko, M. Tikhanovskaya, S. Sachdev and Y.-H. Zhang, *Small to large Fermi surface transition in a single band model, using randomly coupled ancillas*, Phys. Rev. B **103**(23), 235138 (2021), doi:[10.1103/PhysRevB.103.235138](https://doi.org/10.1103/PhysRevB.103.235138), [2103.05009](https://arxiv.org/abs/2103.05009).

[158] E. Mascot, A. Nikolaenko, M. Tikhanovskaya, Y.-H. Zhang, D. K. Morr and S. Sachdev, *Electronic spectra with paramagnon fractionalization in the single-band Hubbard model*, Phys. Rev. B **105**(7), 075146 (2022), doi:[10.1103/PhysRevB.105.075146](https://doi.org/10.1103/PhysRevB.105.075146), [2111.13703](https://arxiv.org/abs/2111.13703).

[159] P. W. Anderson, P. A. Lee, M. Randeria, T. M. Rice, N. Trivedi and F. C. Zhang, *The physics behind high-temperature superconducting cuprates: the 'plain vanilla' version of RVB*, Journal of Physics Condensed Matter **16**(24), R755 (2004), doi:[10.1088/0953-8984/16/24/R02](https://doi.org/10.1088/0953-8984/16/24/R02), cond-mat/[0311467](https://arxiv.org/abs/0311467).

[160] D. E. Rumelhart, G. E. Hinton and R. J. Williams, *Learning representations by back-propagating errors*, Nature **323**(6088), 533 (1986), doi:[10.1038/323533a0](https://doi.org/10.1038/323533a0).

[161] B. Zhou, H.-K. Jin and Y.-H. Zhang, *Variational wavefunction for a Mott insulator at finite U using ancilla qubits*, Phys. Rev. B **112**(11), 115159 (2025), doi:[10.1103/8knn-mr5x.2409.07512](https://doi.org/10.1103/8knn-mr5x.2409.07512).

[162] T. Chalopin, P. Bojović, S. Wang, T. Franz, A. Sinha, Z. Wang, D. Bourgund, J. Obermeyer, F. Grusdt, A. Bohrdt, L. Pollet, A. Wietek *et al.*, *Probing the magnetic origin of the pseudogap using a Fermi-Hubbard quantum simulator*, arXiv e-prints arXiv:2412.17801 (2024), doi:[10.48550/arXiv.2412.17801](https://doi.org/10.48550/arXiv.2412.17801), [2412.17801](https://arxiv.org/abs/2412.17801).

[163] L. Haldar Kendrick, A. Kale, Y. Gang, A. Dennisovich Deters, M. Lebrat, A. W. Young and M. Greiner, *Pseudogap in a Fermi-Hubbard quantum simulator*, arXiv e-prints arXiv:2509.18075 (2025), doi:[10.48550/arXiv.2509.18075](https://doi.org/10.48550/arXiv.2509.18075), [2509.18075](https://arxiv.org/abs/2509.18075).

[164] H.-C. Jiang and S. A. Kivelson, *High Temperature Superconductivity in a Lightly Doped Quantum Spin Liquid*, Phys. Rev. Lett. **127**(9), 097002 (2021), doi:[10.1103/PhysRevLett.127.097002](https://doi.org/10.1103/PhysRevLett.127.097002), [2104.01485](https://arxiv.org/abs/2104.01485).

[165] H.-C. Jiang, S. A. Kivelson and D.-H. Lee, *Superconducting valence bond fluid in lightly doped eight-leg t-J cylinders*, Phys. Rev. B **108**(5), 054505 (2023), doi:[10.1103/PhysRevB.108.054505](https://doi.org/10.1103/PhysRevB.108.054505), [2302.11633](https://arxiv.org/abs/2302.11633).

[166] S. Chatterjee and S. Sachdev, *Fractionalized Fermi liquid with bosonic chargons as a candidate for the pseudogap metal*, Phys. Rev. B **94**(20), 205117 (2016), doi:[10.1103/PhysRevB.94.205117](https://doi.org/10.1103/PhysRevB.94.205117), [1607.05727](https://arxiv.org/abs/1607.05727).

[167] N. P. Armitage, F. Ronning, D. H. Lu, C. Kim, A. Damascelli, K. M. Shen, D. L. Feng, H. Eisaki, Z.-X. Shen, P. K. Mang, N. Kaneko, M. Greven *et al.*, *Doping Dependence of an n-Type Cuprate Superconductor Investigated by Angle-Resolved Photoemission Spectroscopy*, Phys. Rev. Lett. **88**, 257001 (2002), doi:[10.1103/PhysRevLett.88.257001](https://doi.org/10.1103/PhysRevLett.88.257001).

[168] K.-J. Xu, Q. Guo, M. Hashimoto, Z.-X. Li, S.-D. Chen, J. He, Y. He, C. Li, M. H. Berntsen, C. R. Rotundu, Y. S. Lee, T. P. Devereaux *et al.*, *Bogoliubov quasiparticle on the gossamer Fermi surface in electron-doped cuprates*, Nature Physics **19**(12), 1834–1840 (2023), doi:[10.1038/s41567-023-02209-x](https://doi.org/10.1038/s41567-023-02209-x).